Imperial College London
The Francis Crick Institute

Cell cycle remodelling during hESC differentiation: a lesson from single cells

Chiara Borghi
August 2018

Submitted in part fulfilment of the requirements for the degree of Master of Philosophy of Imperial College London

Declaration

I certify that the work presented in this thesis is my own, and that any work carried out by others has been properly acknowledged and appropriately referenced in the text.

Chiara Borghi

The copyright of this thesis rests with the author and is made available under a Creative Commons Attribution Non-Commercial No Derivatives licence. Researchers are free to copy, distribute or transmit the thesis on the condition that they attribute it, that they do not use it for commercial purposes and they do not alter, transform or build upon it. For any reuse or redistribution, researchers must make clear to others the licence terms of this work.

Abstract

The cell cycle is a sequence of events that every cell goes through in order to duplicate its genomic content and segregate it into two daughter cells. Even though the molecular machinery involved in cell cycle control does not vary in different cells, cell cycle dynamics can be very different cells. Human embryonic stem cells (hESCs) have two unique capabilities: they self-renew and differentiate into the three germ layers upon receiving an external stimulus. While their self-renewal state is characterised by a very short cell cycle (~16h) mostly due to a short G1-phase and little checkpoint control, after differentiation they acquire the canonical cell cycle profile of somatic cells with long gap phases and active checkpoint control. Previous studies have highlighted the differences between the pluripotent and the somatic (differentiated) cell cycle but it is still unclear how cells remodel cell division networks to allow for structurally different cell cycles.

In order to explore the mechanisms underlying cell cycle remodelling during hESCs differentiation, a combination of cell cycle biosensors and live cell imaging techniques was established to study how cell cycle remodelling happens in single cells during mesoderm differentiation of hESC. The main difference in cell cycle phases length between hESC and differentiated cells was found to be in G1-phase length. We show that the transition from the short G1-phase of hESCs to the remodelled G1-phase of differentiated cells happened in a switch-like manner. Finally, using perturbation approaches, we demonstrated that cell cycle regulators controlling Cdks activity have a role in G1-phase remodelling. We show that p15, p21 and cyclin A1, important Cdk regulators, are involved in G1-phase lengthening during differentiation. The work presented in this thesis set the foundations for future research looking at cell cycle dynamics in live, single cells during early developmental. The work also highlights hESCs as trackable, ideal system to study changes in cell cycle dynamics during embryonic to somatic transition.

Acknowledgements

First of all, I would like to thank Silvia for welcoming in her lab 2 years ago and seeing potential in me. Never before, I had been so lucky to meet someone so enthusiastic and passionate about science. She always had her door open, ready for scientific discussion or simply a needed advice. Thank you for always pushing me to work harder and do better than the day before. I will always be grateful for the opportunity that you gave me to enter this dynamic scientific world but also a work place where I had the luck to be surrounded by amazing people.

Thanks to everyone in the Quantitative cell biology lab. Thank you to Borzo and Adrienne for always be patiently there to help and advice on scientific matters but also being there always ready for a laugh.
Alix and Rita, I sincerely do not know I would have done it without you two. You took me under your wing from day one and you have always been there ready to help in every situation in and out the lab. I wish the best for you both and I am sure you will achieve anything you set yourselves to do in the future.

I would like to also thank my thesis committee members, present and past, Dr Peter Sarkies, Dr Luis Aragon, Dr John Diffley and Dr Dominique Bonnet for the discussion and input given during these two years. I am also very thankful to have been part of two exceptional scientific communities at the MRC-LMS institute and at the Francis Crick Institute that always provide whit a stimulating scientific environment. A special thanks goes to the FACS facility in both institute that were a constant help during the development of my project and to the hESCU facility at the Crick that welcomed us offering help and advices.

To Antimo, my new family, for listening to the everyday chronicles and always been the logic voice helping me to make sense of my thoughts. No matter what happened during the day, you have always been my safe harbour at night. If this was the beginning, I know that we can deal with everything that will come in the future. E che sempre sia lodata la birretta o digestivo.

Finally, I would like to thank my family. Grazie ai miei genitori, Paola e Daniele e a mia sorella Ilaria. Se non fosse stato per voi non avrei mai scritto neanche una parola di questa tesi e non mi sarei trovata nella posizione in cui sono ora. Grazie per avermi sempre spinto nella direzione migliore soprattutto quando io stessa non riuscivo a riconoscerla e anche se mi ha portato lontano da voi. Grazie per avermi sostenuta nei momenti di difficoltà e incertezza e avermi sempre ricordato quale sia il mio valore. Qui mi fermo perché non siamo i tipi da grandi sbrodolamenti ma anche perché so bene che sappiamo sia io che voi

che ci sarebbero pagine da scrivere per descrivere tutto quello di cui vi sono grata ma questo non è il luogo.

A quelli che se ne sono andati in questi due anni, Carmela e Shanti.

Contents

Chapter 1 Introduction 20

1.1 A cell cycle overview 20

1.2 Cell Cycle of Somatic Cells 22

1.2.1 Checkpoint control and cyclins specificity 22

1.2.2 Negative control of Cdks activity by Cdks inhibitors 24

1.2.3 Control of G1- to S-phase transition in somatic cells 24

1.3 Cell Cycle Control of Embryonic Stem Cells 26

1.3.1 Control of G1- to S-phase transition in embryonic stem cells 26

1.4 Human embryonic stem cells (hESC) as a model to study cell cycle regulation .... during early development 28

1.5 New tools to study cell cycle dynamics 30

1.6 Project aims 32

Chapter 2. Methods 33

2.1 Human embryonic stem cells (hESCs) cell culture 33

2.1.1 Maintaining hESCs 33

2.1.2 Passaging hESCs 34

2.1.3 Differentiating hESCs into mesoderm precursors 34

2.1.4 Long term storage and thawing of hESCs 34

2.2 Biosensors, shRNA and establishment of stable cell lines 35

2.2.1 Lentiviral production for hESC infection 35

2.2.2 Lentiviral based infection of hES cells 35

2.2.3 Fluorescence Activating Cell Sorting (FACS) 36

2.2.4 Inducible over-expression and shRNA constructs 36

2.3 Microscopy 36

2.3.1 Imaging 36

2.3.2 Immunofluorescence (IF) 38

2.4 Data Analysis 39

2.4.1 Analysis of cell cycle dynamics 39

2.4.2 Immunofluorescence data and statistical analysis 44

2.5 Cloning and Molecular Biology 45

2.5.1 Construction of modified Fucci (SA) biosensor 45

2.5.2 Polymerase chain reaction (PCR) ... 46
2.5.3 Restriction digest of vector ... 46
2.5.4 Purification of gel bands from agarose gel ... 47
2.5.5 Gibson Isothermal Assembly based cloning ... 47
2.5.6 Transformation of E.coli Dh5α ... 48
2.5.7 Isolation of plasmid DNA ... 48
2.5.8 RT-qPCR ... 48

Chapter 3. Results ... 50

3.1 Cell cycle dynamics changes during differentiation in human embryonic stem cells (hESCs) ... 50

3.1.1 Gap phases length changes during BMP4-driven differentiation of hESCs ... 50
3.1.2 Correlation amongst different cell cycle phases during BMP4-driven differentiation of hESCs ... 56
3.1.3 Interdependency of G1-phase and G2-phases length is different in hESCs and differentiated cells ... 58

3.2 Cell cycle dynamics changes during differentiation in lineages during hESCs differentiation ... 60

3.3 G1-phase length changes during differentiation in single cells. ... 63

3.4 Cell cycle regulators might be responsible for G1-phase remodelling ... 65

3.4.1 p15 and p21 expression increases during differentiation and their overexpression induce G1-phase lengthening in hESCs ... 66
3.4.2 Cyclin A1 downregulation effects G1-phase lengthening in hESCs ... 69

Chapter 4. Discussion ... 71

4.1 Cell cycle dynamics of hESCs changes during BMP4-driven differentiation ... 71

4.2 The activity of cyclin dependent kinases might be responsible for G1-phase remodelling ... 72

4.2.1 P15 and p21 overexpression induces G1-phase lengthening ... 73
4.2.2 Cyclin A1 down-regulation induces G1-phase lengthening ... 74

4.3 G1-phase is different in somatic and hES cells ... 75

4.4 The cell cycle remodels after 3 days of BMP4 treatment, but how many cell divisions is this? ... 78

4.5 Cell cycle biosensors and live cell imaging: advantages and disadvantages ... 80

4.6 hES cells as a novel model system to study cell cycle remodelling ... 81

Chapter 5. Future perspectives and final conclusions 83

5.1 Cdk activity is key for cell cycle remodelling during hES differentiation 83

5.2 Cell fate specificity in cell cycle remodelling 83

Final Conclusions 85

References 86

List of Figures

Figure 1.1 Cell cycle structure 20
Figure 1.2 Cell cycle progression goes through three major checkpoints 22
Figure 1.3 Cyclins/Cdks complexes through cell cycle progression 23
Figure 1.4 Schematic representation of G-phase control mechanisms 25
Figure 1.5 Cell cycle profile during differentiation as measured by propidium iodide staining 27
Figure 1.6 Derivation of human embryonic cells from the blastocyst 29
Figure 2.1 Pipeline for quantitative analysis of live cell imaging experiments 37
Figure 2.2. Cell cycle dynamics measured in hESC with the biosensor PCNA-YFP, NLS-mCherry 40
Figure 2.3 Cell cycle dynamics measured in hESC with the biosensor Fucci(SA) 41
Figure 2.4. Cell cycle dynamics measured in hESC with the biosensor Fucci(CA) 42
Figure 2.5. G1-phase length measured in hESC with the biosensor Cdt1-YFP and NLS-mCherry 43
Figure 2.6 Pipeline for quantitative analysis of IF experiments 44
Figure 2.7 Schematic representation of construction of modified Fucci (SA) biosensor 45
Figure 3.1 Duration of cell cycle phases as measured by stable hES cell line expressing PCNA-YFP and NLS-mCherry biosensor and imaged every 20 minutes 52
Figure 3.2 Duration of cell cycle phases was measured with stable hES cell line expressing PCNA-YFP and NLS-mCherry biosensor and imaged every 10 minutes 53
Figure 3.3 Duration of cell cycle phases was measured with stable hES cell line expressing Fucci (CA) biosensor and imaged every 10 minutes 55
Figure 3.4 Comparison of cell cycle dynamics in hES and BP4-treated cells using PCNA-YFP and NLS-mCherry biosensor 57
Figure 3.5 Comparison of cell cycle dynamics in hES and BMP4-treated cells using Fucci(CA) biosensor 58
Figure 3.6 Interdependency between percentage of time spent in G1 and in the other cell cycle phases changes with differentiation 59
Figure 3.7 Schematic comparing graded or switch–like transition in G1-phase length during differentiation 60
Figure 3.8 Cell cycle dynamics changes during differentiation in cell lineages 61
Figure 3.9 G1-phase remodels after 2-3 divisions (F2 and F3) 62
Figure 3.10 G1-phase length increases during BMP4-driven differentiation in two different cell lines 64
Figure 3.11 G1-phase length increases during BMP4-driven differentiation in lineages 64
Figure 3.12 Volcano plots 65

Figure 3.13 p21 and p15 mRNA and protein levels increase during differentiation 67
Figure 3.14 Normalized expression of p15 and p21 in overexpressing inducible cell line expressing Cdt1-YFP and NLS-mCherry 68
Figure 3.15 Overexpression of p15 or p21 in hESCs increases G1-phase length 68
Figure 3.16 Cdt1-YFP can be used to plot G1-phase length to visualise lengthening due to overexpression of p15 and p21 in two consecutive divisions (lineages) 69
Figure 3.17 shRNA against cyclin A1 increases G1-phase length in hESCs 70
Figure 4.1 Experimental workflow used to determine the correlation between cell fate/commitment to differentiation and cell cycle in single cells 76
Figure 4.2 Correlation between cell cycle phases and commitment 77
Figure 4.3 Pipeline to study the correlation between differentiation markers expression and cell division during BMP4-driven differentiation 78
Figure 4.4 Differentiation markers are expressed after at least 2 divisions in hESC during BMP4-driven differentiation 79
Figure 5.1 Cell cycle remodels with different speeds depending on cell fate 84

List of Tables

Table 1 Summary of main differences between ES and somatic cell cycle 28

Table 2 - Commonly used reagents for hES cell culture in this thesis 33

Table 3 List of plasmids used to generate stable hESCs lines 35

Table 4 - List of antibodies used for IF 38

Table 5 - List of PCR primers used in this thesis 46

Table 6 – qPCR primers used in this thesis 49

Abbreviations

Au	Arbitrary units
BMP4	Bone Morphogenic protein 4
bp	Base pair
BrdU	5-bromo-2'deoxyuridine
BSA	Bovine serum albumin
CAK	Cdk-Activating Kinase
CDK	Cyclin dependent kinase
cDNA	Complementary DNA
CKI	Cyclin-dependent kinase inhibitor
DAPI	4',6-diamindino-2-phenylindole
dH_2O	Distilled water
DMEM	Dulbecco's modified Eagle's medium
DNA	Deoxyribonucleic acid
dNTPs	Deoxynucleotide (dNTP) solution mix
DOX	Doxycycline
EdU	5'Ethynyl-2'-deoxyuridine
eIF2α	Eukaryotic initiation factor 2 α
em	Emission wavelength
ex	Excitation wavelength
FACS	Fluorescence activated cell sorting
FUCCI	Fluorescent Ubiquitination-based Cell Cycle Indicator
GFP	Green fluorescent protein
GUSB	Glucuronidase beta
h	Hours
hES	Human embryonic stem cell
ICM	Inner Cell Mass
IdU	(5-Iodo-2'-deoxyuridine
IF	Immunofluorescence
IVF	In Vitro Fertilization
kb	Kilobase
LB	Lysogeny broth
LED	Light emitting diode

M	Mitosis
MAD	Mean absolute deviation
mCherry	monomeric red fluorescent protein
MCM-2	DNA replication licensing factor MCM2
mES	mouse embryonic stem cell
mins	minutes
mL	millilitre
mM	millimolar
MMT	Thiazolyl blue tetrazolium bromide
NEB	Nuclear envelope breakdown
NER	Nuclear envelope reformation
NLS	Nuclear localization signal
nm	nanometre
p-	phosphorylated
PAX2	paired box gene 2
PBS	phosphate buffered saline
PCR	Polymerase chain reaction
PCNA	Proliferation cell nuclear antigen
PEI	polyethylenimine
qPCR	quantitative polymerase chain reaction
r	Pearson correlation coefficient
R^2	Coefficient of determination
Rb	Retinoblastoma protein
RNA	Ribonucleic acid
rpm	Revolutions per minute
RT	Reverse transcriptase
shRNA	Short hairpin RNA
SOC	Super optimal broth
TAE	Tris-acetate-EDTA buffer
Tris	Trisaminomethane
µl	Microliter
µM	MicroMolar
µm	Micrometre
VSVG	vesicular stomatitis Indiana virus G protein

WST-1	
WT	wild type
XTT	Tetrazolium salt
YFP	Yellow fluorescent protein

Chapter 1. Introduction

1.1 A cell cycle overview

The cell cycle is the highly regulated series of events that a cell goes through during its life that leads to duplication and segregation of its DNA into two daughter cells. This process is divided into four distinct phases, chronologically: G1-phase, during which the cell grows and prepares for DNA replication; S-phase, when replication takes place; G2-phase that gives time to the repair complex to check genomic integrity and mitosis when the genomic material is segregated and the two daughter cells are born (Figure 1.1).

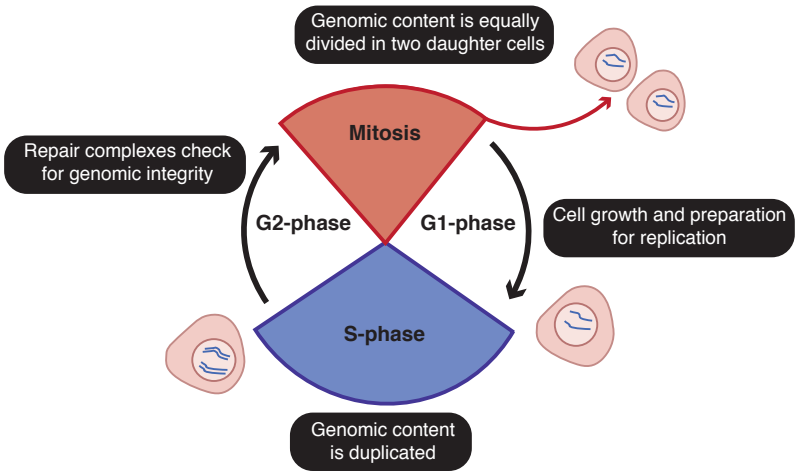


Figure 1.1 Cell cycle structure. The cell cycle is divided in four phases: G1, S, G2 and mitosis. Each phase has a specific function with the final goal of correctly segregating genomic material in two daughter cells.

The main effectors that control cell cycle processes are a family of proteins called cyclin-dependent kinases (Cdks). Cdks are serine/threonine kinases whose activity is regulated by the binding to their regulatory counterpart called cyclins that are synthesized and degraded in a timely manner during cell cycle. As a consequence, Cdks' activity display a cyclical activation dynamic that is responsible for initiation of different cell cycle events. Both Cdks and cyclins were firstly discovered almost 50 years ago in budding yeast (*Saccharomyces cerevisiae*) and fission yeast (*Schizosaccharomyces pombe*) (Hartwell, Mortimer et al. 1973, Nurse, Thuriaux et al. 1976) and although their number changes, they are conserved in all eukaryotes (Cao, Chen et al. 2014). Both *S. cerevisiae* and *S. pombe* only have a single Cdk (Cdc28 and Cdc2 respectively) which controls the whole cell cycle progression, while mammalian cells possess many different Cdk-cyclin complexes that each contribute to the progression through different cell cycle phases (Santamaria, Barriere et al. 2007, Malumbres and Barbacid 2009).

Cell cycle progression is controlled by different mechanisms that ensure faithful transmission of genetic information from generation to generation. These restrictive control mechanisms are fundamental to keep the four cell cycle phases in the correct temporal order to ensure that chromosomal DNA is correctly replicated and then distributed equally to each daughter cell. These sophisticated control mechanisms couple extracellular signals to the cell cycle machinery and have strategically placed restriction points safeguarding genomic integrity, as well as forward direction of cell cycle progression. These signals provide positive or negative growth control cues and their absence drives proliferation, cells arrest in G1 and quiescence or differentiation. Some of the mechanisms involved in regulation of cell cycle progression are:

- Checkpoint control – external and internal signals are incorporated by the cells to ensure that one phase only starts after full and correct completion of the previous one (Hartwell and Weinert 1989, Barnum and O'Connell 2014);
- Cyclical expression of cyclins – during the cell cycle, cyclins are expressed, degraded and form complexes with Cdks in a cyclical manner controlling the progression through the different cell cycle phases (Murray and Kirschner 1989, Nurse 1994);
- Levels of Cdk activity – during the cell cycle, Cdk activity increases, triggering different cell cycle phases. Early cell cycle events will be triggered by low levels of Cdk activity, while late events will be triggered by higher levels of Cdk activity (Swaffer, Jones et al. 2016);
- Cdk inhibitor activity – Cdk inhibitors integrate external stimuli and interact with cyclin-Cdk complexes to inhibit their activity (Besson, Dowdy et al. 2008).

Although the proteins that regulate cell division are fundamentally the same, the dynamics of cell cycle varies extensively throughout different species and even tissues in the same organism. Differences in cell cycle length can be seen within human cell types, for example a typical rapidly proliferating human cell has a total cycle time of 24 hours in which the phases have an approximate duration of ~11 hours for G1-phase, ~8 hours for S-phase, ~4 hours for G2 and ~1 hour for mitosis where G1-phase length accounts for most of the variability in cell cycle duration.

Dissimilarly human embryonic stem cells (hESCs) show a very different cell cycle profile with a cell cycle length of approximately 16 hours. These cells undergo rapid cell/nuclear divisions alternating rounds of M phase and interphase without fully formed gap phases in which a high proportion of time (approximately 65 %) is devoted to S phase (Becker, Ghule et al. 2006). Later, as the cells transition through the embryonic development, the cell cycle acquires two identifiable gap phases (White and Dalton 2005).

The difference in cell cycle dynamics between somatic and embryonic cells have been studied in many different mammalian cell types. For example, murine ES cells has been estimated to have a cell cycle duration of about 8-10 h (Stead, White et al. 2002) and 15h for the rhesus monkey ES cells (Fluckiger, Marcy et al. 2006). It is believed that the temporal difference between embryonic and somatic cell cycles in mammalian cell resides in different dynamics of gap phases.

1.2 Cell Cycle of Somatic Cells

Somatic cell divisions are long and asynchronous with long G1 and G2 phases. During the cell cycle, cells monitor the environment that provides positive or negative cues like growth factors and nutrients as well as evaluate the integrity of their genome. In the absence of signals that drive proliferation, cells arrest in G1 and quiescence or they may undergo apoptosis.

1.2.1 Checkpoint control and cyclin specificity

To keep cell cycle events in the correct order and timely it is fundamental that the cell has a control system that tightly controls the progression through the cell cycle (Figure 1.2). A series of biochemical switches of which the central components are Cdks, lead the cell through the three major regulatory checkpoints: G1/S checkpoint, G2 checkpoint and the spindle checkpoint. These checkpoints control cell cycle progression and ensure that one phase does not begin until full completion of the previous one.

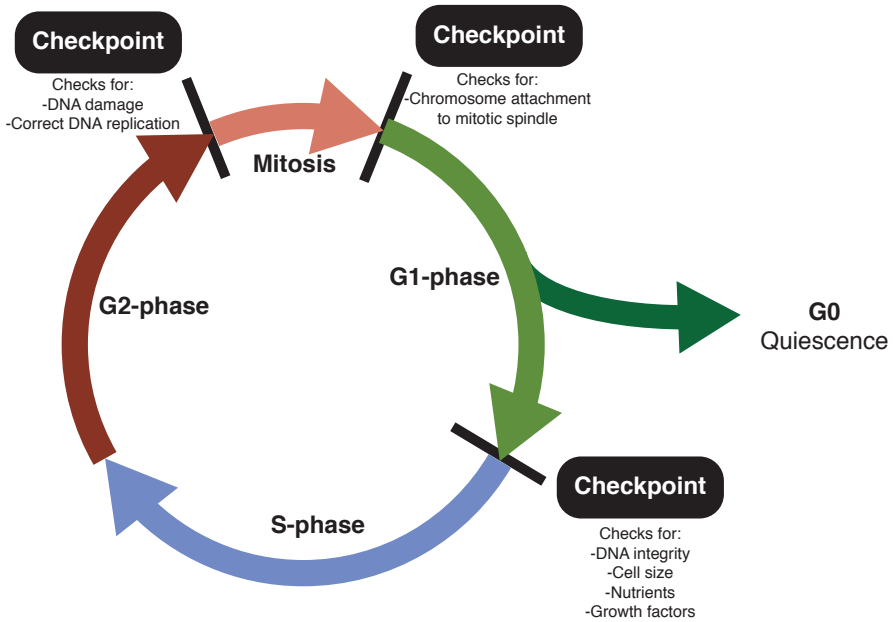


Figure 1.2 Cell cycle progression goes through three major checkpoints. Cell cycle checkpoints are fundamental to ensure an orderly and timely progression of the cell cycle. During G1-phase the cell controls if the environment is favourable and the cell has the correct size and correct amount of DNA; in G2-phase the cells check for completed replication and integrity of DNA; during mitosis the cells verify the correct assemble of chromosomes on the mitotic spindle.

Cyclin-dependent kinases (Cdks) go through changes in their enzymatic activities in cyclical activation and inactivation phases (Figure 1.3). Their catalytic functions are tightly regulated to ensure that downstream substrates are activated or inhibited at precise times during the cell cycle. If uncontrolled, Cdk activity can lead to catastrophic events on cell cycle progression affecting genomic integrity and growth control. The activation of Cdks is dependent on the assembly of Cdks with its cyclin partner. In fact, Cdk expression levels remain constant throughout the cell cycle while cyclins levels oscillate. Cyclins have an unstable nature and they are synthesised and degraded at precise times during the cell cycle, so they can be divided in four classes based on the timing of their expression and their function in the cell cycle: G1 cyclins, G1/S cyclins, S cyclins and M cyclins. Their levels are regulated both at a transcriptional level and at the level of protein stability. The oscillatory regulation of cyclin levels generates waves of Cdk activity (Nigg 1995, Gerard and Goldbeter 2009) that is triggered by the binding and allows a series of conformational changes to adopt the catalytic active form (Jeffrey, Russo et al. 1995), which involves phosphorylation-dependent conformational changes to the Cdk catalytic subunit. The progression through each phase of the cell cycle requires the activation of at least one phase-specific Cdk complex. Each cyclin-Cdk complex promotes the activation of the next complex in the sequence ensuring that the cycle progresses in an ordered fashion (Figure 1.3).

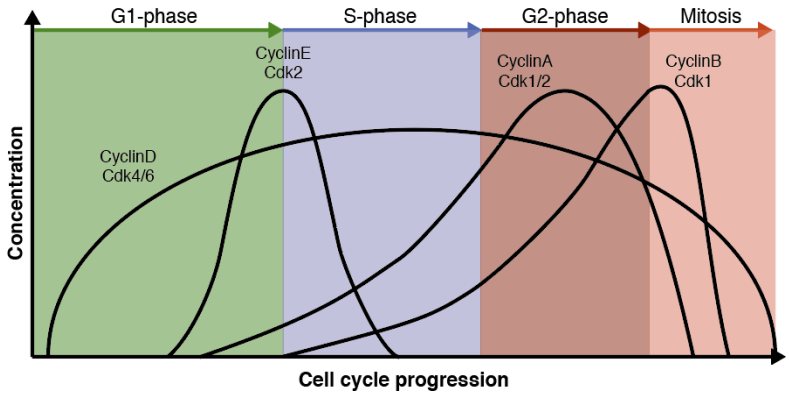


Figure 1.3 Cyclins/Cdks complexes through cell cycle progression. Cyclins are differentially expressed during the cell cycle. They form active complexes with specific cyclin dependent kinases (Cdks) that drive the different cell cycle phase. Early G1-phase is driven by cyclin D/Cdk4/6 complex; late G1-phase and S-phase beginning are regulated by the cyclin E/Cdk2 complex; cyclin A/Cdk2 and cyclin A/Cdk1are responsible for S-phase termination; start of mitosis is regulated by cyclin B/Cdk1.

Cyclin binding alone is, however, not sufficient to fully activate Cdks, which requires also the phosphorylation of a threonine residue adjacent to the kinase active site (T150). This phosphorylation is catalysed by Cdk-activating kinases (CAKs) that show a constant high level of activity throughout the cell cycle and don't seem to be regulated by any known pathway. Whereas the activating phosphorylation of Cdks is not regulated, two inhibitory phosphorylations on Tyr 15 and Thr 14 have important functions in the regulation of Cdk activity. The phosphorylation state of these two sites depends on the balance

between kinase and phosphatase activities. The two main enzymes involved in this balance are Wee1 and Cdc25.

1.2.2 Negative control of Cdk activity by Cdk inhibitors

The final mechanism that the cells use to control Cdk activity is provided by Cdk inhibitors (CdkIs), which can be upregulated in response to diverse physiological cues such as growth factors, cytokines, cell–cell contact, cell-extracellular matrix interactions or, in response to DNA damage, cell senescence, and differentiation. These enzymes can be divided in two groups based on their structure and mechanism of Cdk inhibition: Cip/Kip family and INK4 family. The Cip/Kip family whose members can control different cyclin-Cdks complexes by interacting with both subunits is comprised of: $p21^{Cip1}$, $p27^{Kip1}$ and $p57^{Kip2}$. These proteins can block the cell-cycle progression by inhibiting G1/S and S Cdks. The INK4 family display a specificity for Cdk4 and Cdk6 where they act by reducing cyclin binding affinity and consist of: $p15^{Ink4B}$, $p16^{Ink4A}$, $p18^{Ink4C}$, $p19^{Ink4D}$ (Nakayama and Nakayama 1998). In general, CdkIs provide an effective means of arresting cell division by binding to and inhibiting Cdk-cyclin complexes by steric inhibition, blocking access to substrates or ATP and, by destabilization of Cdk-cyclin interactions.

Control of Cdk activity is key to proper functioning of cell division and as described, this control involves many players that together ensure the correct functioning of the cell cycle machinery. Interestingly in simple eukaryotic organisms such as fission yeast, Cdk1 has been shown to be sufficient to drive the full cell cycle (Coudreuse and Nurse 2010). On the other hand, multiple Cdks and cyclins are involved in cell cycle regulation in mammalian cells (Malumbres and Barbacid 2009, Satyanarayana and Kaldis 2009).

1.2.3 Control of the G1- to S-phase transition in somatic cells

As previously described, in mammalian cells, cell division is divided in four phases and the progression through these phases is highly regulated in particular at the transition points. These checkpoints can be divided in two types of checkpoint: the first one includes cell-intrinsic checkpoints (G1/S checkpoint, G2/M checkpoint and M phase checkpoint) that depends on intrinsic signals, for example, the integrity of the genome; secondly there is cell-extrinsic checkpoint that depends on mitogenic signals, such as growth factors, and control the passage from early G1 to late G1 (Mailand, Falck et al. 2000) (Figure 1.4). This last checkpoint is also known as Restriction point (R point) and it is when the cell makes the decision to undergo a new round of replication and enter S phase or switch to quiescent state (G0). This transition from early G1 to late G1 is mainly regulated by the complex formed by cyclin D and Cdk 4/6. Cyclin D starts to be expressed in early G1-phase and contrary to the other cyclins does not oscillate. Instead its levels rise in response to mitogenic signals (Lukas, Bartkova et al. 1996) and forms an activity complex

in conjunction with Cdk4/6. This complex has the main function of inactivating the Retinoblastoma tumor suppressor protein (Rb) (Sherr and McCormick 2002) that leads to the expression of cyclin E (Lukas, Herzinger et al. 1997). In early G1 phase, the retinoblastoma tumor suppressor (Rb) binds and inhibits transcription factor E2F responsible for the transcription of S-phase promoting genes. After hyper-phosphorylation by the activity of cyclinD-Cdk4/Cdk6 complexes and upon reaching a threshold level of cyclin E-Cdk2 activity in mid-to-late G1, Rb becomes fully inactivated. The inactivation of Rb allows the activation of the transcription factors E2F that are responsible for upregulating the expression of genes required for the G1 to S phase transition such as cyclin E or Cdc25A and that are involved in DNA replication. The expression cyclin E and Cdc25A results in the formation and activation of cyclin E-Cdk2 complexes that drive the G1-S transition and regulate S- and G2-phase events activating the replication machinery (Bertoli, Skotheim et al. 2013). This step is fundamental for the DNA damage response and the start of the DNA synthesis S-phase.

Contrasting the effects of these forward pathways and Cdks activity, cyclins-Cdks complexes are subjected to another level of control that involves Cdks inhibitors. Ink4 family members can inhibit cyclin D-Cdk4 and cyclin D-Cdk6 complexes and other members of the Cip/Kip family (p21, p27, p57) are direct inhibitors of the cyclinE-Cdk2 complexes.

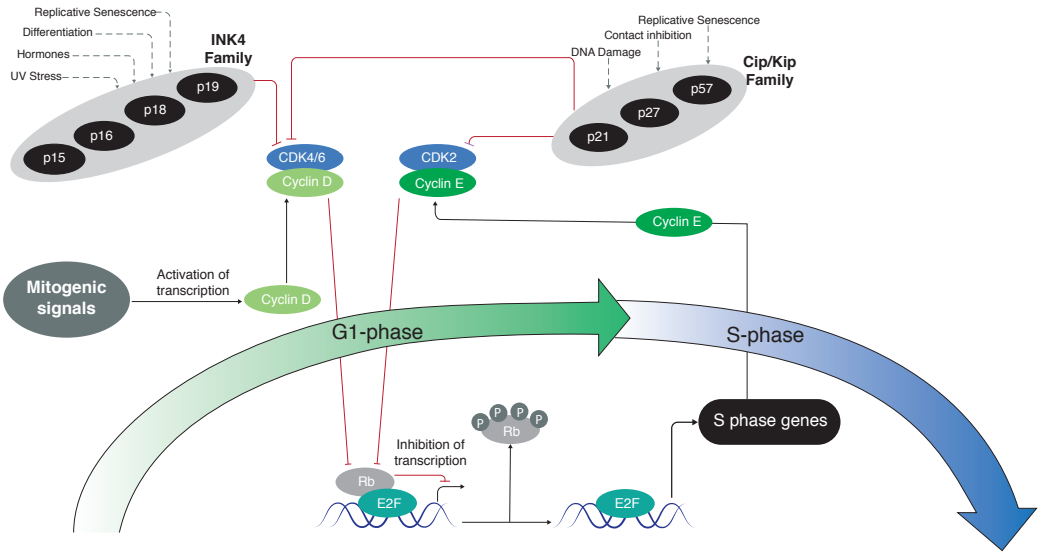


Figure 1.4 Schematic representation of G-phase control mechanisms. Simple diagram showing a simplified G1-phase regulatory network.

1.3 Cell Cycle Control of Embryonic Stem Cells

An exception to the cell cycle structure described so far is represented by pluripotent stem cells. These cells are less reliant on exogenous growth factors, are not subject to contact inhibition and do not undergo quiescence on growth factor withdrawal (Savatier, Lapillonne et al. 1996, Schratt, Weinhold et al. 2001). Pluripotent cells of early embryos undergo rapid cell divisions alternating rounds of M phase and interphase without fully formed gap phases and in which a high proportion of time, approximately 60 %, is devoted to S phase (Artus, Babinet et al. 2006, Fluckiger, Marcy et al. 2006). Mammalian embryonic stem (ES) cells divide with a short generation time compared to the one observed for somatic cells. For example, the cell cycle duration of murine ES cells has been estimated to be around 8-10 h (Stead, White et al. 2002), 15h for the rhesus monkey ES cells (Fluckiger, Marcy et al. 2006) and 8-16h in human ES cells (Becker, Ghule et al. 2006). A few studies have shown that the cell cycle regulating cyclins D1, D2 and D3 are increased in G1 and cyclin D2, A, E are increased in G2 compared with somatic cells (Fujii-Yamamoto, Kim et al. 2005). Moreover, all the Cdks appear to be in their active complexes with their cyclin regulatory partners (Stead, White et al. 2002). This evidence contrasts with the control of cell cycle regulation in somatic cells. While knowledge of the differences between the embryonic and the somatic division cycles has relied on research with model organisms (frog eggs, mouse, fruit fly and zebrafish embryos), mammalian cell lines and yeast cells a lot less is known between cell cycles of embryonic cells and their differentiated counterparts.

1.3.1 Control of G1- to S-phase transition in embryonic stem cells

The temporal difference between embryonic and somatic cell cycle seems to reside in gap phases' dynamics (Table 1). Both murine and human ES cells have cell division cycles lacking fully formed G1 and G2 phases and cells spend approximately 65% of the cell cycle duration in S phase (Becker, Ghule et al. 2006). As cells transition through embryonic development, the cell cycle acquires longer gap phases (Figure 1.5). With differentiation, cells accumulate in G1 phase and cell cycle length increases over 16 hours, as seen in somatic cells (White and Dalton 2005). Recent studies have also solidified the idea that a short cell cycle and in particular a short G1 is necessary for maintaining ES cell pluripotency (Julian, Carpenedo et al. 2016).

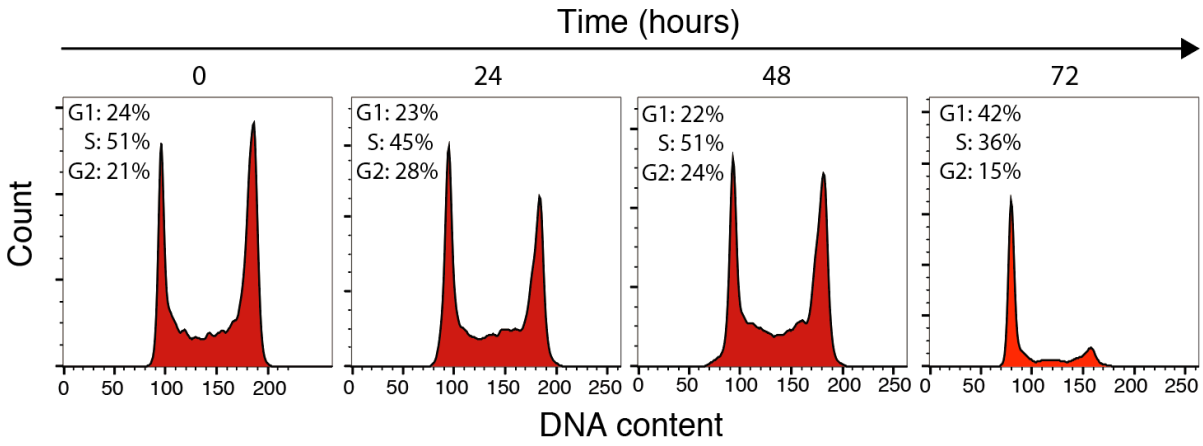


Figure 1.5 Cell cycle profile during differentiation as measured by propidium iodide staining

Studies conducted in mESCs suggested Cdk2 activity (that is high and precociously expressed in these cells), to be responsible for the rapid cell cycle progression (Koledova, Kramer et al. 2010). The periodic activity of this kinase in its active complex with cyclin E, typical of a somatic cell, is lost in embryonic stem cells which have a cyclin E/Cdk2 activity independent of cell-cycle phase. Consequently, Cdk2 suppresses the Rb family members, leaving the transcription of E2F dependent genes constitutively active during the cell cycle. The absence of cell cycle regulated Cdk2 activity can be partially explained by persistent levels of its two regulatory subunits, cyclin E and cyclin A. High levels of these two cyclins are restricted to specific stages in the cell cycle of somatic cells. On the contrary, Cyclin A and Cyclin E cyclical expression is lost in embryonic stem cells. Besides the constitutive activation of the Cyclin E-Cdk2 complex, a shortened G1 phase is also attributed to weak expression of CDK inhibitory proteins of the INK and Cip/Kip families (Savatier, Lapillonne et al. 1996, Ballabeni, Park et al. 2011). A short G1-phase of ES cells is therefore the result of lack of checkpoint control due to the downregulation of cell cycle brakes such as Rb and Cdks inhibitors and the up-regulation of cell cycle drivers such as cyclins and Cdks (Koledova, Kramer et al. 2010, Kapinas, Grandy et al. 2013).

In the early stages of differentiation, cells start to lose pluripotency genes and the cell cycle starts to remodel with the establishment of a fully formed G1 phase and activation of R-point control occurs as part of the developmental program (White and Dalton 2005). This coincides with the switch of cell cycle-control mechanisms from having a constantly high level of Cdks activity to a cell cycle-regulated Cdks activity. As ES cells differentiate, Cdk4/Cdk6-Cyclin D and Cdk2-Cyclin E activity become cell cycle-regulated and responsive to external signals, leading to G1 phase lengthening. In differentiated cells, Cdk activity is inhibited during G1 due to degradation of cyclins and the presence of inhibitor proteins, like p21 and p15. Changes in cyclin transcription, cyclin stability, and CdkI levels are all likely to be factors that contribute to this switch in cell cycle control. It has also been hypothesized that a rapid progression through G1 phase is important to minimize potential exposure to differentiation signals and maintain

the self-renewing state (Julian, Carpenedo et al. 2016) even though this mechanism is not yet fully understood.

G1-phase control in ES cells has been studied extensively using fixed cells at a population level and paradoxically the molecular mechanisms which lead to lengthening of G1-phase are still poorly understood. Moreover, most of the knowledge currently available on the topic has been acquired using mouse ES cells. The aim of this thesis was to investigate to follow individual human ES cells by live cell imaging to see how and when the cell cycle remodels during differentiation at a single cell level.

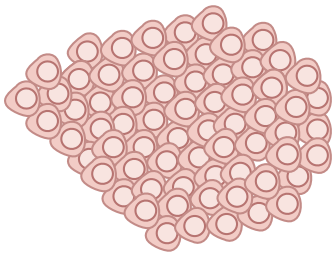
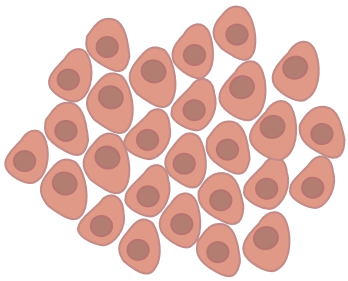
Embryonic stem cells	Somatic cells
	
• Cyclins do not show cyclical expression	• Cyclins have a cyclical expression
• All Cdks are in active complexes with their cyclin partner	• Cdks are in active complexes with their cyclin partner in a cyclical manner
• Low levels of CDK inhibitors	• Higher levels of CDK inhibitors
• No check-point control regulating G1- to S-phase transition	• Check-point control regulate G1- to S-phase transition
• Do not rely on external stimuli to progress through G1-phase	• Respond to external stimuli like mitogenic signals and differentiation cues

Table 1 Summary of main differences between ES and somatic cell cycle

1.4 Human embryonic stem cells (hESC) as a model to study cell cycle regulation during early development

For more than 40 years, pluripotent cells from the murine embryonic epiblast during late pre-implantation and early post-implantation stages of development have been used to study cell cycle and its molecular mechanisms (Solter, Skreb et al. 1971, Snow and Bennett 1978). Notably, the study of these cells *in vivo* with direct biochemical and molecular characterization methods are not generally feasible due to difficulties in obtaining sufficient cell numbers. To circumvent this problem, murine and human embryonic stem cells have since then been used extensively as an *in vitro* model to study specific aspects of early embryonic development (Pedersen 1994) to represent the inner cell mass (ICM) of preimplantation stage blastocysts (Lake, Rathjen et al. 2000).

Human embryonic stem cells (hESCs) have been originated from the ICM of a blastocyst stage pre-implantation embryo, donated after *in vitro* fertilisation (IVF) treatment in 1998. The essential characteristics of ES cells include: derivation from the preimplantation or preimplantation embryo; prolonged undifferentiated proliferation, and stable developmental potential to form derivatives of all three embryonic germ layers even after prolonged culture (Thomson, Itskovitz-Eldor et al. 1998). These cells can remain in a proliferative condition and maintain their two main characteristics, pluripotency and self-renewal ability, thanks to a unique transcriptional profile. After the derivation of these cells, specific protocols have been developed to reproduce the differentiation processes for the three germ line lineages, demonstrated by their capacity of teratomas formation in mice (Thomson, Itskovitz-Eldor et al. 1998).

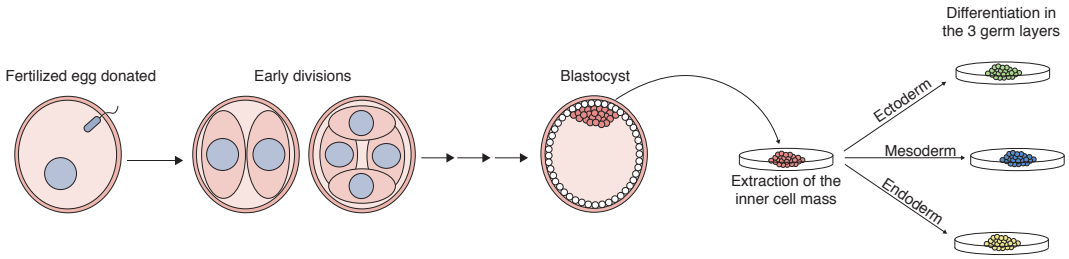


Figure 1.6 Derivation of human embryonic cells from the blastocyst. Fertilized eggs donated after IVF treatments were cultured in vitro until the formation of the pre-implantation blastocyst. At this stage, the inner cell mass (ICM) was extracted and cultured *in vitro*. These cells are the basis of hES cell lines and can be kept in culture and self-renew indefinitely. Different differentiation protocols have been developed in the years allowing to differentiate these cells in the 3 germ layers: ectoderm, mesoderm and endoderm.

The derivation of hES cells has opened new doors to study both early developmental process and cell cycle regulation in these cells. They offer many advantages such as:

- They grow in 2D culture allowing tracking of single cells
- Protocols are available to differentiate towards the 3 germ layers and require from 3 to 5 days.
- They are easy to manipulate
- They are an important model to study human development and diseases.

For the studies conducted in this thesis, bone morphogenetic protein 4 (BMP4) was used in combination with fibroblast growth factor (FGF) to induce mesoderm differentiation in hESCs (Yu, Pan et al. 2011).

1.5 New tools to study cell cycle dynamics

Cell cycle studies started in the 70's and allowed a deep understanding of this fundamental process during the last 50 years. Although knowledge of the cell cycle has grown immensely, the techniques used in the field have not evolved at the same pace. Cell cycle assays were mainly focused on specific cell cycle phases and looked at cell cycle at population level, missing a more direct and quantitative approach with single cell resolution. In general, these methods can be classified as based on: DNA synthesis (IdU, EdU and BrdU), cellular metabolism (MMT, XIT and WST-1) and proliferation protein (PCNA, Ki67 and MCM-2). These methods involve invasive steps and cell manipulation that interfere with the natural physiology and temporal dynamics of cell cycle. Moreover, these approaches provide either a snapshot of the cell cycle or an average for a cell population, losing information about dynamics and variability between cells within the population.

In order to further the studies on cell cycle dynamics employing less invasive methodologies, new tools, called biosensors, have been developed in the last 15 years employing fluorescence cell cycle phase reporters. The rationale behind the creation of these tools was to exploit the expression dynamics of certain cell cycle proteins that were tagged with a fluorophore in order to be used as a probe for different cell cycle phases. In 2000, PCNA was fused for the first time with GFP and used to study the dynamics of DNA factories in live cells (Leonhardt, Rahn et al. 2000). This protein is a fundamental member of the replication machinery (Bravo, Frank et al. 1987, Prelich, Tan et al. 1987) and it is loaded on the DNA during S-phase showing as nuclear speckles. Recently, mRuby-PCNA has been used in live cell imaging experiments as an all-in-one cell cycle reporter allowing for cell cycle analysis, cell tracking and classification (Zielke, Korzelius et al. 2014).

In 2008, the FUCCI (Fluorescent Ubiquitination-based Cell Cycle Indicator) biosensor, one of the most important technologies in the field was published by Sakaue-Sawano and colleagues. This biosensor harnesses the oscillatory properties of two proteins, Cdt1 and Geminin involved in the DNA replication control machinery (Nishitani, Lygerou et al. 2000), whose protein levels oscillate inversely during the cell cycle (Sakaue-Sawano, Kurokawa et al. 2008). The biosensor is comprised of two plasmids encoding a truncated Geminin (1-110) tagged with mAG (monomeric Azami-Green) and truncated Cdt1 (30-120) tagged with mKO2 (monomeric Kusabira-Orange). Both proteins are truncated in order to minimize the effect of over-expressing these proteins in the cells. Geminin levels peak during G2-, S- and M-phase while Cdt1 levels are high in G1-phase (Shiomi, Suenaga et al. 2014). After the original Fucci system was published, some modifications to its design were performed by different groups. Fucci reporters based on other organism versions of Cdt1 and Geminin were created for zebrafish, mouse and fly (Sugiyama, Sakaue-Sawano et al. 2009, Abe, Sakaue-Sawano et al. 2013, Zielke, Korzelius et al. 2014). However, both

the original and the following modification of the FUCCI system allowed to distinguish only G1-phase from the rest of cell cycle. In 2016 and 2017, two new FUCCI biosensors were published: FUCCI 4 (Bajar, Lam et al. 2016) and FUCCI (CA) (Sakaue-Sawano, Yo et al. 2017). The FUCCI 4 system was the first sensor employing four different cell cycle proteins tagged with four different fluorescent probes that enabled to observe the four cell cycle phases at the same time in a single snapshot of a population. The FUCCI (CA) biosensor employs the same proteins of the original FUCCI with the distinction of the Cdt1 fragment in the FUCCI (CA) is Cdt1(1-110) (Sakaue-Sawano, Yo et al. 2017). This fragment has a different degradation dynamics and labels G1-phase but also G2-phase and mitosis. This modification allows to distinguish all four cell cycle phases (for more details see methods section in Chapter 2).

These new tools, combined with advances in microscopy and image analysis, allow studying quantitatively cell cycle dynamics in single cells during multiple division cycles and have revolutionized the way experiments can be performed.

1.6 Project aims

The work reported in this thesis aimed to investigate how the cell cycle remodels hESC during differentiation. Specifically, when and how cell cycle changes occur in individual cells during the process of differentiation. Live cell imaging techniques and cell cycle biosensors were employed to quantitatively characterise cell cycle dynamics in hESCs and specifically G1-phase remodelling during differentiation. BMP4-driven differentiation was used in this work to differentiate hESCs towards the mesoderm lineage.

Specific project aims:

- Establish methodologies to monitor and quantitatively measure changes in cell cycle dynamics during hESC differentiation.

- Characterise quantitatively cell cycle remodelling during BMP4-driven differentiation of hESC in single cells.

- Understand when G1-phase changes with differentiation and how it changes (whether it is a graded or switch-like transition).

- Test whether key cell cycle regulators highlighted in previous studies from the lab (p15, p21, Cyclin A1) affect G1-phase length and its dynamics.

Chapter 2. Methods

2.1 Human embryonic stem cells (hESCs) cell culture

All experiments in this thesis were performed using H1 and H9 (hESC) cell lines. Both cell lines were derived from cleavage stage human embryos obtained by in vitro fertilization (IVF) for clinical purposes and then donated to scientific research (Thomson, Itskovitz-Eldor et al. 1998). H1 and H9 cell lines were derived from two different embryos, H1 had a normal XY karyotype and H9 had a normal XX karyotype. Since 1998, these cells have been a fundamental object of research and have been used in hundreds of published experimental works (Guhr, Kurtz et al. 2006).

Table 2 - Commonly used reagents for hES cell culture in this thesis

Reagent or Resource Cells	Source	Cat.no
H1, H9 wild-type hES	WiCell	WA01, WA09
293T packaging cells	Sigma	12022001-1VL
Inhibitors and Recombinant proteins		
BMP4	ThermoFisher (Life technologies)	PHC9534
Rock inhibitor (Y-27632)	Stem Cell Technologies	129830-38-2
Polybrene	Millipore Ltd	TR-1003-G
Polyethylenamine (PEI)	Sigma	764965-1G
Doxycycline	Sigma	D9891
Puromycin	ThermoFisher (Life technologies)	A1113803
Media and Buffers		
mTeSR1	Stem Cell Technologies	85870
TeSR-E5	Stem Cell Technologies	5916
DMEM:F12	ThermoFisher (Life technologies)	11320033
OptiMEM	ThermoFisher (Life technologies)	51985026
mFRESR	Stem Cell Technologies	5855
PBS	Sigma	D8537-6X500ML
Gentle dissosiaciton buffer	Stem Cell Technologies	7174
Matrigel	Corning	354230

2.1.1 Maintaining hESCs

Both cell lines (H1 and H9) were cultured at 37°C and 5% CO2 in feeder-free conditions on Matrigel (Corning)-coated plates (usually 6-wells plates). Plates were prepared diluting Matrigel in DMEM:F12 medium to a final concentration of 100μg/ml. Appropriate amount of solution (depending on well size) was added to each well and left to set for 1 hour at room temperature prior to platting cells. Ready-to-use plates were kept at 4°C for a maximum of 2 weeks.

2.1.2 Passaging hESCs

Cells were fed daily using mTeSR1 (StemCell Technologies), split 1:2 or 1:3 every 3-4 days and routinely tested for mycoplasma. Confluent cultures (80%-90% confluency) were washed with PBS and incubated with Gentle Dissociation Buffer (StemCell Technologies) for 3 minutes at room temperature. Dissociation buffer was aspirated and fresh mTeSR1 medium was added to the cells. Cell lifters were used to gently detach the cells that were then placed in a new well.

2.1.3 Differentiating hESCs into mesoderm precursors

Growth factor bone morphogenic protein 4 (BMP4) was routinely added (every 24 hours) at a concentration of 50ng/mL to the media to drive differentiation towards the mesoderm lineage (Xu et al., 2002).

2.1.4 Long term storage and thawing of hESCs

In order to freeze stock cells, hES cells were stored in liquid nitrogen tanks at -160°C. Cells were washed twice with PBS and then 1mL of mTeSR1 per well was added. Using cell lifters, the colonies were gently broken down in small fragments, dislodged from the plate and transferred to a 15mL tube. The suspension was centrifuged at 1000 rpm for 5 minutes and the pellet was re-suspended in 1 mL of cold mFreSR (StemCell Technologies) added drop-wise. The mixture was promptly transferred to a cryotube and stored into a fresh isopropanol-containing freezing box. The box was kept at -80°C for a maximum of 24 hours after which cryotubes were moved to a liquid nitrogen tank for long term storage.

To thaw hESC, a frozen cryotube was placed into 37°C water bath for 1-2 minutes after which its content was transferred to a 15mL tube and 2mL of mTeSR1 was added drop-wise. Cells were centrifuged at 1000 rpm for 5 minutes and the pellet was gently re-suspended in 1mL of mTeSR1 and plated in a Matrigel-coated plate. ROCK inhibitor (Sigma Y-27632) [10μM] was added in the media at the same time of plating to help adhesion and left for a maximum of 24 hours.

2.2 Biosensors, shRNA and establishment of stable cell lines

Stable cell lines expressing cell cycle biosensors, shRNA for down-regulation of cell cycle genes or construct for overexpressing cell cycle regulators differentiation were obtained employing lentiviral infection and used to monitor cell cycle dynamics.

Table 3 List of plasmids used to generate stable hESCs lines

Plasmid Name	Backbone	Gene of interest	Fluorophore	Source	Scheme
NLS-FKBP-mCherry	pCSII-EF1α	NLS	mCherry	QCB lab	
hCdt1-YFP	pCSII-EF1α	hCdt1 (aa 30-120)	YFP	QCB lab	
hGMNN-mCherry	pCSII-EF1α	hGMNN (aa 1-100)	mCherry	QCB lab	
PCNA-YFP	pCSII-EF1α	PCNA	YFP	QCB lab	
Modified Fucci (SA)	pCSII-EF1α	hCdt1 (aa 30-120) & hGMNN (aa 1-100)	mCherry & YFP	This thesis	
Fucci (CA) 15446	pCSII-EF1α	hCdt1 (aa1-1-100) & hGMNN (aa 1-100)	mCherry & mVenus	Sakaue-Sawano et al., 2017	
Inducible Over-expression p15	pLvX	Over-expression p15	None	QCB lab	
Inducible Over-expression p21	pLvX	Over-expression p21	None	QCB lab	
Inducible shCyclin A1	pRRL	shCyclin A1	GFP	QCB lab	

2.2.1 Lentiviral production for hESC infection

Lentiviral production was performed using HEK 293T cells. Cells were seeded at ~50% confluency in medium composed of DMEM (Gibco) and 10% FBS (Gibco). Media was switched to mTeSR1 one day after plating. For lentivirus production, lentivirus assembly vectors (PAX2 and VSV-G), expression vector of interest (Table 3) and Polyethyleninmine (PEI) were mixed in Optimem and incubated for 15 minutes at room temperature as follows: [PEI (µg) : DNA/PAX2/VSV-G (µg) ratio 3:1; DNA : PAX2 : VSV-G ratio 5:2:1].

The mixture was added to HEK 293T cells in mTeSR1 media and cells were left to incubate for 48 hours. Virus-containing media was collected twice, 48 and 72 hours after transfection, where virus titre was shown to be the highest. The virus-containing media was collected and spinned down at 2500rpm for 5 minutes to remove any trace of HEK 293T cells. The supernatant containing viral particles was aliquoted in 1 mL vials, placed in dry ice and stored at -80°C or added directly to cells.

2.2.2 Lentiviral based infection of hES cells

H1 and H9 cells were infected overnight using 12 µg of polybrene per mL of virus-containing media for 12 hours. The morning after infection, cells were fed with fresh media. Infected cells with constructs

containing puromycin selection cassette were selected by adding puromycin [1μg/mL] to mTeSR1 media. Otherwise, cells were sorted using Becton Dickinson FACS Aria III Influx machine (The Francis Crick FACS Facility) by low to medium expression levels of desirable reporters to prevent potential effects of overexpression.

2.2.3 Fluorescence Activating Cell Sorting (FACS)

Cells were prepared for FACS starting with a PBS wash followed by incubation with gentle dissociation buffer for 10 minutes at 37°C. Buffer was carefully removed and PBS was added to cells and the mixture was centrifuged at 1000 rpm for 5 minutes. The pellet was re-suspended in a solution of PBS + 1% BSA at room temperature and the cell containing suspension was filtered using a 70μm cell strainer. After FACS, cells were centrifuged at 1000rpm for 5 minutes and the pellet re-suspended in fresh mTeSR1 media. ROCK inhibitor (10μM) was added to the media to help attachment for a maximum of 24 hours.

2.2.4 Inducible over-expression and shRNA constructs

The inducible over-expression constructs for the cell cycle regulators p15, p21 were embedded in the pLvX-TetONE-Puro vector using Gibson Isothermal assembly technique (See 2.5.5). The shRNA construct used to down-regulate CyclinA1 levels was obtained from the predictive algorithm provided by Zuber's lab (pRRL genome top prediction) (Fellmann, Hoffmann et al. 2013). Specific ultramers for Cyclin A1 were ordered from Sigma-Aldrich and the lentiviral vector was constructed in the pRRL backbone. The ultramers showing higher levels of downregulation, as measured by qPCR, were used for the experiments described in this thesis.
All constructs were transfected into HEK 293T cells for lentivirus production and used to infect hES cells. Transduced cells were selected with puromycin (1μg/mL). Doxycycline (1μg/mL) was added to cells in order to induce expression of inducible constructs one day prior to the start of the experiment. To verify overexpression or down-regulation of genes of interest, RT-qPCR was performed (see 2.5.8). pLvX empty vector and shEmpty vector were used as negative controls for the experiments.

2.3 Microscopy

2.3.1 Imaging

Imaging was performed using two different microscopes: the ScanR, a fully motorized and automated inverted epifluorescence microscope system IX83 (Olympus) combined with the CellVivo (Olympus) or

the IncuCyte Zoom® (Essen Bioscience). Temperature, humidity and CO2 levels were controlled to insure cell viability.

Typically, ScanR images were acquired using a 20x plan (UCPLFLN) fluorescence objective (NA 0.7) and a sCMOS (Orca Flash 4.0, Hamamatsu) camera. LED-based illumination (SpectraX LED, Lumenco) was used for excitation. Excitation (ex) and emission (em) filters were as follows: DAPI [ex:391/20nm, em:440/521/607/700]; YFP [ex:509/22nm, em:515-560nm]; mCherry [ex:554/23nm, em:440/521/607/700nm]; Alexa-647 [ex:650/13nm, em:690/50nm].

Incucyte Zoom images were acquired with a 20x plan fluorescence objectives and a CCD camera. Fluorescence excitation (ex) and emission (em) were as follows: Green channel [ex:440-480, em:504-544]; Red channel [ex:565-605nm, em:625-705nm].

Live cell imaging experiments started at day 0 by plating the cells at various confluences in 96-well plates (Greiner Bio-OneLtd) or 96-well Incucyte ImageLock plates. Cells were let attaching overnight and imaging was started the following morning (to avoid induced synchronicity due to splitting). A typical experiment to follow cell cycle dynamics would monitor cells for 36 to 120 hours with images taken every 10 or 20 minutes (Figure 2.1). In specific experiments, after live cell imaging, cells were fixed and stained with antibodies for immunofluorescence (IF).

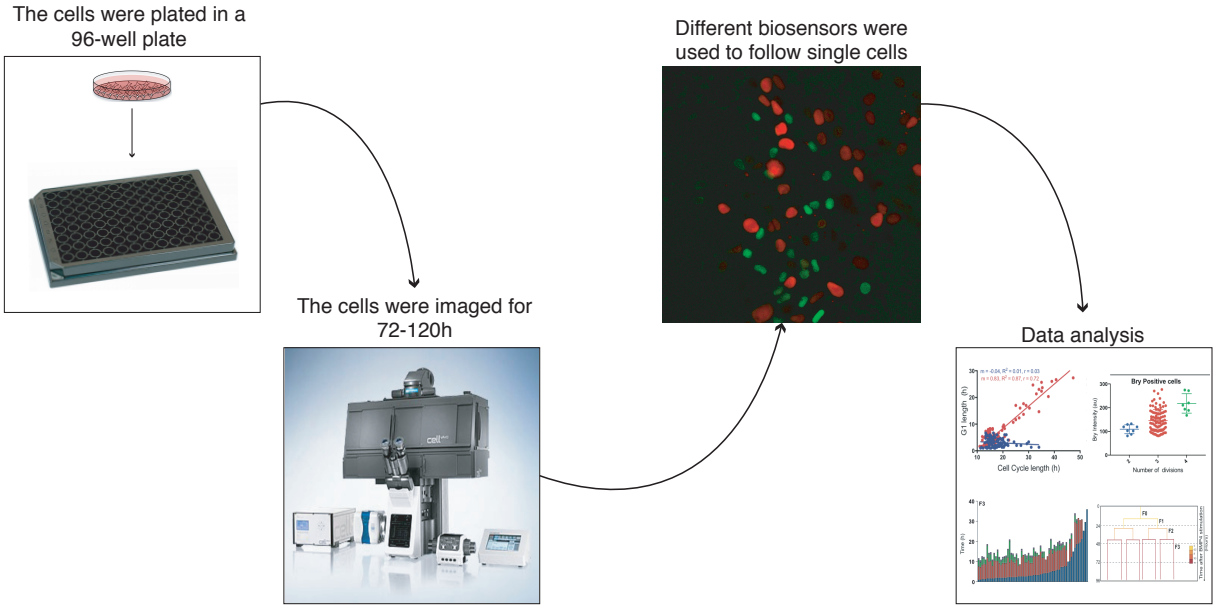


Figure 2.1 Pipeline for quantitative analysis of live cell imaging experiments. Cells were seeded in a 96-well plate 24 hours prior to the start of the experiment. Typically, cells where imaged from 36 to 120 hours. Different cell cycle biosensors were used to follow cell cycle dynamics followed by image analysis to quantify different features of cell cycle in single cells. This was followed by data and statistical analysis.

2.3.2 Immunofluorescence (IF)

Cells were washed twice with PBS before fixation with 4% paraformaldehyde in PBS for 10 minutes at room temperature. Cells were washed three times with PBS for 5 minutes before permeabilization using 0.3% Triton X-100 in PBS for 5 minutes at room temperature. Cells were washed three times with PBS for 5 minutes followed by an 1 hour incubation in blocking buffer containing 10% fetal bovine serum and 3% bovine serum albumin in PBS at room temperature. Primary staining was performed incubating the cells overnight at 4°C with primary antibodies (listed in Table 4) diluted in blocking buffer. The next morning, cells were washed three times with 0.3% Tween in PBS. Secondary staining was performed incubating the cells with secondary antibody diluted in blocking buffer for 1 hour at room temperature. The nuclei were stained using DAPI (0.5 μg/mL) to allow for tracking of cells and facilitate image analysis.

Table 4 - List of antibodies used for IF

Protein	Source	Cat.no	Diluition
Primary antibodies			
GATA3	CST	5852	1:1000
SOX2	CST	3579	1:400
CDX2	Abcam	157524	1:200
Brachyury	R&D System	AF2085	1:1000
p21	Abcam	109520	1:500
p15	Abcam	88304	1:100
Secondary antibodies			
Alexa-488 anti-goat	Life technologies	A11055	1:200
Alexa-647 anti-rabbit	Life technologies	A21244	1:200
Alexa-350 anti-rabbit	Life technologies	A10039	1:200
Alexa-647 anti-mouse	Life technologies	A21235	1:200

2.4 Data Analysis

2.4.1 Analysis of cell cycle dynamics

In order to measure cell cycle dynamics in single cells, stable H1 and H9 cell lines were created with different cell cycle biosensors. Relying on more than one biosensor allows to avoid artefacts, to measure individual cell cycle phases and ensures more accurate quantitative measurements, since not all sensors allow for all cell cycle phases to be clearly defined.

2.4.1.1 Measuring cell cycle dynamics using PCNA-YFP, NLS-mCherry biosensor

To measure all cell cycle phases in the same cell, a stable cell line expressing PCNA-YFP, a protein involved in DNA replication and repair, and the nuclear marker NLS-mCherry was created. Nuclear localization sequence (NLS) is the sequence PKKKRKV of amino acids, firstly discovered in the SV40 Large T-antigen, responsible for the nuclear import of a protein containing it. This sequence is recognised and bound by an importin responsible for the translocation through the nuclear pore in the nucleus.
After mitosis, when the nuclear envelope reforms (NER), both PCNA and NLS re-localise in the nucleus marking the beginning of G1-phase. At the beginning of S-phase, PCNA starts to be loaded to the DNA highlighting speckles in the nucleus, which disappear at the beginning of G2-phase (Sporbert, Domaing et al. 2005). When the nuclear envelope breaks down (NEB), marking the beginning of mitosis, both PCNA and NLS go to the cytoplasm (Figure 2.2). The formation and disappearance of PCNA speckles measurements are reasonably subjective, but the same criteria were used for all the experiments shown to avoid variability between measurements.

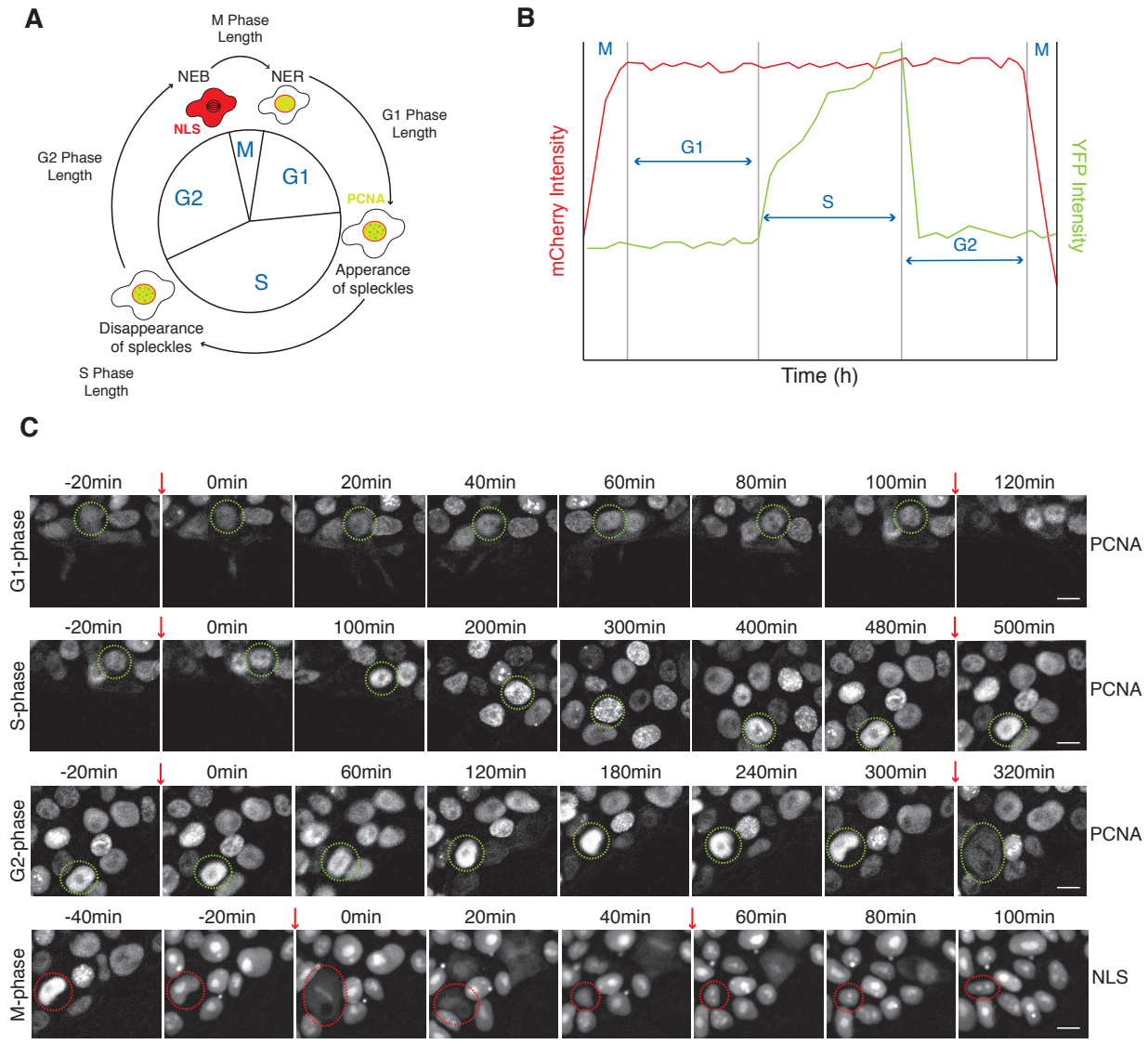


Figure 2.2. Cell cycle dynamics measured in hESC with the biosensor PCNA-YFP, NLS-mCherry. A. Schematic of the biosensor proteins appearing during the cell cycle and their correspondent colour. **B.** Schematic of duration measurements for cell cycle phases performed using fluorophores intensity with the biosensor PCNA-YFP, NLS-mCherry. **C.** Representative images showing how cell cycle phases lengths were measured in single cells with this cell cycle biosensor. The red arrows identify the beginning and the end of each phase. Green (PCNA-YFP) and red (NLS-mCherry) dotted circles mark the followed cell. Scale bars is 10 μm.

2.4.1.2 Measuring cell cycle dynamics using Fucci sensors

The Fucci technology harnesses the oscillatory properties of proteins that mark cell-cycle transitions using genetically encoded fluorescent probes. Specifically, it takes advantage of the cell cycle-dependent ubiquitination of two proteins, Cdt1 and Geminin, that can be used as indicators for cell cycle progression. During the cell cycle SCF^{Skp2} and APC^{Cdh1} E3 ligase activities, that are responsible for the proteolysis and consequent degradation of Cdt1 and Geminin respectively, oscillate reciprocally. Consequently, the protein levels of their substrates fluctuate in the same cell cycle-dependent manner.

Both Fucci sensors employed in this study are comprised of two proteins, Cdt1-mCherry and Geminin-mVenus, and the difference between the two sensors resides in the Cdt1 domain of the biosensor. The Fucci (SA) sensor employs a Cdt1 (aa30-120) domain that is a substrate of SCF^{Skp2} E3 ligase, resulting in the possibility to distinguish between G1-phase and the rest of the cell cycle marked by Geminin (aa 1-100) (Figure 2.3).

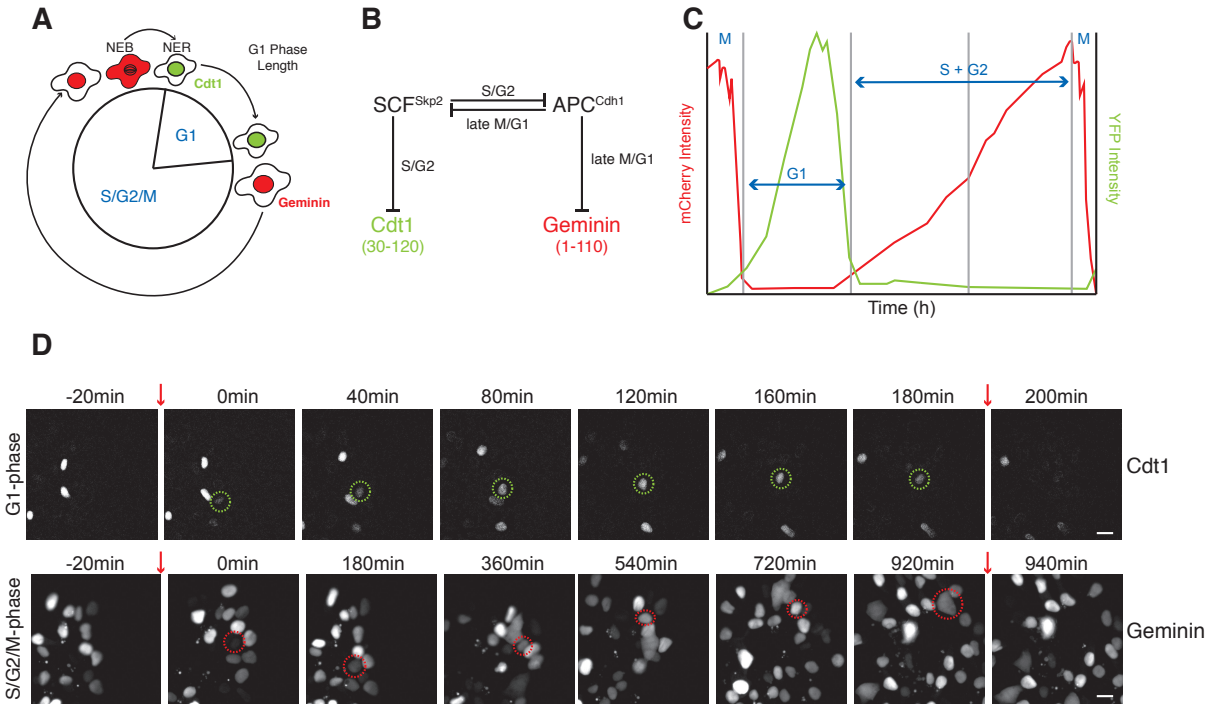


Figure 2.3 Cell cycle dynamics measured in hESC with the biosensor Fucci(SA). A. Schematic of the biosensor proteins appearing during the cell cycle and their correspondent colour. **B.** SCF^{Skp2} and APC^{Cdh1} control levels of Cdt1 an Geminin in a cell cycle-dependent manner **C..** Schematic of duration measurements for cell cycle phases performed using fluorophores intensity with the biosensor Cdt1-YFP, Geminin-mCherry. **D.** Representative images showing how cell cycle phases lengths were measured in single cells with this cell cycle biosensor. The red arrows identify the beginning and the end of each phase. Green (Geminin-mCherry) and red (Cdt1-YFP) dotted circles mark the followed cell. Scale bar is 10 μm.

The Fucci (CA) sensor employs a Cdt1 (1-110) domain that is a substrate of the CUL4^{Ddb1}-mediated pathway, active only during S-phase. This makes Cdt1-mCherry present in cells starting from G2-phase until the end of G1-phase, while Geminin-mVenus behaves the same way as in the Fucci(SA) sensor. In other words, the Fucci (CA) allows to distinguish the different interphase phases G1, S and G2 (Figure 2.4).

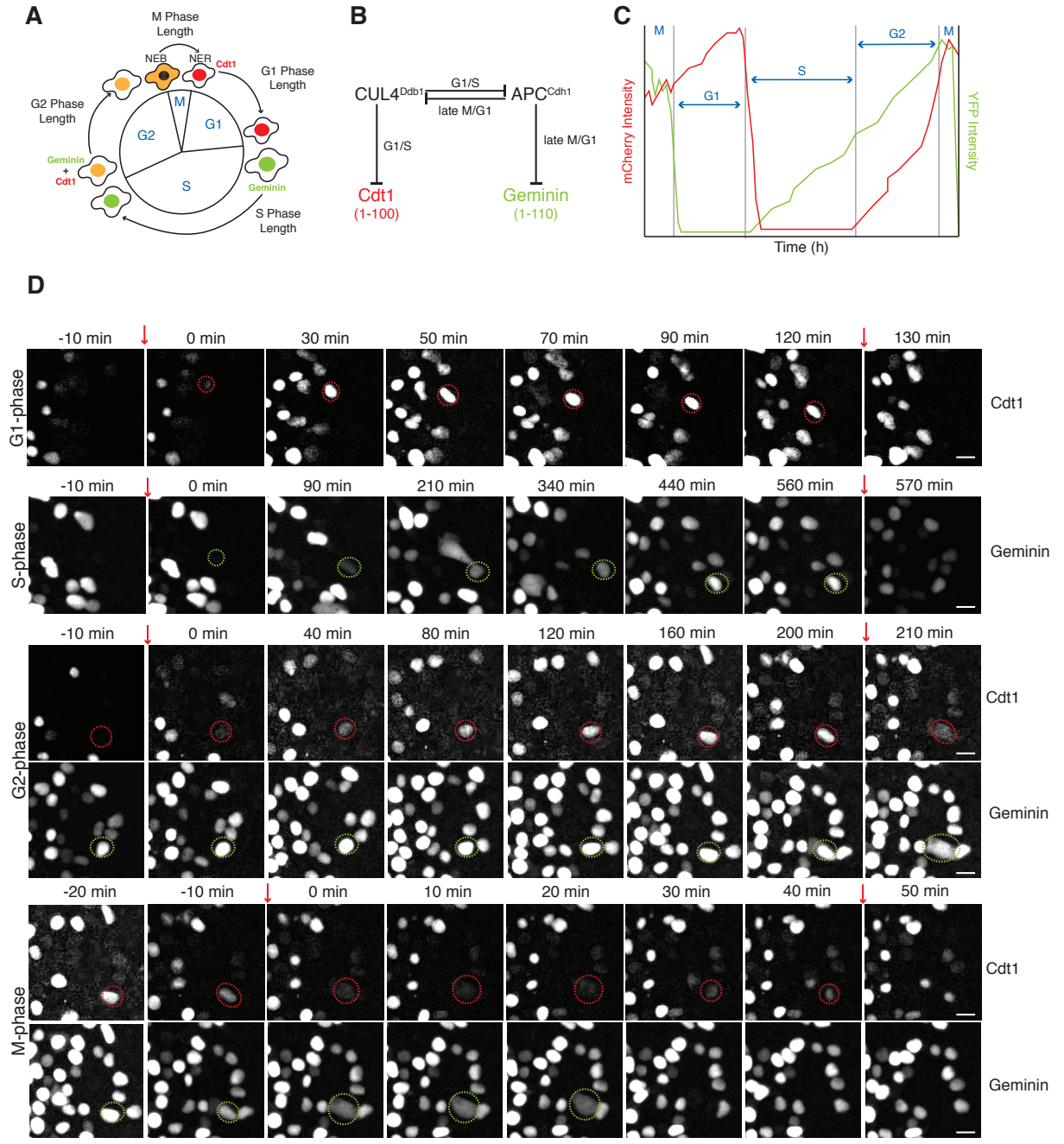


Figure 2.4. Cell cycle dynamics measured in hESC with the biosensor Fucci(CA). A. Schematic of the biosensor proteins appearing during the cell cycle and their correspondent colour. **B.** CUL^{Ddb1} and APC^{Cdh1} control levels of Cdt1 an Geminin in a cell cycle-dependent manner. **C.** Schematic of duration measurements for cell cycle phases performed using fluorophores intensity with the biosensor Cdt1-mCherry, Geminin-mVenus. **D.** Representative images showing how cell cycle phases lengths were measured in single cells with this cell cycle biosensor. The red arrows identify the beginning and the end of each phase. Green (Geminin-mVenus) and red (Cdt1-mCherry) dotted circles mark the followed cell. Scale bar is 10 μm.

2.4.1.3 Measuring G1 length using Cdt1-YFP, NLS-mCherry sensor

To measure G1-phase length a truncated Cdt1 (30-120aa) was used in combination with the nuclear biosensor NLS-mCherry. Cdt1 is one of the essential factors of the pre-replication complex which is assembled in late mitosis on G1-phase on the DNA and then disassembled at the G1/S transition by ubiquitin (Ub)-mediated proteolysis (Sakaue-Sawano et al., 2008). The Cdt1 used in this sensor is an adaptation of the original Fucci (SA) sensor. NLS-mCherry was used both to easily track the cells and to measure time between nuclear envelope breakdown (NEB) and nuclear envelope reformation (NER), a proxy for cell cycle length (Figure 2.5)

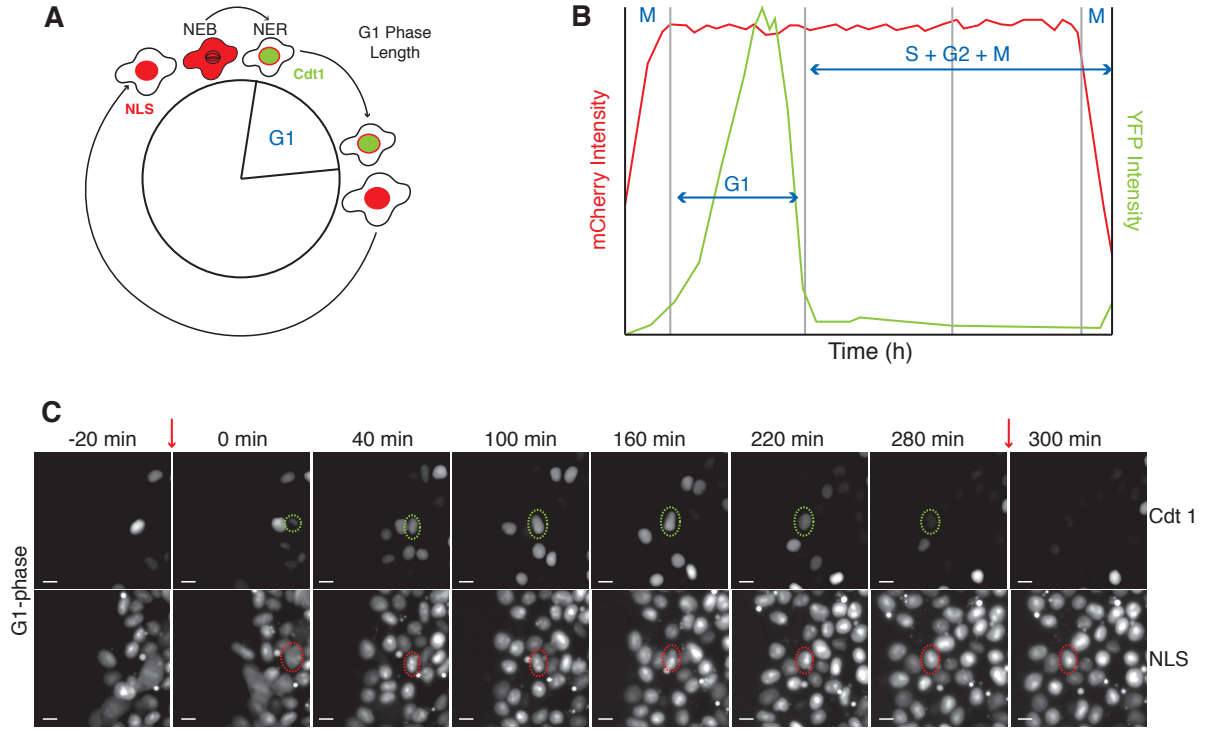


Figure 2.5. G1-phase length measured in hESC with the biosensor Cdt1-YFP and NLS-mCherry. A. Schematic of the biosensor proteins appearing during the cell cycle and their correspondent colour. **B.** Schematic of duration measurements for cell cycle phases performed using fluorophores intensity with the biosensor Cdt1-YFP, NLS-mCherry. **C.** Representative images showing how G1-phases length was measured in single cells with this cell cycle biosensor. The red arrows identify the beginning and the end of each phase. Green (Cdt1-YFP) and red (NLS-mCherry) dotted circles mark the followed cell. Scale bar is 10 μm.

2.4.2 Immunofluorescence data and statistical analysis

Automated-image analysis was performed using Fiji (NIH) and Cell Profiler software. Individual nuclei were identified through DAPI staining, which was used to make cell/nuclear masks. The levels of protein expression were measured/quantified by the mean intensity of a specific signal within the masks. Means were then normalized by mean intensity of DAPI (Figure 2.6).

Mann-Whitney and Kolmogorov-Smirnov tests, for non-parametric distributions were used to estimate p-values and were calculated using Prism7. Trend lines (m), coefficient of determination (R^2), Pearson correlation (r) were calculated using Prism7. Mean absolute deviations (MAD) were calculated at http://www.alcula.com/calculators/statistics/mean-absolute-deviation.

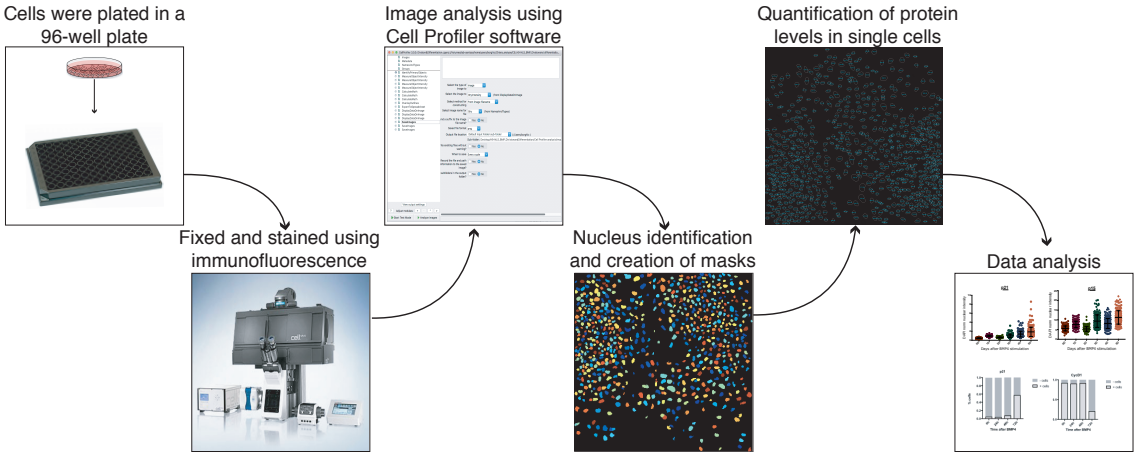


Figure 2.6 Pipeline for quantitative analysis of IF experiments. Cells were seeded in 96-well imaging plates and allowed to settle before the start of the experiment. After the experiment, cells were fixed and stained for immunofluorescence. Plates were imaged and images were analysed using Cell Profiler Software. Nuclear staining was used to create masks for quantification of protein levels in single cells. This was followed by data and statistical analysis.

2.5 Cloning and Molecular Biology

2.5.1 Construction of modified Fucci (SA) biosensor

Before the Fucci (CA) biosensor was available (Sakaue-Sawano, Yo et al. 2017), two constructs [Geminin aa1-110 fused to mCherry and Cdt1 aa 30-120 fused to YFP] necessary to obtain the Fucci biosensor were embedded in two separate vectors (Sakaue-Sawano, Kurokawa et al. 2008). This meant that two sequential hESCs infections and respective selection via FACS sorting were necessary to get the complete biosensor. To overcome this problem, it was necessary to fuse both constructs in the same vector. In order to do so, the pCSII-EF1α mCherry-hGMNN (aa 1-110) plasmid was cut with XbaI (as described in 2.5.3) and two DNA fragments encoding for an IRES sequence and YFP tagged.

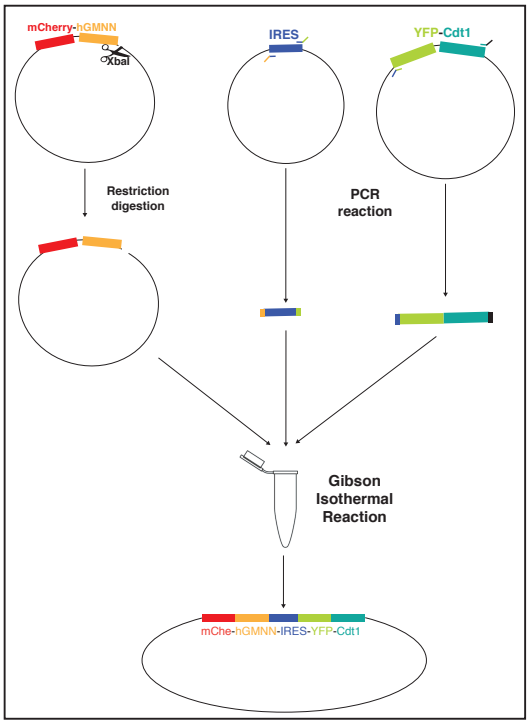


Figure 2.7 Schematic representation of construction of modified Fucci (SA) biosensor. Vector containing mCherry-hGMNN was digested with XbaI in order to obtain an open vector. IRES and Cdt1-YFP were amplified by PCR to obtain fragments with overlapping sequences. The three elements were used to perform Gibson Isothermal reaction. A fused vector containing mCherry-hGMNN-IRES-YFP-Cdt1 (modified Fucci (SA)) was obtained.

Cdt1 (aa 30-120) were amplified by PCR (as described in 2.5.2) such that there was a 30bp overlapping sequence respectively with the backbone and Cdt1-YFP or IRES and the backbone. These three components were fused together using Gibson Isothermal assembly technique (Figure 2.7).

2.5.2 Polymerase chain reaction (PCR)

To selectively amplify DNA fragments (IRES and Cdy1-YFP), a polymerase chain reaction (PCR) was performed. The reaction mixture generally contained a final volume of 50µl consisting of:

- 5µL of Pfu High Fidelity Buffer (10x)
- 2.5U Pfu
- 1µL of 10mM dNTPs
- 100ng template DNA
- 25pmol Primer 5' (sense)
- 25pmol Primer 3' (anti-sense)
- top up to 50µL with dH_2O

The mixture was then place on a thermocycler machine and the following protocol was initiated:

- 1 cycle of 3 minutes of initial denaturation at 94°C
- 30 cycles of: 15 seconds denaturation at 94°C, 30 seconds at annealing temperature (ideal for each pair of primers), 60 seconds of elongation at 68°C
- 1 cycle of further extension for 5 minutes at 68°C.

5µL of PCR reaction was then run on an agarose gel to confirm single band with the correct size and the PCR product was purified with Qiagen PCR purification kit.

Table 5 - List of PCR primers used in this thesis

Fragment	Forward Primer	Reverse Primer
IRES	TGGCAGAAAAACGGAGAAAGGCGCTG TAATCCCCCCCCCCCCTAACG	CAGCTCCTCGCCCTTGCTCACCA TGGTGGCGGCCATATTATCATC
CDT1-YFP	TCCTTTGAAAAACACGATGATAATATG GCCGCCACCATGGTGAGCAAGG	ATAAGCTTGATCCCTCGATGTTAC TCTAGTTAGATGGTGTCCTGGTCC TGC

2.5.3 Restriction digest of vector

In order to obtain the pCSII-EF1α mCherry-hGMNN (aa 1-110) open vector, 5µg of vector were digested using XbaI restriction enzyme. 10U of enzyme was mixed with compatible buffer and topped up with dH_2O to the final volume of 20µL. The mixture was incubated 1 hour at 37°C followed by a heat inactivation step at 65°C for 20 minutes. To prevent re-ligation in the following cloning step of the

incompletely digested DNA, the restricted DNA was 5'dephosphorylated with a unit of Shrimps alkaline phosphatase for 1 hour at 37C.

2.5.4 Purification of gel bands from agarose gel

1% (w/v) of agarose was added to 1xTAE (Tris Acetate EDTA) buffer and let to dissolve in the microwave.
50x TAE buffer was prepared in water accordingly:

- 2M Tris/acetate
- 50mM EDTA
- pH 8.5

The solution was left to cool down before adding 1µL/mL ethidium bromide and transferred to a gel support. After solidification, 20µL of DNA dephosphorylation reaction were loaded onto the gel using 6x DNA loading buffer and 10Kb ladder (New England Biolabs) for DNA size quantification. DNA gel bands were then excised from the gel and purified using Qiagen Gel Extraction Kit according to manufacturer's instructions.

2.5.5 Gibson Isothermal Assembly based cloning

In order to fuse both Fucci biosensor constructs (Cdt1 and Geminin) in one vector, three DNA fragments were purified and used to perform the Gibson Isothermal assembly cloning (Gibson, Young et al. 2009). For a final volume of 5µL, equimolar amounts of DNA fragments were calculated based on the (bp) and concentration (ng/mL). The combined DNA was added to 15µL of isothermal assembly master mix and incubated for 1 hour at 50°C.

The final isothermal assembly reaction (total volume 20µL) contained:

- 5µL mixed DNA fragments
- 0.08U of T5 Exonuclease
- 0.5U of Phusion High Fidelity DNA Polymerase
- 80U of Taq DNA Ligase
- 4µL of 5x Reaction Buffer

5x Reaction buffer was prepared in water as follows:

- 500nM of Tris HCl pH 7.5
- 50nM of $MgCl_2$
- 1mM of dGTP
- 1mM of dATP
- 1mM of dTTP
- 1mM of dCTP
- 50mM of DTT
- 5mM of NAD+
- 250mg/mL of PEG-8000

The reaction mix was purified using Qiagen QIAquick PCR Purification Kit according to the manufacturer's instructions and used to transform *E.coli* Dh5α (as described in 2.5.6).

2.5.6 Transformation of E.coli Dh5α

All DNA constructs used in this study were obtained using chemically competent *E.Coli* Dh5α cells (Sigma). These cells were thawed in ice for 30 minutes after which 0.5μg of plasmid DNA of interest was added and incubated on ice for 20 minutes. A heat-shock of 45 seconds at 42°C was performed to the cells to facilitate the uptake of plasmid DNA, followed by a 2 minutes incubation in ice. 250μL of S.O.C Medium were added to the cells and the mixture was then spread on ampicillin (100μg/mL)-containing LB agar plates and incubated overnight at 37°C.

2.5.7 Isolation of plasmid DNA

After overnight incubation on LB plates, bacteria colonies were picked and incubated for 8 hours in 5mL of LB medium containing Ampicillin (100μg/mL) in a horizontal shaker at 37°C. The cultured bacteria were then transferred to a 200mL flask of LB media with fresh antibiotic and incubated overnight at 37°C in the shaker. Cells were centrifuged at 4000 rpm for 15 minutes at 4°C and the HiSpeed-Plasmid Maxi Kit 9 (Qiagen) was used according to the manufacturer's instruction to obtain highly concentrated plasmid DNA. DNA concentration was determined using a Nanodrop spectrometer (Fisher Scientific).

2.5.8 RT-qPCR

RNA extraction was performed using TRI reagent (Life Technologies) and MaXtract High Density tubes (Qiagen) according to manufacturer's instructions. RNA purity and quantity were assessed using a

Nanodrop spectrometer (Fisher Scientific), considering an absorbance ratio of 1.8-2 for A260/280 suitable for further analysis. Treatment with DNase was performed to remove possible genomic DNA contamination. cDNA was obtained from 1μg of RNA using QuantiTect Reverse Transcription Kit (Qiagen) according to manufacturer's instructions. qRT-PCR was performed using iTaq SYBR Green qPCR master mix (Bio-Rad) on a QuantStudio 7 Flex Real-Time PCR System. Primers pairs are listed in **Table 6**. Glucuronidase beta (GUSβ) were used as an invariant housekeeping gene to normalize measured transcripts. Fold change expression was calculated using $2^{-\Delta\Delta CT}$ (Livak) method (Livak and Schmittgen 2001).

PCR conditions were as follows:

- 1 cycle at 95°C for 3 minutes
- 40 cycles at 95°C for 5 seconds and 60C for 30 seconds.

Table 6 – qPCR primers used in this thesis

Gene	Forward Primer	Reverse Primer
GUS*β*	CCGAGTGAAGATCCCCTTTTTA	CTCATTTGGAATTTTGCCGATT
CCNA1 (cyclin A1)	AATTGTGCCTTGCCTGAGTG	GAGGTGAAGTTCTGGAAGTGC
CDKN1A (p21)	CTGGAGACTCTCAGGGTCGAA	CGGATTAGGGCTTCCTCTTG
CDKN2B (p15)	ACTAGTGGAGAAGGTGCGAC	GCGCTGCCCATCATCATG

Chapter 3. Results

3.1 Cell cycle dynamics changes during differentiation in human embryonic stem cells (hESCs)

3.1.1 Gap phases length changes during BMP4-driven differentiation of hESCs

To investigate how the cell cycle remodels during BMP4-induced differentiation in single cells, a live cell imaging approach was employed. Different cell cycle phases were measured using stable hES cell lines expressing PCNA-YFP and NLS-mCherry as described in section 2.4.1 (Figure 2.2). G1-length was measured from the end of mitosis (nuclear envelope reformation, NER) to the start of S-phase (with the appearance of PCNA speckles); S-phase was monitored by the appearance to the disappearance of PCNA speckles; G2-phase was defined as the time between the end of S-phase (disappearance of nuclear speckles) to the beginning of mitosis (nuclear envelope breakdown, NEB); mitosis was measured as the time between NEB to NER. Total cell cycle length was defined by the time between two consecutive NER events. In order to induce differentiation, cells were treated with BMP4 and imaged using the IX83 inverted epifluorescence microscope every 20 minutes for 4 days.

After three days of BMP4 stimulation, hES colonies completely changed morphology, from being small (10μm long cells) and tight to being large (>50μm) and flat and spread when compared with cells that were left untreated (Figure 3.1A). S-phase and mitosis did not show any change in length (Mean=8.71 and 8.09 hours for S-phase and Mean=0.91 and 0.87 hours for mitosis in hESCs and differentiated cells respectively) or variability (MAD=2.17 and 1.90 for S-phase and MAD=0.21 and 0.19 for mitosis in hESCs and differentiated cells respectively). Mean absolute deviation, MAD, is a measure of the variation in a population of how much the data values differ from the mean. Conversely, G1-phase length increased with differentiation from 3.08 hours in hES cells to 7.43 hours in differentiated cells. Moreover, when plotting the measurements for single cells, cell-to-cell variability was evident as seen by the measured mean absolute deviation. The extent of this variation increased when comparing hESC and BMP4-treated cells (MAD=1.38 in hESC, MAD=4.98 in differentiated cells. On the other end, G2-phase length showed an opposite trend, with hESC having a G2-phase duration of 4.73 hours that decreased significantly in differentiated cells down to 2.41 hours. The cell-to-cell variability measured for G2-phase length showed a MAD value of 1.93 in hESCs and 0.62 in differentiated cells (Figure 3.1B).
G1-phase length showed significant change, when comparing hESCs and differentiated cells (*p-value* <0.0001 by KS test). When comparing G2-phase length in hESCs and BMP4 treated cells a significant

difference was highlighted (*p-value* <0.0001 by KS test). S-phase and mitosis length showed no significant difference between the two conditions (Figure 3.1C).

These results show that during BMP4-driven differentiation of hESCs, G1- and G2-phase length and variation change while S-phase and mitosis length remains the same.

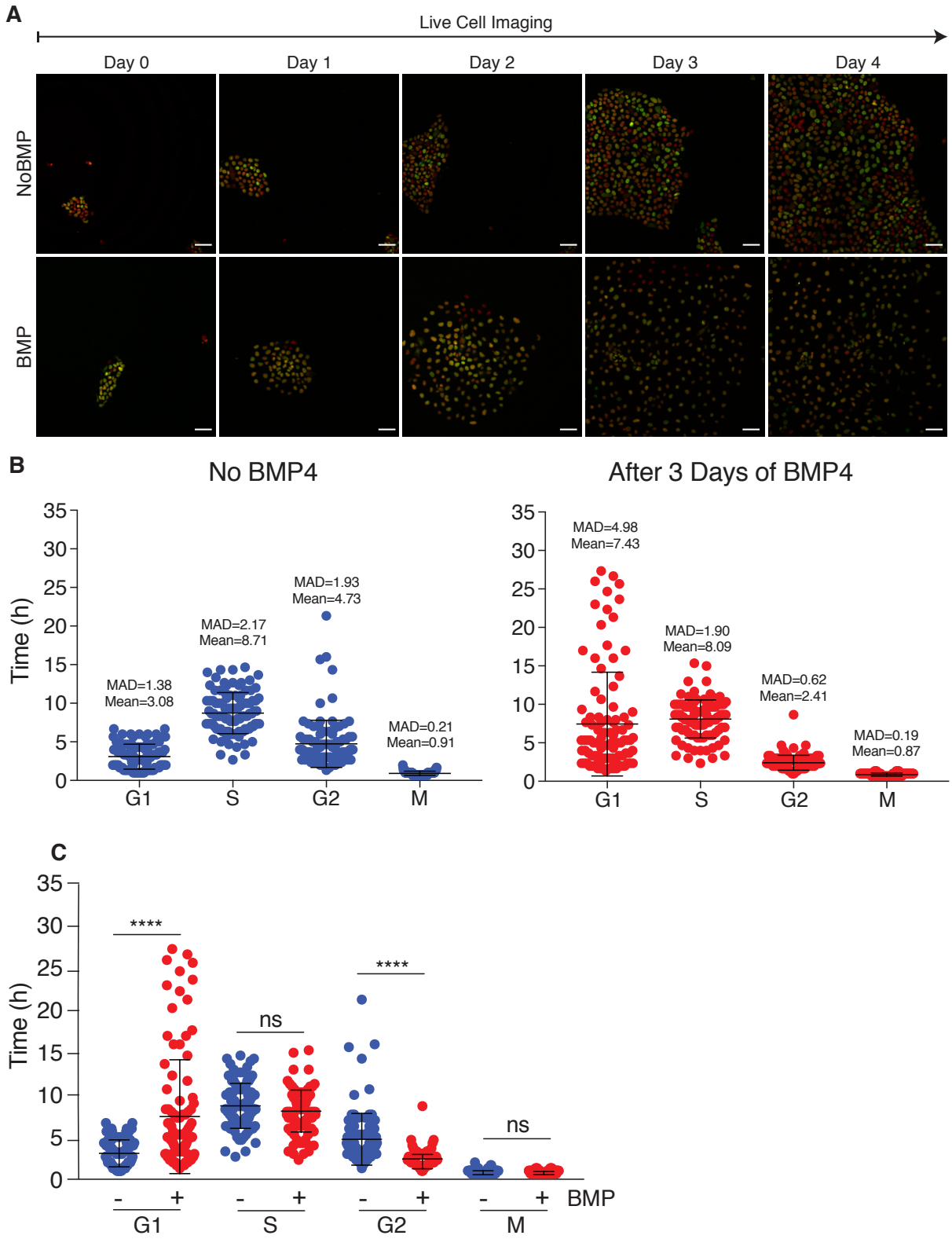


Figure 3.1 Duration of cell cycle phases as measured by stable hES cell line expressing PCNA-YFP and NLS-mCherry biosensor and imaged every 20 minutes. A. Representative images of stable hES cell lines expressing PCNA-YFP and NLS-mCherry biosensors in presence or absence of BMP4 (50 ng/ml). Scale bar=100μm. **B.** Length of cell cycle phases was measured in single cells by live cell imaging for hESCs and differentiated cells after 3 days of BMP4 treatment. Mean and mean absolute deviation are shown (n>100). **C.** Cell cycle phases length in hESCs and differentiated cells was compared and statistically tested employing KS test. (ns= not significant; **** p<0.0001) (n>100).

To make sure that these measurements were not affected by acquisition frequency, the same experiment was performed acquiring images every 10 minutes to increase temporal resolution. This difference in sampling time showed no effect on the previously observed length of cell cycle phases (Figure 3.2). These results show that imaging at different frame frequencies has no effect on the measured cell cycle dynamic changes during differentiation.

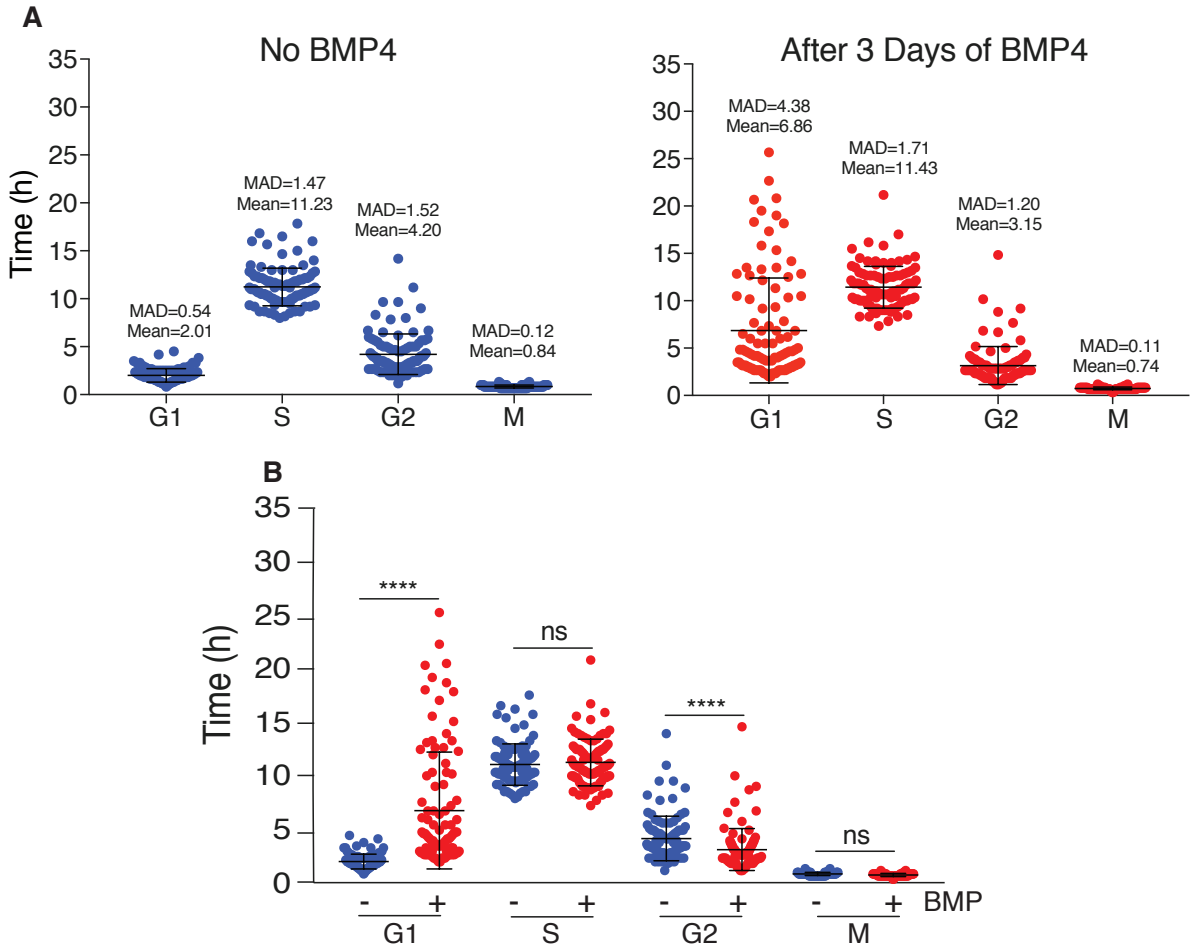


Figure 3.2 Duration of cell cycle phases was measured with stable hES cell line expressing PCNA-YFP and NLS-mCherry biosensor and imaged every 10 minutes. A. Cell cycle phases length was measured in each cell by single cell live imaging for hESCs and differentiated cells after 3 days of BMP4 treatment. Mean and mean absolute deviation are shown (n>100). **B.** Cell cycle phases length in hESCs and differentiated cells was compared and statistically tested employing KS test. (ns= not significant; **** p<0.0001) (n>100)

In order validate these measurements, collect more robust data and avoid artefacts introduced by using only one cell cycle biosensor, a different cell line was employed. A stable cell line expressing Fucci (CA) biosensor was built and used to measure cell cycle phases length in hES cells and differentiated cells. As detailed in the methods section, the Fucci (CA) sensor is comprised of two elements: Cdt1-mCherry (aa 1-110) and Geminin-mVenus (aa 1-100). G1-length was measured by the nuclear envelope reformation (NER) to the disappearance of Cdt1 signal; S-phase was monitored by the appearance of Geminin signal to the appearance of Cdt1 intensity; G2-phase was defined as the time between the appearance of Cdt1 signal and the nuclear envelope breakdown (NEB); mitosis was measured form the NEB to the NER. Total cell cycle length was defined by the time between two consecutive NER events. More details on how duration of cell cycle phases was measured can be found in section 2.4.1 (Figure 2.4)

The experiment was conducted by treating cells for 4 days with BMP4 while imaging them in the IX83 inverted epifluorescence microscope every 10 minutes. Fucci (CA) cells were morphologically differentiated after BMP4 treatment for 3 days compared with untreated cells. Cells were imaged for an additional day in order to measure full cell cycle length of cells that started dividing at day 3 (Figure 3.3A). G1-phase length increased with differentiation from 2.06 hours in hES cells to 7.08 hours in differentiated cells. Cell-to-cell variability increased, as seen before, when comparing hESC and BMP4-treated cells (MAD= 0.50 in hESC, MAD=4.98 in differentiated cells). G2-phase length showed again an opposite trend, hESC had a G2-phase duration of 3.41 hours compared to 2.83 hours in differentiated cells. Population variability measured for this phase was of 1.62 in hESCs and 1.04 in differentiated cells. S-phase and mitosis lengths did not vary (Mean=10.45 and 10.22 hours for S-phase and Mean=0.89 and 0.91 hours for mitosis in hESCs and differentiated cells respectively) as well as variability (MAD=1.62 and 1.36 for S-phase and MAD=0.12 and 0.14 for mitosis in hESCs and differentiated cells respectively) (Figure 3.3B).

G1-phases length showed significant change, as seen before, when comparing hESCs and differentiated cells (*p-value*<0.0001 by Kolmogorov-Smirnov test) while G2-phase length displayed a less significant difference (*p-value*=0.02 by Kolmogorov-Smirnov test). S-phase and mitosis length showed no significant difference between the two conditions (Figure 3.3C).

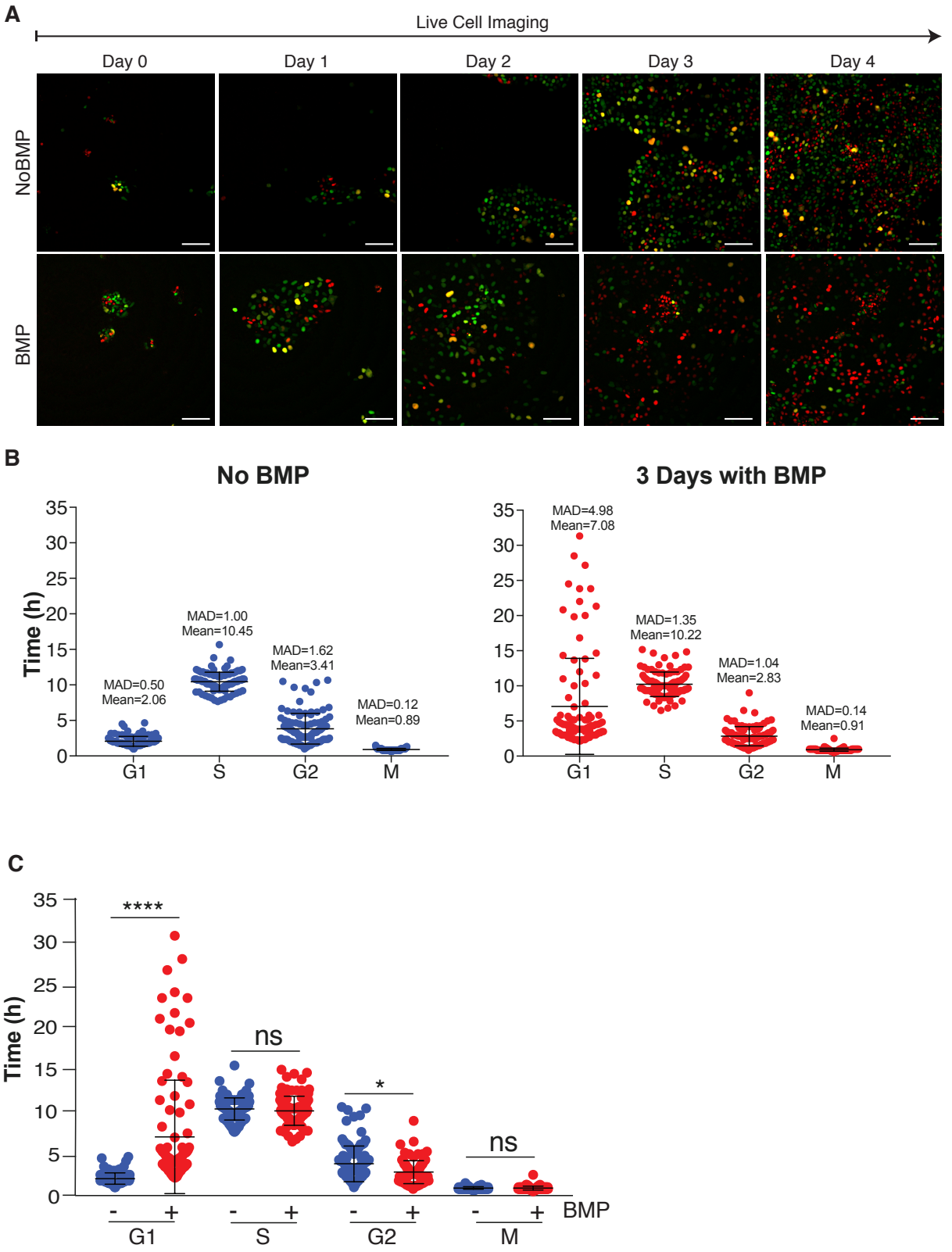


Figure 3.3 Duration of cell cycle phases was measured with stable hES cell line expressing Fucci (CA) biosensor and imaged every 10 minutes. A. Representative images of stable hES cell lines expressing Fucci (CA) biosensor in presence or absence of BMP4 (50 ng/ml). Scale bar=100µm. **B.** Cell cycle phases length was measured in each cell by single cell live imaging for hESCs and differentiated cells after 3 days of BMP4 treatment. Mean and mean absolute deviation are shown (n>100). **C.** Cell cycle phases length in hESCs and differentiated cells was compared and statistically tested employing KS test. (ns= not significant; **** p<0.0001) (n>100).

These measurements confirmed what was previously seen using PCNA-YFP and NLS-mCherry biosensor. The slight difference seen in G2-phase might be due to difficulty, when using Fucci (CA) biosensor, in defining a strict boundary between S- and G2-phase. The end of S-phase and the beginning of G2-phase are defined by the appearance of the Cdt1-mCherry signal that combined with the Geminin-mVenus signal shows as a yellow/orange fluorescence. Detecting two signals (Cdt1-mCherry and Geminin-mVenus) is more challenging to detect than a single signal and as a result the boundary between S-phase and G2-phase was more challenging to define.

Taken together, these results suggest that while both S-phase and mitosis length remain constant during BMP4-driven differentiation, G1-phase length significantly increases. In addition, G2-phase duration decreases with differentiation but challenges in quantifying it results in less robust measurements.

3.1.2 Correlation amongst different cell cycle phases during BMP4-driven differentiation of hESCs

To further characterise the cell cycle remodelling process, correlations between each phase and total duration of cell division for single cells were analysed. Length of cell cycle phases and cell cycle were measured as previously described (see 2.4.1) using hESC stable cell line expressing PCNA-YFP and NLS-mCherry biosensor. BMP4-treated and untreated cells were imaged in the ScanR inverted epifluorescence microscope every 20 minutes for 4 days.

When looking at hES cells both S-phase and G2-phase length correlate with total duration of cell cycle (Pearson correlation coefficient: *r* – S-phase= 0.56; G2-phase=0.84). On the other hand, mitosis and G1-phse length do not show any correlation with cell cycle length (Pearson correlation coefficient: *r* – G1-phase= -0.12; mitosis=0.14). When comparing these results to differentiated cells, it was seen that S-phase and mitosis remain similarly correlated with time between divisions (Pearson correlation coefficient, *r* – G2-phase=0.47; Mitosis=0.18). Contrarily changes were observed in the correlation of G1- and G2-phase. The correlation between G1-phase duration and cell cycle length strikingly increased while the one with G2-phase length decreased in BMP4 treated cells (Pearson correlation coefficient, *r* – G1-phase=0.93; G2-phase=0.10) (Figure 3.4A)

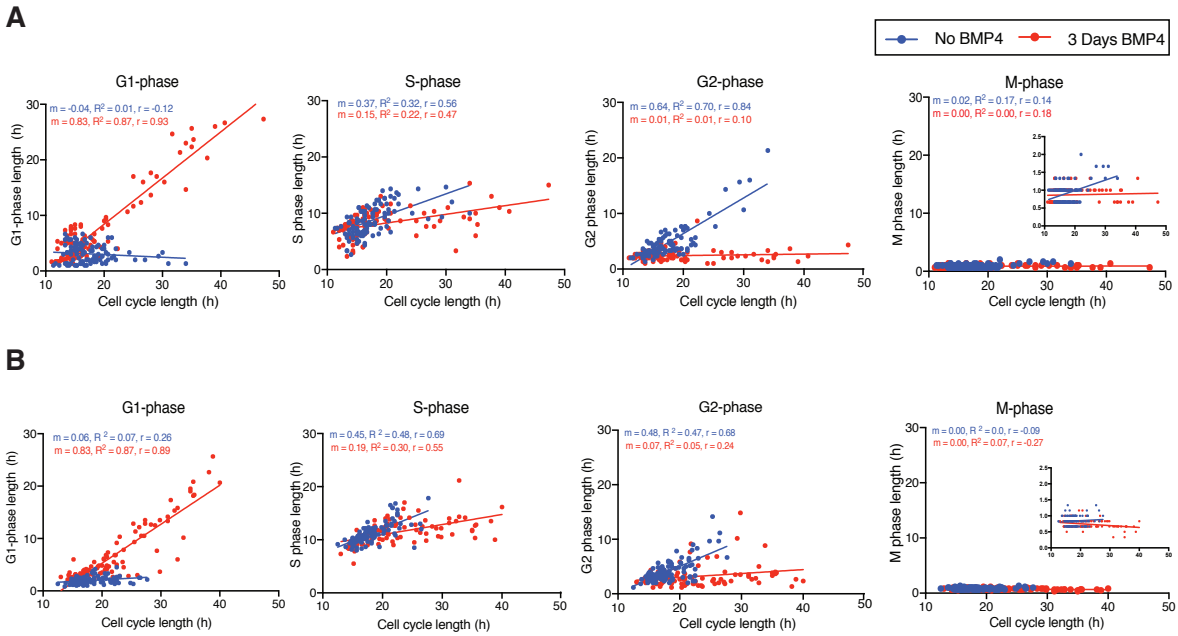


Figure 3.4 Comparison of cell cycle dynamics in hES and BP4-treated cells using PCNA-YFP and NLS-mCherry biosensor. **A.** Each cell cycle phase length was plotted as a function of total cell cycle length in hESCs (blue dots) and differentiated cells (red cells) as measured by live-cell imaging, with acquisition of images every 20 minutes. Slope of trend line (m), coefficient of determination (R^2) and Pearson correlation coefficient (r) are shown. (n>100) **B.** Each cell cycle phase length was plotted as a function of total cell cycle length in hESCs (blue dots) and differentiated cells (red cells) as measured by live-cell imaging, with acquisition of images every 10 minutes. Slope of trend line (m), coefficient of determination (R^2) and Pearson correlation coefficient (r) are shown. (n>100)

As previously, to confirm whether these quantifications did not depend on sampling time, the same measurements were repeated acquiring images every 10 minutes to increase temporal resolution (Figure 3.4B). Increasing the sampling frequency did not highlight any difference compared to lower sampling frequency results.

Finally, to gain more robust data on cell cycle dynamics and avoid artefacts due to using a specific biosensor, the stable cell line expressing Fucci (CA) biosensor, previously used in 3.1, was employed to perform the same measurements. The results showed comparable trends to what was previously seen with the PCNA-YFP and NLS-mCherry. Both S-phase and mitosis do not show significant differences in correlation when comparing hESCs against differentiated cells (Pearson correlation coefficient: *r* – G2-phase in hESCs= 0.53, Differentiated cells=0.31; mitosis in hESCs=0.39, differentiated cells=0.05) (Figure 3.5). Low correlation is present between G1-phase length and cell cycle length in hESCs as opposed to 3 days of BMP4-driven differentiation (Pearson correlation coefficient, *r* – hESCs=0.58; Differentiated cells=0.97); G2-phase displays opposite behaviour (Pearson correlation coefficient, *r* – hESCs=0.82; Differentiated cells=0.34).

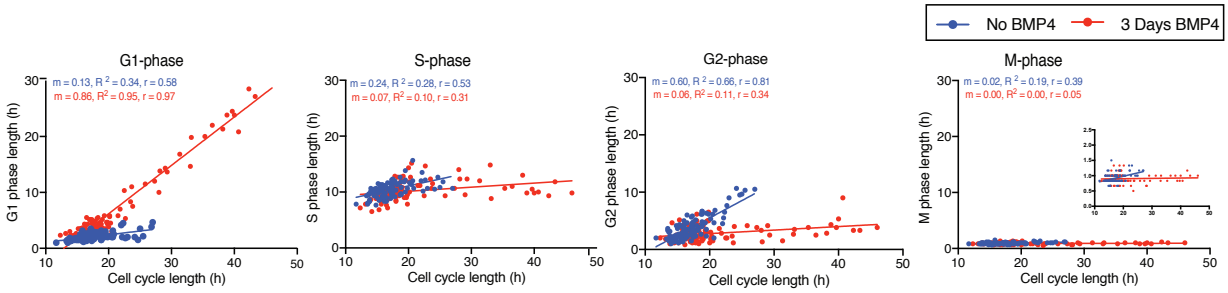


Figure 3.5 Comparison of cell cycle dynamics in hES and BMP4-treated cells using Fucci(CA) biosensor. Every cell cycle phase length was plotted as a function of total cell cycle length in hESCs (blue dots) and differentiated cells (red cells) as measured by live-cell imaging, with acquisition of images every 10 minutes. Slope of trend line (m), coefficient of determination (R^2) and Pearson correlation coefficient (r) are shown. (n>100)

In hES cells, cell cycle duration does not depend on G1-phase length while the opposite is true in differentiated cells. On the other hand, G2-phase shows a reverse behaviour being correlated to cell cycle length in hESCs and losing correlation in differentiated cells. S-phase in both hESCs and BMP4-treated cells is correlated with cell cycle length while mitosis is remains temporally insulated from previous cell cycle events as previously shown by Araujo et al., 2016 (Araujo, Gelens et al. 2016). Taken together, these observations show differences in the correlation between cell cycle duration and cell cycle phases length of hES and BMP4 treated cells suggesting that there might be differences in the regulatory mechanisms underlying G1- and G2-phase control.

3.1.3 Interdependency of G1-phase and G2-phases length is different in hESCs and differentiated cells

In the previous paragraph, absolute cell cycle duration of individual cells was plotted. However, pluripotent and differentiated cells cycles have very different lengths even cells within the same population (pluripotent and BMP4-treated) have different cell cycle duration, as shown by the MAD values. The question arises on how these correlations look when the values are normalized by these differences. In order to do this, the percentage of time that single cells spent in each of the cell cycle phase was calculated using the measurement obtained in 3.1.2. This allowed to normalize each cell cycle phase length by the total cell cycle length.

After observing that G1-phase was the one that changed the most during BMP4-driven differentiation, it was investigated how its duration is correlated with the other cell cycle phase in hESCs and differentiated cells. To avoid artefacts and increase the data robustness this analysis was performed for the three different conditions seen previously (3.1.2). The dependency of each cell cycle phase with G1 is shown in Figure 3.6.

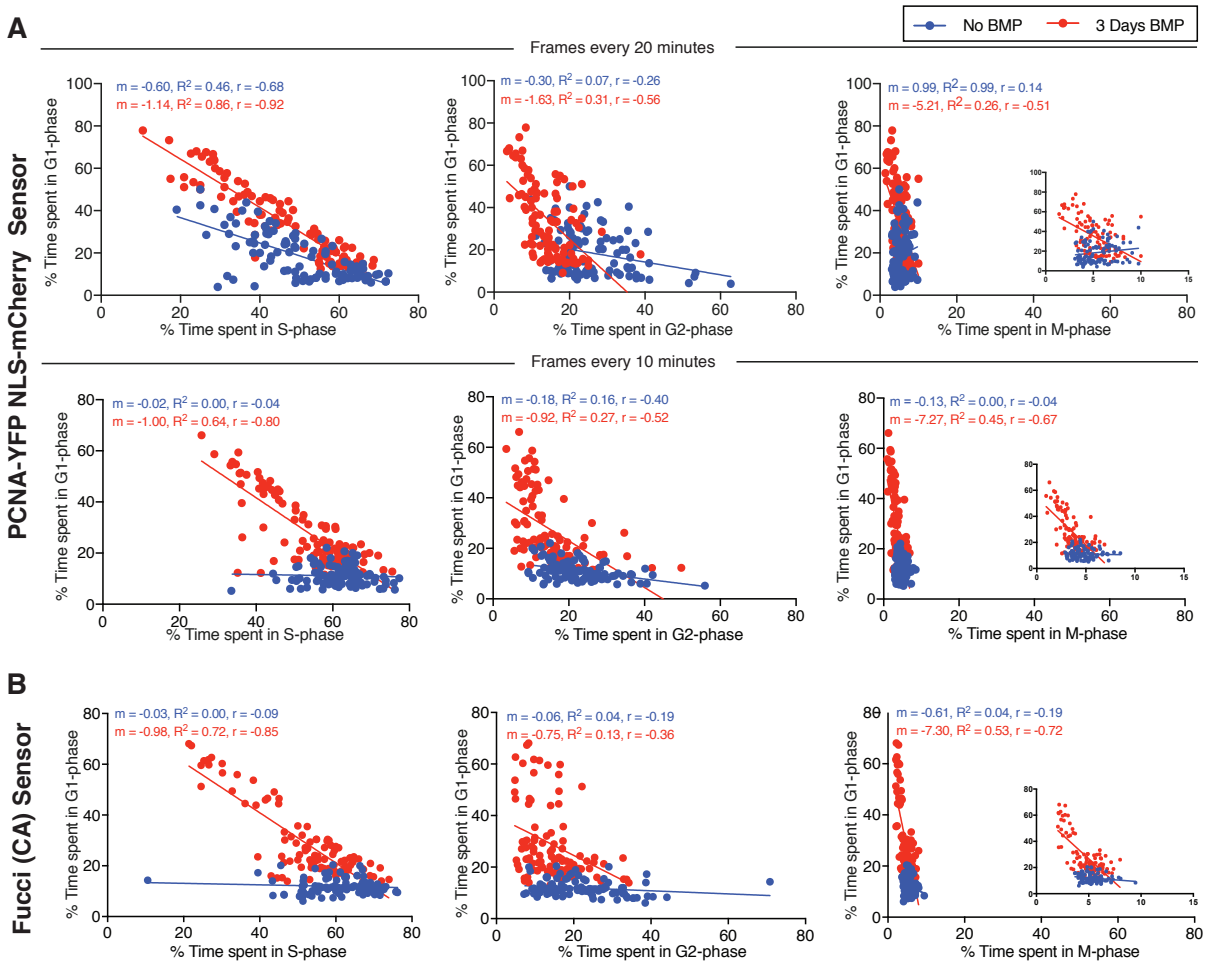


Figure 3.6 Interdependency between percentage of time spent in G1 and in the other cell cycle phases changes with differentiation. A. Stable hESC line expressing PCNA-YFP and NLS-mCherry where imaged either every 20 or 10 minutes. Percentage of time spent in S-phase, G2-phase and mitosis as function of percentage of time spent in G1-phase in hESCs (blue dots) and differentiated cells (red dots) as measured by live cell imaging. Slope of trend line (m), coefficient of determination (R^2) and Pearson correlation coefficient (r) are shown. (n>100). B. Stable hESC line expressing Fucci(CA) biosensor where imaged either every 10 minutes. Percentage of time spent in S-phase, G2-phase and mitosis as function of percentage of time spent in G1-phase in hESCs (blue dots) and differentiated cells (red dots) as measured by live cell imaging. Slope of trend line (m), coefficient of determination (R^2) and Pearson correlation coefficient (r) are shown. (n>100)

In differentiated cells (red dots), percentage of time spent in G1-phase was always inversely correlate with the percentage of time spent in the other cell cycle phases while hESCs showed low to no correlation. These results interestingly show that G1-phase length not only is remodelled during early BMP4-driven differentiation but also that its interdependence with other cell cycle phases changes as well.

3.2 Cell cycle dynamics changes during differentiation in lineages during hESCs differentiation

In previous paragraphs, measurements of cell cycle dynamics were performed in hESCs and differentiated cells looking at two static states. To further characterise the remodelling process of hESC, cell cycle changes were measured to understand whether the remodelling process happens as a graded or switch-like transition (Figure 3.7). For this analysis, we quantified how many divisions cells underwent before remodelling their cell cycle.

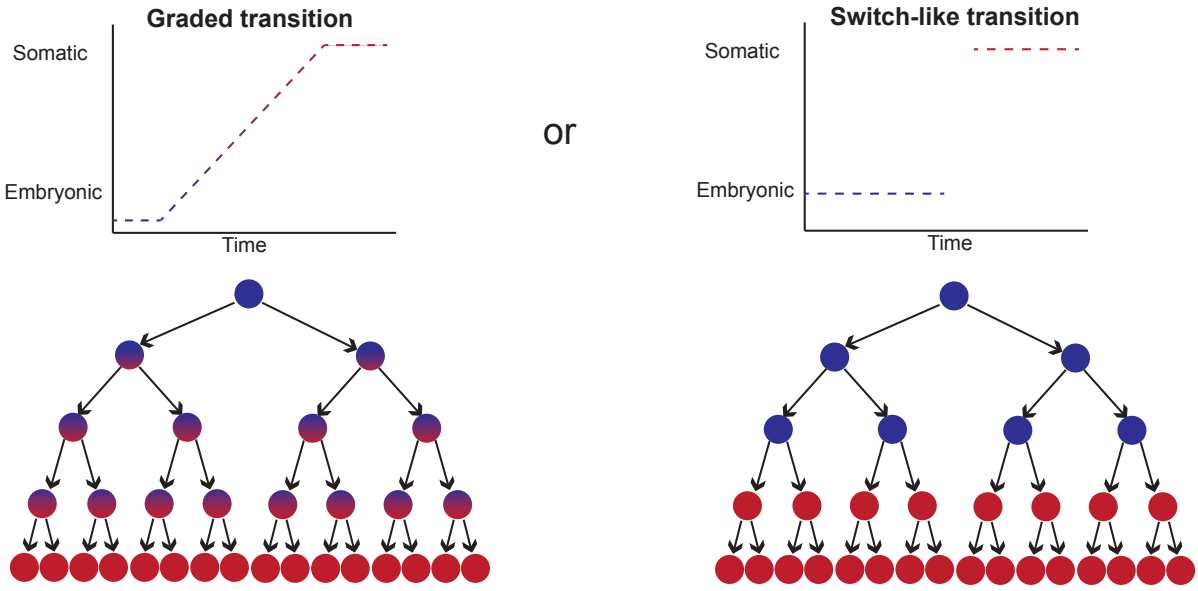


Figure 3.7 Schematic comparing graded or switch–like transition in G1-phase length during differentiation. If G1-length remodelling was graded, each division cells would have longer G1-phase whilst with a switch-like transition cells would all show low G1-phase length in the first divisions and fully remodelled G1-phase in the following division.

In order to do so, hESCs stable cell line expressing the PCNA-YFP and NLS-mCherry biosensor was employed. Cells were treated with BMP4 for 4 days and imaged every 20 minutes using the IX83 inverted epifluorescence microscope, as seen in section 3.1.1. At day 0 of the experiments "mother cells" were randomly selected and followed in their lineage for three divisions during BMP4-driven differentiation (F0: "mothers", F1: "daughters", F2:"grand-daugthers", F3:"great-grand-daughters"). The length of each cell cycle phase was measured as previously explained in 2.4.1. This allowed to measure cell cycle dynamics through time instead of only quantifying two different states (hESC and differentiated cells).

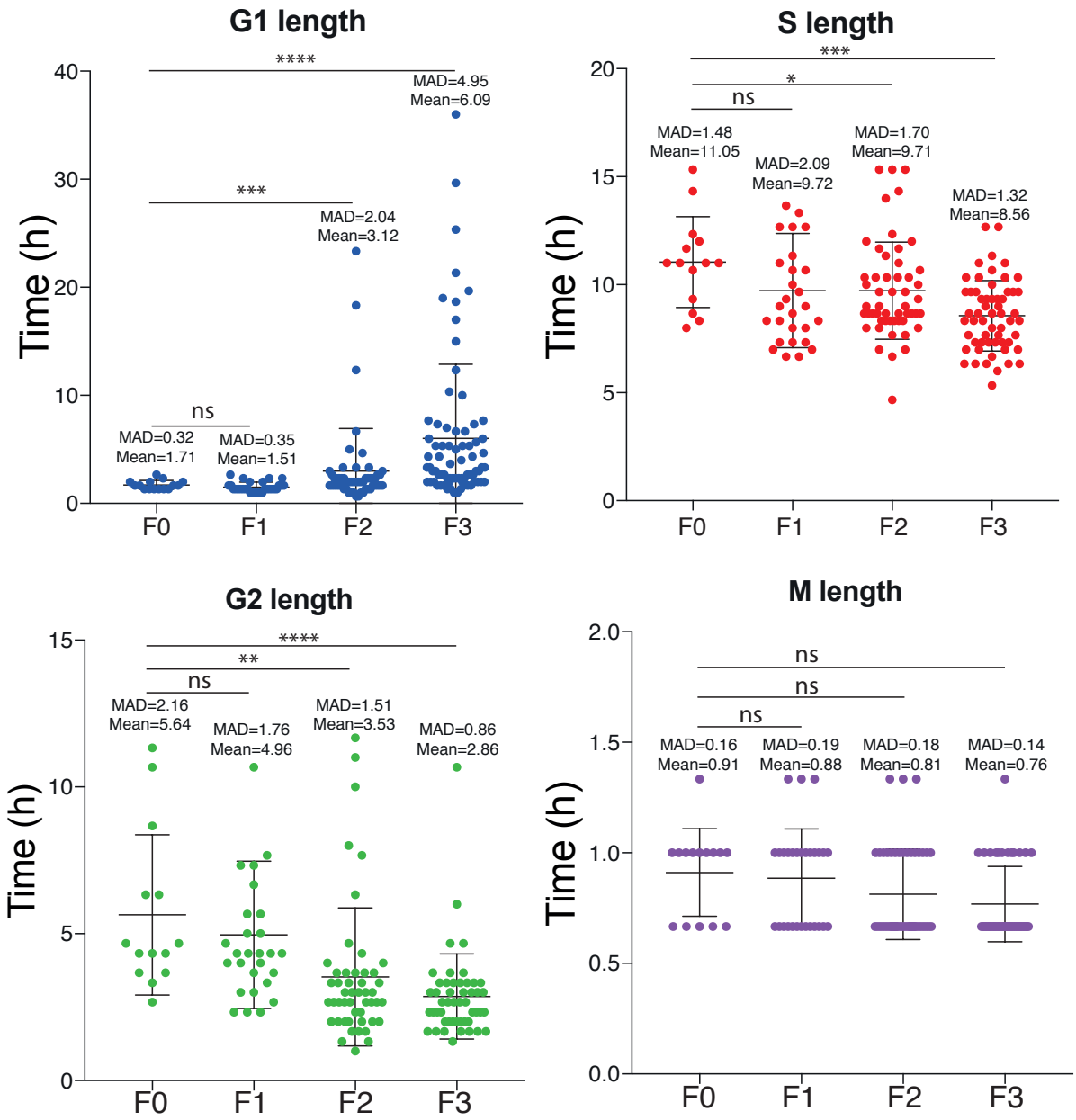


Figure 3.8 Cell cycle dynamics changes during differentiation in cell lineages. Each panel represents a cell cycle phase and its length during sequential division in BMP4-driven differentiation. Cell cycle phases length was measured using stable cell line expressing PCNA-YFP and NLS-mCherry combined with single cell live imaging. Cells were imaged for 4 days in presence of BMP4. Mean and mean absolute deviation are shown (initial n=14, final n~100). Cell cycle phases length was compared and statistically tested employing KS test. (ns= not significant; *p<0.05, **p<0.01***p<0.001, **** p<0.0001)

As expected, no changes were detected in mitosis length during differentiation (Mean: F0=0.91; F1=0.88; F2=0.81; F3=0.76 hours and MAD: F0=0.16; F1=0.19; F2=0.18; F3=0.14). S-phase and G2-phase length showed a slight decrease after each division (S-phase mean: F0=11.05; F1=9.72; F2=9.71; F3=8.56 hours and MAD: F0=1.48; F1=2.09; F2=1.70; F3=1.32 and G2-phase mean: F0=5.64; F1=4.96; F2=3.53; F3=2.86 hours and MAD: F0=2.16; F1=1.76; F2=1.51; F3=0.86). When considering

significance in changes of these two cell cycle phases, it is important to remember that the dataset size for the two first divisions was lower compared with the second two division.

Interestingly, G1-phase length displayed a drastic change after the second and third divisions. While the first two cell cycle, G1-phase duration remained similar and never exceeded 3.5 hours (F0: Mean= 1.71, MAD=0.32; F1: Mean=1.51, MAD=0.35). In the two following divisions, remodelled cells appeared and G1-phase length increased as follows: (F2: Mean=3.12, MAD=2.04; F3: Mean=6.09, MAD=4.95) (Figure 3.8). These results show that the cell cycle changes abruptly after 2 divisions in a switch-like manner and G1-phase duration has the highest length variation during BMP4-driven differentiation when looking at sequential divisions.

This striking change in G1-phase duration is highlighted when plotting the cell cycle profile for each cell as a bar graph. G1-phase length shows to be the cell cycle phases that remodels the most during BMP4-driven differentiation (Figure 3.9).

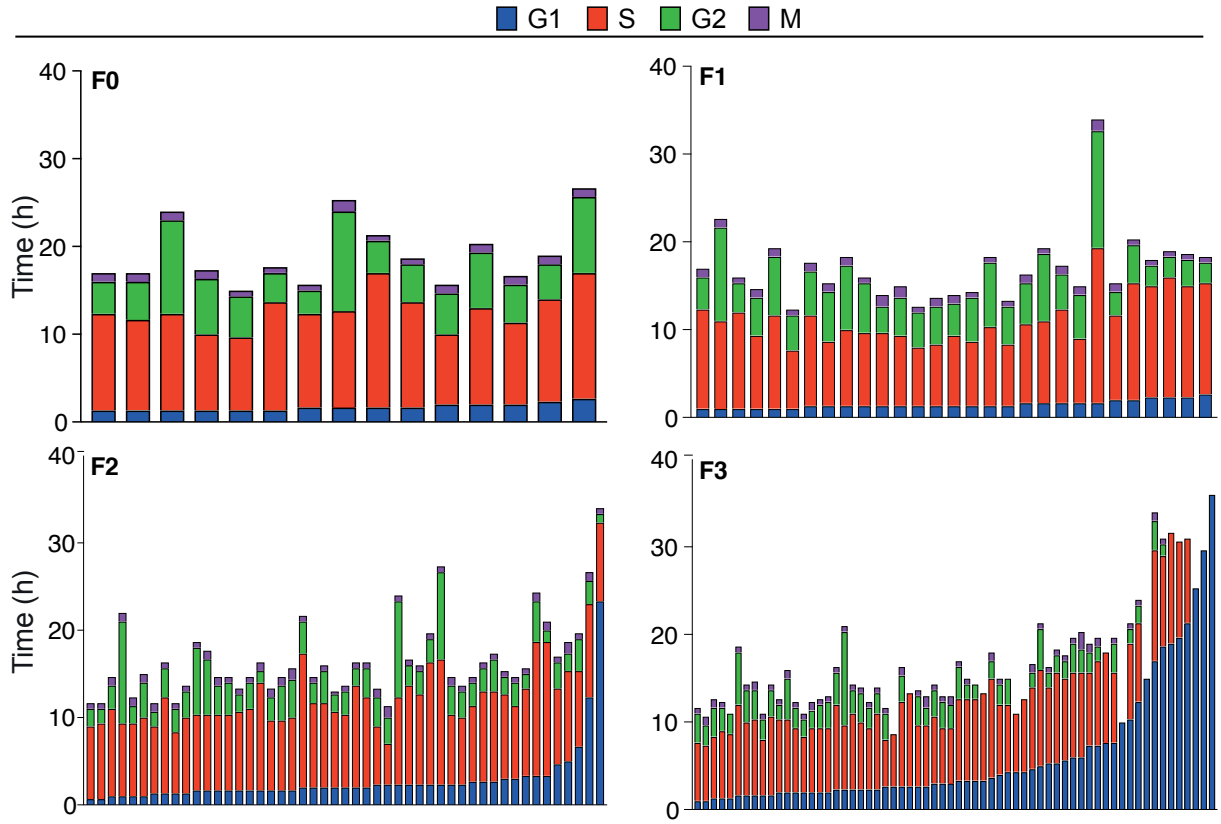


Figure 3.9 G1-phase remodels after 2-3 divisions (F2 and F3). Each plot represents a population of sister cells followed in sequential divisions during BMP4-driven differentiation. Each bar exemplifies a cell and its cell cycle profile. Each colour represents a cell cycle phase (G1-phase=blue; S-phase=red; G2-phase=green; mitosis= purple).

In conclusion, these preliminary results showed that G1-phase seem to remodel during BMP4-driven differentiation in a switch-like manner. Further measurements will be required to increase the dataset size and improve the robustness of these conclusions. Moreover, further validation using different biosensors, such as the Fucci (CA), would be fundamental to solidify these conclusions.

3.3 G1-phase length changes during differentiation in single cells.

After analysing the whole cell cycle, further studies were performed focusing on G1-phase since our results showed it to be the cell cycle phase that mostly remodelled during BMP4-driven differentiation.
To investigate how G1-phase remodels at single cell level, a live cell imaging approach was employed in conjunction with stable cell line expressing Cdt1-YFP and NLS-mCherry as described in section 2.4.1 (Figure 2.5). G1-length was measured from nuclear envelope reformation (NER) and the beginning of Cdt1 signal to the disappearance of Cdt1. NLS-mCherry was used as a nuclear marker to track the cells. Cells were treated with BMP4 and imaged in the Incucyte Zoom Microscope every 20 minutes for 4 days. G1-phase length measurements were performed for each day of the differentiation process and gave a further insight into how this phase length remodels at population level in single cells.
The first two days of the differentiation process did not show any significant change in G1-phase length (Day 0: Mean= 4.47 hours, MAD=0.65; Day 1: Mean= 4.27, MAD=0.70). From day 2 a slight increase in G1-phase length occurred together with an increase in cell-to-cell variability (Mean= 4.85 hours, MAD=1.08).After 3 days of BMP4 treatment a larger percentage of cells showed a significant change in G1-phase dynamic (Mean= 10.28 hours, MAD=5.43, $p<0.0001$) (Figure 3.10, left panel) resembling the data obtained with the previous sensors (see 3.1.1). These results show that G1-phase starts to remodel after two days of BMP4 stimulation in H1 hES cells. At day 3 of BMP4 treatment a significant number of cells have remodelled its G1-phase.

In order to confirm these observations are not specific to which cell line was used, differentiation of H9 hESCs expressing Cdt1-YFP and NLS-mCherry biosensor were monitored. In the first two day of BMP4 treatment no change was observed in G1-phase length (Day 0: Mean=5.7 hours, MAD=0.72; Day 1: Mean=5.6 hours, MAD=1.03). At day 2 a significant increase in G1-phase duration was observed (Mean=6.9 hours, MAD=0.96, $p<0.0001$). Finally, at day 3 more cells started to display a remodelled G1-phase (Mean= 10.8 hours, MAD=3.73). The results obtained were comparable with the previous ones with a difference in the change in G1 length from day 1 to day 2. H9 cells displayed a more significant change from day 1 to day 2 (Figure 3.10, right panel) that might be due to their higher tendency to spontaneously differentiate observed in culture.

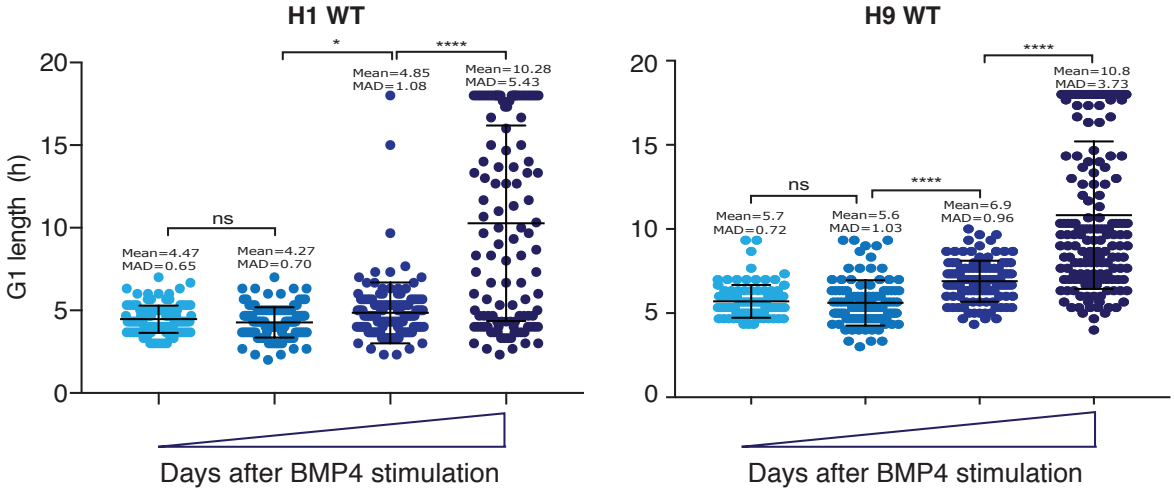


Figure 3.10 G1-phase length increases during BMP4-driven differentiation in two different cell lines. Left panel: G1-phase length measured by single live cell imaging at different time of BMP4 stimulation in H1 WT cells expressing Cdt1-YFP and NLS-mCherry. Mean and mean absolute deviation (MAD) are shown. KS test was performed to calculate *p-values* (ns= not significant; * p>0.02; **** p<0.0001) (n>100). Right panel: Same measurements were performed using H9 WT cells expressing Cdt1-YFP and NLS-mCherry. Mean and mean absolute deviation (MAD) are shown. KS test was performed to calculate *p-values* (ns= not significant; **** p<0.0001) (n>100).

Finally, preliminary results using H1 WT cell line expressing Cdt1-YFP and NLS-mCherry looking at remodelling of G1-phase during BMP4-driven differentiation in lineages confirmed what previously seen with the PCNA-YFP and NLS-mCherry biosensor (see 3.2). Instead of using dot plots, the data was plotted as genealogical tree where each branch represented the mean of G1-phase length during differentiation (Figure 3.11).

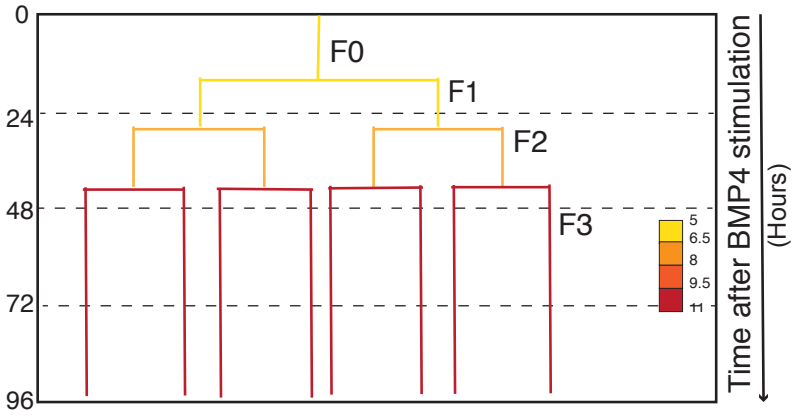


Figure 3.11 G1-phase length increases during BMP4-driven differentiation in lineages. Mean of G1-phase length genealogy during hES cell differentiation. G1-phase length was measured for different lineages during BMP4-driven differentiation. Vertical bars represent individual cells, horizontal bars denote cell division events. Colour scale indicates mean G1-phase length.

Taken together these results confirm the described data on section 3.2 and suggest that G1-phase remodels in a switch-like manner during BMP4-driven differentiation whereby after 2 divisions G1-phase lengthens. Further lineage analysis will be fundamental to increase confidence in these conclusions.

3.4 Cell cycle regulators might be responsible for G1-phase remodelling

While trying to understand the mechanisms underlying cell cycle remodelling during BMP4-driven differentiation in hESCs, RNA seq was performed comparing pluripotent and differentiated cells. hES and BMP4 treated cells were synchronized in G1/S and G2/M phases of the cell cycle and levels of nascent transcript compared (Gharibi et al., unpublished).

When focusing on cell cycle GO terms, to identify putative genes which might be implicated in the observed G1 lengthening, only ~15 genes out of 150 described cell cycle genes were differentially expressed between hES and differentiated cells. This suggested that contrary to other genes, cell cycle genes might not change dramatically at mRNA level during differentiation.

Among these genes, three cell cycle regulators involved in G1- to S-phase transition with altered mRNA between hESC and differentiated cells. Specifically, p15 and p21 mRNA levels were up-regulated in differentiated cells compared with hES cells while CyclinA1, is down-regulated (Figure 3.12). Moreover, when perturbing their expression levels in hESCs, they affected differentiation dynamics (data not shown) (Gharibi et al., unpublished). All three proteins are known to be involved in G1-to S-phase transition regulation: p15 and p21 belong to the CDKs inhibitors class of protein and specifically inhibit CDK4/6 and CDK1/2 respectively; Cyclin A1, one of the isoforms of Cyclin A, forms the active complex with CDK2, important in G1/S-phase transition (as described in 1.2.2).

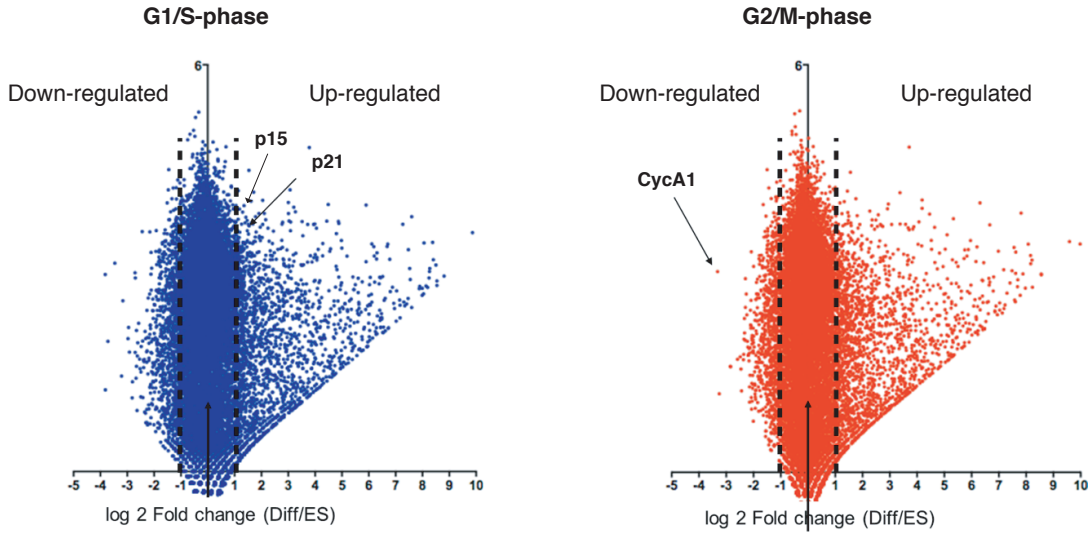


Figure 3.12 Volcano plots

In order to test if these cell cycle regulators were involved with G1-phase remodelling, stable cell line expressing inducible over-expression constructs for p15 and p21 and inducible shRNA construct against Cyclin A1 were used. These were combined with cell cycle biosensors to measure changes in G1-phase length.

3.4.1 p15 and p21 expression increases during differentiation and their overexpression induce G1-phase lengthening in hESCs

First, p15 and p21 protein and mRNA levels were studied in H1 hES cells treated with BMP4 for 5 days in order to induce differentiation. Protein levels were measured by immunofluorescence assay (IF) while mRNA levels were measured by RT-qPCR. Protein levels of both p21 and p15 were quantified using Cell Profiler software and protein intensity was normalised by nuclear staining.

Both protein levels increased after 3 days of BMP4 treatment (Figure 3.13A), which correlate well with what previously shown is the timeline of G1-phase length remodelling. qPCR experiments showed slightly different dynamics of p21 and p15 at transcription level. Both genes show a drastic increase in transcription from day 4 to day 5 of BMP4 treatment. However, during the first 3 days p21 showed a steady increase (up to 10-fold) of mRNA levels while p15 plateau after a first 5-fold increase (Figure 3.13B). Taken together, these results showed that in fact these two CDKs inhibitor increase, both at protein and mRNA level, during differentiation.

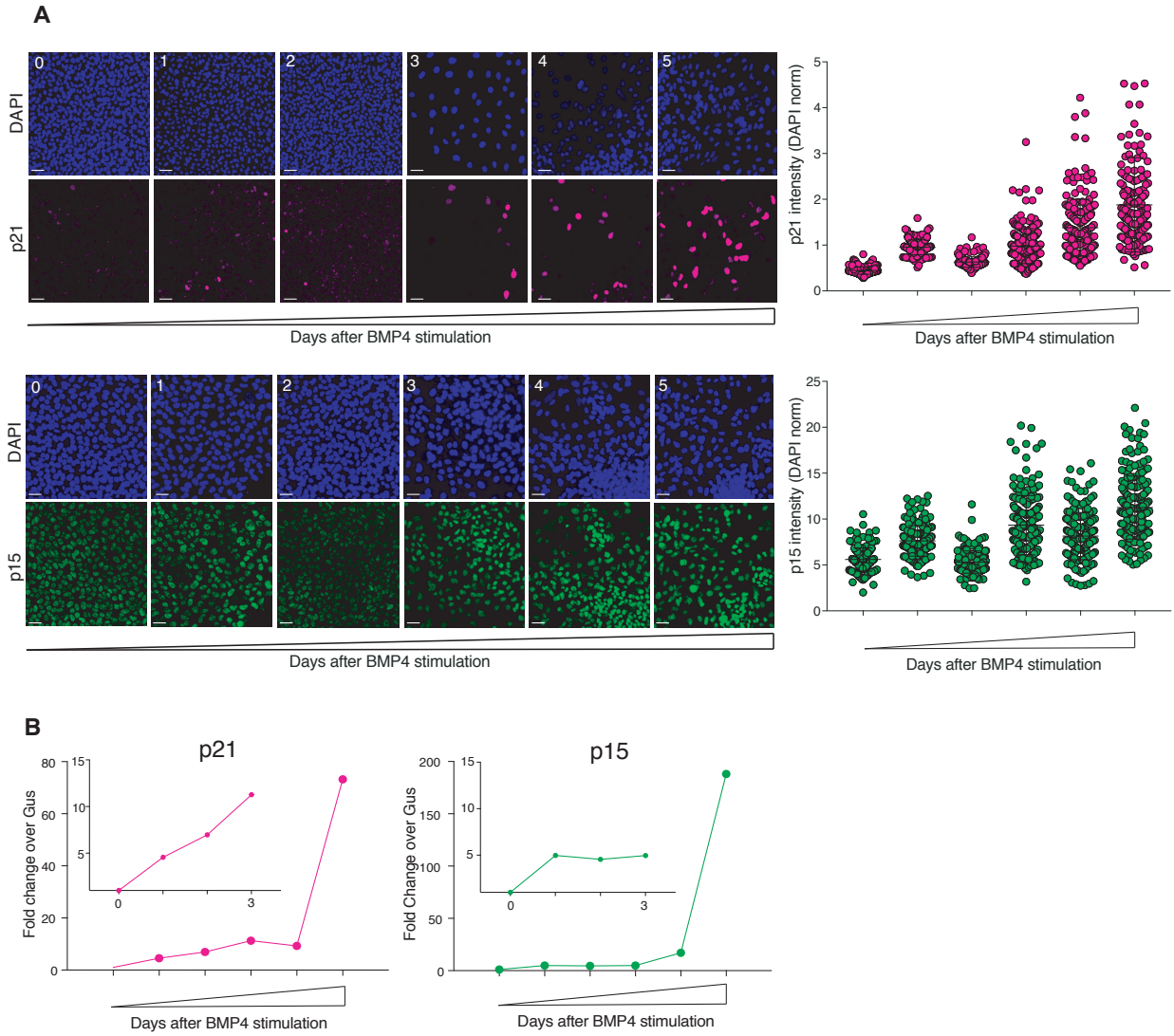


Figure 3.13 p21 and p15 mRNA and protein levels increase during differentiation. A. Immunostaining and corresponding quantification of p21 and p15 protein levels during a 5 days treatment of hESCs with BMP4. Protein intensity was quantified using Cell Profiler and approximately 5000 cells were analysed for each condition. For image clarity only 200 randomly chosen cells were plotted. Both p21 and p15 protein intensity was normalised using nuclear staining (DAPI). Scale bar is 20µm. **B.** mRNA levels normalised by GUSB (housekeeping gene) are plotted for both p21 and p15 during a 5 days treatment on hESCs with BMP4. The smaller panels zoom on the first 3 days of BMP4 treatment.

In order to investigate further the role of p15 and p21 in G1-phase lengthening, H1 expressing the Cdt1-YFP and NLS-mCherry were stably transfected with a doxycycline-inducible p15 or p21 construct. The inducible empty vector was transfected as well and used as a control in all experiments. The overexpression of both genes was measured by qPCR and cells showed an overexpression of about 800 folds for p15 and 13 folds for p21 in comparison to empty vector line (Figure 3.14).

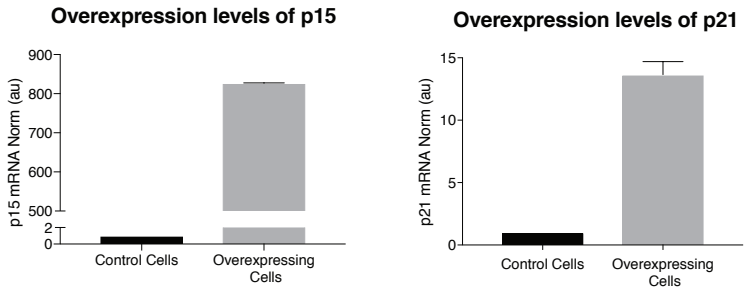


Figure 3.14 Normalized expression of p15 and p21 in overexpressing inducible cell line expressing Cdt1-YFP and NLS-mCherry. Normalized expression of p15 and p21 were measured by qPCR in hES cell lines expressing empty vector (control cells) or p15 or p21 inducible overexpressing vector and Cdt1-YFP and NLS-mCherry. Mean and standard deviation is shown (n=3).

G1-phase length was measured as previously described using Cdt1-YFP and NLS-mCherry biosensors (as described in 2.4.1). hES cells were transferred from mTeSR1 to TeSR E5 (a basal media to differentiate hESCs), doxycycline (Dox) was added and cells were imaged for 2 days in order to measure G1-phase dynamics in single cells. Ectopically expressing p15 and p21 lengthened G1-phase significantly when compared to untreated cells (p15: No Dox=4.89 hours and Dox=7.29 hours; p21: No Dox=5.76 hours and Dox=7.04 hours).

In order to ensure that TeSR E5 media did not have any effect on the G1-phase lengthening, G1-phase duration was measured in control cells for the full length of the experiment and did not show any effect (Figure 3.15).

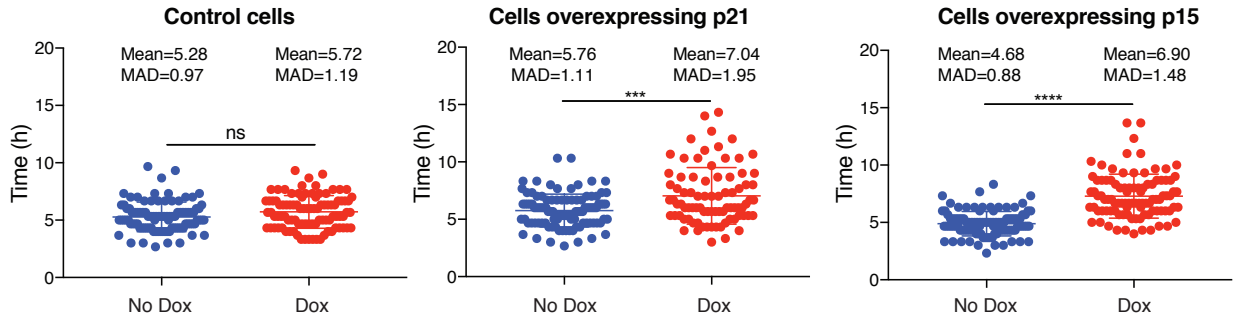


Figure 3.15 Overexpression of p15 or p21 in hESCs increases G1-phase length. Left panel G1-phase length measured by live-cell imaging in control cells in TeSR E5 in presence or absence of doxycycline. Mean and MAD are shown above in hours. KS test was performed to calculate *p-values* (ns= not significant) (n>100). Central panel G1-phase length measured by live-cell imaging in cells transduced with p15 inducible overexpression vector in TeSR E5 in presence or absence of doxycycline. Mean and MAD are shown above in hours. KS test was performed to calculate *p-values* (**** $p<0.0001$) (n>100). Right panel G1-phase length measured by live-cell imaging in cells transduced with p21 inducible overexpression vector in TeSR E5 in presence or absence of doxycycline. Mean and MAD are shown above in hours. KS test was performed to calculate *p-values* (**** $p<0.0001$) (n>100).

In order to observe G1-phase lengthening in lineages, the experiment was analysed following cells during two sequential divisions. Cdt1-YFP intensity was measured in every frame using Fiji and normalised by maximum intensity. G1-phase length was plotted as a function Cdt1-YFP intensity in time. Similarly to previous results, the G1-phase length of the second cell cycle division in cells overexpressing p15 or p21

was longer compared to control cells, as seen from the increasing length of the trace of Cdt1-YFP (Figure 3.16).

Taken together these results showed suggest that p15 and p21 expression of both induce lengthening of G1-phase length in hES cells.

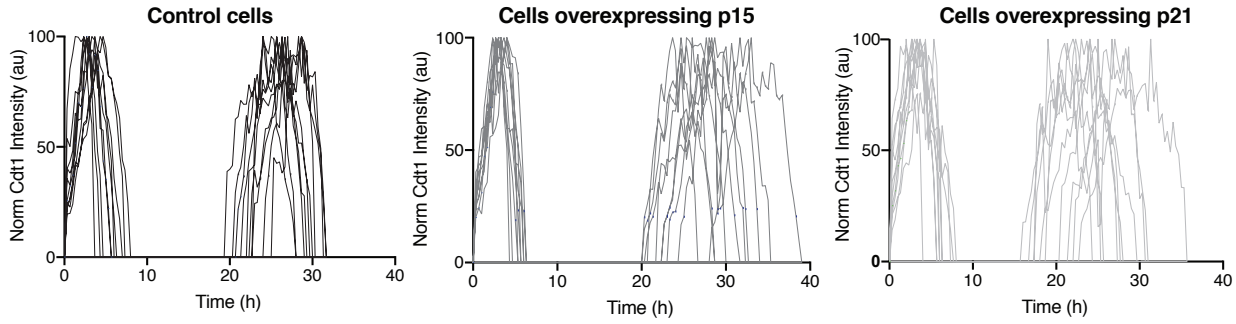


Figure 3.16 Cdt1-YFP can be used to plot G1-phase length to visualise lengthening due to overexpression of p15 and p21 in two consecutive divisions (lineages). Measurements of G1-phase length in stable hES cell lines expressing Cdt1-YFP and NLS in combination with the overexpression of p15, p21 or control empty vector
were used show G1-phase remodelling as a function of Cdt1-YFP normalized intensity in time. Cells were followed during two sequential divisions after adding doxycycline and imaged every 20 minutes. Cdt1-YFP intensity was measured in every frame, the highest value was set at a value of 100 and the others were normalized accordingly (n=10)

3.4.2 Cyclin A1 downregulation affects G1-phase lengthening in hESCs

Finally, in order to verify if Cyclin A1 has a role in G1-lengthening in hES cells, H1 expressing the Fucci(CA) biosensor were stably transfected with a doxycycline-inducible short hairpin RNA (shRNA) against CyclinA1. Fucci (CA) cells transfected with shEmpty vector were used as a control in the experiment. In this experiment, the Fucci(CA) biosensor was employed instead of Cdt1-YFP and NLS-mCherry due to the presence of a GFP fluorophore present in the shRNA vector that would have interfered with the Cdt1-YFP signal. The expression of shRNA against Cyclin A1 showed a down-regulation of about ~25% of Cyclin A1 protein after induction with doxycycline (Figure 3.17A).

Cells were imaged for two days in order to measure G1-phase length as previously described (2.4.1). Cells were transferred from mTeSR1 to TeSR E5, doxycycline was added to induce shRNA expression and cells were imaged for 2 days in order to measure G1-phase duration. We saw that G1-phase length was modestly, yet significantly, longer in the cells with down-regulation of Cyclin A1 (No dox: mean=1.87 hours; Dox: mean=2.46) (Figure 3.17). In conclusion, the down-regulation of cyclin A1 shows a significant effect on G1-phase length in hESCs.

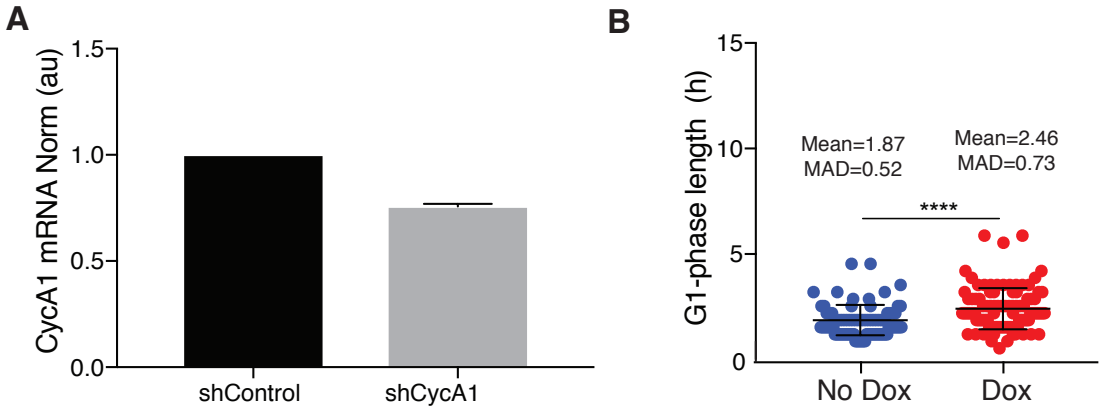


Figure 3.17 shRNA against cyclin A1 increases G1-phase length in hESCs. A. Levels of down-regulation of Cyclin A1 in inducible shRNA cell line expressing Fucci(CA) biosensor. Normalized downregulation was measured by qPCR in hES cell lines expressing empty vector (control cells) or shRNA against cyclin A1. Mean and standard deviation is shown (n=3). **B.** G1-phase length measured by live-cell imaging in cells transduced with shRNA against cyclin A1 in TeSR E5 in presence or absence of doxycycline. Mean and MAD are shown above in hours. KS test was performed to calculate *p-values* (**** $p<0.0001$) ($n>100$).

Chapter 4. Discussion

4.1 Cell cycle dynamics of hESCs changes during BMP4-driven differentiation

The first studies looking at the characteristics of hESCs cell cycle go back a little over 10 years ago when Becker and colleagues firstly investigated the abbreviated cell cycle of human ES cells. In their work, they employed techniques such as FACS analysis of DNA content, BrdU incorporation and Ki67 staining. They determined that 65% of hESCs reside in S-phase, 19% in G1-phase and 15.5% in G2-phase with a total cell cycle duration of 16 hours. Moreover, using a combination of BrdU incorporation and cell cycle inhibitors, G1-phase length was measured to be around 3 hours (Becker, Ghule et al. 2006). These first studies allowed to defy the short cell cycle duration of hESCs as one of the defining characteristics of self-renewal. Following studies showed that cell cycle and G1-phase lengthened within 3 days of early lineage reprogramming.

One of the aims of the work presented in this thesis was to study cell cycle remodelling by applying new techniques, employing cell cycle biosensor and live cell imaging, in order to obtain a quantitative understanding of how cell cycle changes in single cells during differentiation. This approach would be beneficial, allowing to study the dynamic change in cell cycle and its phases and avoiding the eventual artefacts that synchronization of cells can produce. Employing different types of cell cycle biosensors, such as PCNA coupled with NLS and the Fucci (CA) sensor, we were able to show differences in cell cycle phases length during hES differentiation. While S-phase and mitosis remained similar in hESCs and differentiated cells, G2-phase duration mildly decreased in its length following differentiation. The biggest variation was seen in G1-length that increased from 3 hours in hESCs to 7 hours in cells stimulated with BMP4 (Figure 3.1). These measurements, allowed for analysis of correlation between each phase with the overall cell cycle length, highlighting cell cycle trends in hES and differentiated cells (Figure 3.4). For example, S-phase and mitosis correlation with cell cycle length did not change with differentiation. S-phase duration correlated with cell cycle length in both hESCs and differentiated cells while mitosis duration was uncoupled from cell cycle length as seen before (Araujo, Gelens et al. 2016). On the other hand, duration of G2-phase changed correlation with differentiation while G1-phase showed the opposite behaviour. This type of analysis provides a further layer of information that allows to distinguish between pluripotent and differentiated cells. Analysis of correlations is a potentially helpful tool to understand whether events are coupled or uncoupled and can reveal memory. Importantly, in this case, they show that Gap phases are regulated differently in hES and differentiated cells.

In addition, analysis of cell lineages through cell division provided insight on whether the cell cycle remodelling process happens as a switch-like or graded transition. Our single-cell, real-time approach combining two different cell cycle biosensors (PCNA-YFP and NLS-mCherry; Cdt1-YFP and NLS-mCherry) and live cell imaging suggested that cell cycle and specifically G1-phase length remodels in a switch-like manner after 2 cell cycle divisions (Figure 3.9).

These preliminary results can be used in the future to understand the molecular mechanisms involved in cell cycle regulation in hES and differentiated cells. Moreover, they represent a step toward, a new way of studying cell cycle dynamics in single cells during the differentiation, that can add on the knowledge acquired though the classical population-based approaches.

4.2 The activity of cyclin dependent kinases might be responsible for G1-phase remodelling

The somatic cell cycle is a series of ordered events that is highly regulated to ensure that the genomic material of a mother cells is correctly replicated and equally divided in two daughter cells. Cell cycle progression is strictly regulated at the molecular level by the phase-specific activity of cyclin-dependent kinases (CDKs) that are activated by their regulatory subunits, cyclins. The main function of Cdks activation is to drive cell cycle progression in an orderly and timely manner. Moreover, Cdk activity is modulated at regulatory points by many different regulators: Cdk activating complex (CAK), Cdk phosphatases (es. Cdc25 proteins), kinases (es. Wee1) and Cdks inhibitors (Koledova, Kramer et al. 2010). Embryonic stem cells seem to lack some of these control mechanisms with the different Cdks constitutively active at any time in the cell cycle. Moreover, Cdk inhibitors show extremely low expression while cyclins have highly, non-cycling expression (Koledova, Kramer et al. 2010).

Studies conducted on the regulatory complex responsible for G1- to S-phase transition, Cdk2/cyclinE revealed an important role for Cdk2 in cell cycle regulation in hESCs. Down-regulation of this protein in these cells lead to changes in cell morphology and cell cycle arrest in G1-phase combined with downregulation of pluripotency markers and differentiation towards extraembryonic lineages. At the same time Cdks inhibitors (p27 and p21) showed an increased expression (Neganova, Zhang et al. 2009). Recent studies showed that Cdk1 potentially also has a fundamental role in hESCs cell cycle and maintenance of pluripotency. This kinase has been previously proven to be the master regulator of mammalian cell cycle (Santamaria, Barriere et al. 2007) and it is involved entry into and progression through mitosis. In hESCs, Cdk1 is highly expressed and known to directly bind Oct4, one of the main pluripotency factors, to establish pluripotency while inhibiting Cdx2, a differentiation factor (Li, Wang et al. 2012). Moreover, it has been shown that Cdk1 is regulated by Sox2 and Nanog (Boyer, Lee et al.

2005) and its down-regulation in these cells leads to loss of pluripotency and up-regulation of lineage specific markers (Neganova, Tilgner et al. 2014).

4.2.1 P15 and p21 overexpression induces G1-phase lengthening

Cdks activity seems to be fundamental in cell proliferation in hESCs, determining their cell cycle profile and maintaining their pluripotency state. RNA seq data (Gharibi et al., unpublished) previously obtained in the lab comparing hES and BMP4-treated (differentiated) cells showed that only three known regulators of Cdk activity are expressed differently at mRNA level (p15, p21 and cyclin A1). We sought to investigate their role in cell cycle remodelling.

Both p15 and p21 are Cdk4/6 and Cdk2 inhibitors respectively and are known to been involved in G1-phase regulation. During BMP4-driven differentiation, their levels increase at mRNA and protein levels (Figure 3.13). To verify whether they could have both an effect on G1-phase remodelling, we overexpressed them in stable hESC lines expressing Cdt1-YFP and NLS-mCherry biosensors in order to measure G1-phase and cell cycle length. In both cases, G1-phase length significantly increased in overexpressing cells comparatively to control hESCs (Figure 3.15). These results suggest a role for these proteins in G1-phase lengthening.

In agreement with these observations, previous studies performed in mouse ES cells showed that p21, combined with p27 played a role in the control of G1-phase length. In this case, the combined downregulation of p21 and p27 led to shorter G1-phase due to a loss of Cdk inhibition. The latter is responsible for the phosphorylation of Rb proteins that control progression through G1-phase. Even though mESCs and hESC have been derived from the same stage of development, their transcriptional profiles show differences between the two (Warrier, Van der Jeught et al. 2017). Another example, in which p21 has been shown to be fundamental in regulating cell cycle transitions, was given by Spencer and colleagues (Spencer, Cappell et al. 2013). They studied the decision undertaken by somatic cells between the proliferative and quiescent state and discovered that p21 is necessary and sufficient to determine Cdk2 activity levels in nascent cells. Depending on the levels of Cdk2 activity after mitosis the cells will either undergo proliferation (high Cdk2) or remain quiescent (low Cdk2) (Spencer, Cappell et al. 2013).

Finally, both p21 and p15 have been previously linked to differentiation processes. p21 is crucial in adult stem cells for restricting stem cell self-renewal in hematopoietic stem cells (Cheng, Rodrigues et al. 2000), forebrain stem cells (Kippin, Martens et al. 2005) and in myoblast differentiation in combination with p57 (Zhang, Wong et al. 1999) and fibroblasts differentiation in tandem with p16 (Stein, Drullinger et al. 1999). p15 on the other hand, is involved in neuronal differentiation together with p16 (Lois, Cooper et al. 1995) and in megakaryocytic differentiation (Teofili, Martini et al. 2001).

Interestingly, it has also been shown that both p21 and p15 are regulated by the TGF-beta pathway to block the cell cycle in G1-phase in many types of cancer (Hannon and Beach 1994, Robson, Gnanapragasam et al. 1999) and in the aging process (Carlson, Hsu et al. 2008).

4.2.2 Cyclin A1 down-regulation induces G1-phase lengthening

Cyclin A1 is one of the isoforms of cyclin A present in mammalian cells and it is abundantly expressed in the testes and in the male germline during meiosis in mouse (Sweeney, Murphy et al. 1996) while it is present at low levels in most other tissues. Moreover, it has been shown to be expressed in hematopoietic progenitor cells and in acute myeloid leukaemia (Muller-Tidow, Ji et al. 2004). Cyclin A2 is the isoform know to be ubiquitous in all somatic cells and it is expressed throughout S- and G2-phase and rapidly degraded at the onset of mitosis during the mitotic cell cycle (Geley, Kramer et al. 2001). Cyclin A1, on the other hand, shows a slightly different kinetics at protein level appearing to increase earlier during the cell cycle, in G0/G1 and then rising more gradually compared to cyclin A2 (Yang, Muller et al. 1999). The role of cyclin A1 in somatic cells still remains unknown.

Studies performed in mESCs highlighted the high abundance of cyclin A1-Cdk complexes compared to fibroblast, moreover cyclin A1-Cdk complexes are shown to predominate over cyclin E-Cdk complexes in these cells. This observation points towards a cyclin A1 dependency for cell cycle progression in mES cells (Kalaszczynska, Geng et al. 2009). However, the physiological role of cyclin A1 remains not completely understood.

Data from RNA seq analysis performed in our lab, showed that was one of the most significant genes that decreased at mRNA level during differentiation raising the hypothesis that cyclin A1 might be important for pluripotent cell division cycles. In order to verify if cyclin A1 has any effect on hES cell cycle, a stable H1 hES cell line expressing the Fucci (CA) biosensor and a shRNA against cyclin A1 was built. We saw that down-regulating cyclin A1 has a significant effect on G1-phase lengthening. However, when analysing these results, it is important to take in consideration the fact that these experiments were both performed in the male hES cell line, H1 confirm that this phenotype is not specific for male cells and to confirm cyclin A1 role in hES cell cycle, it would be ideal to repeat the experiments in a female hES cell line, such as H9 hESCs.

4.3 G1-phase is different in somatic and hES cells

As previously stated in the introduction of this thesis, cell cycle control in somatic and hES cells is different. Specifically, G1- to S-phase transition and G1-phase length are drastically different in these two cell types. Moreover, this work showed how G1 remodels during BMP4-driven differentiation, increasing its length in a switch-like manner and changing its correlation with total cell cycle duration (no correlation observed in hES cells, positive correlation established after 3 days of BMP4 treatment), potentially indicating that in pluripotent cell cycles G1-phase is not coupled to the other cell cycle phases (see results 3.1.2).

Overall the difference between G1-phase in hES and differentiated cells can be summarized as:

- Cyclins' expression: somatic cells have cyclic expression of cyclins while hESCs do not.
- Cdk activities: somatic cells have a Cdk activities that reflects the cyclic expression of cyclins while in hESCs Cdks are always in their active complexes with cyclins.
- Checkpoints regulation: differentiated cell cycle is regulated by checkpoint control while in hESCs checkpoints are downregulated.
- Response to external stimuli: to overcome checkpoint control somatic cells can integrate external stimuli to move forward in the cell cycle while hESCs do not rely on them to progress through cell cycle.

This last characteristic of hES cells can lead to some interesting questions. Since these cells do not rely on external cue to differentiate, we wondered whether hESCs retain prerequisite to be in G1-phase in order to integrate differentiation signals, the same way somatic cells do.
In order to investigate whether cells could read stimuli to differentiate in a cycle-dependent manner, a stable hES cell line expressing a modified version of the Fucci (SA) biosensor (described in 2.4.1), that allowed to distinguish between G1-phase and S/G2/M phases. Moreover, a marker for early mesoderm specification, GATA3, was employed to identify committed cells. This protein has been identified in the lab as a marker for early commitment in response to BMP4-treatment via the SMAD signalling pathway (Gunne-Braden et al., unpublished). hES cells expressing the modified Fucci (SA) biosensor were imaged for 16 hours prior to BMP4-stimulation, in order to know their cell cycle history and in which cell cycle phase cells were when they received the stimulus to differentiate. BMP4 was then added and cells were imaged for further 5 hours. At the end of this time, BMP4 was washed away and cells were fixed and stained for GATA3, allowing to determine how many and which cells were expressing the early commitment marker and importantly, where in the cell cycle these cells were when BMP4 was added. By

imaging cells for 16 hours prior to BMP4 stimulation, it was possible to pin down where cells were in the cell cycle when they received the stimulus to differentiate (Figure 4.1).

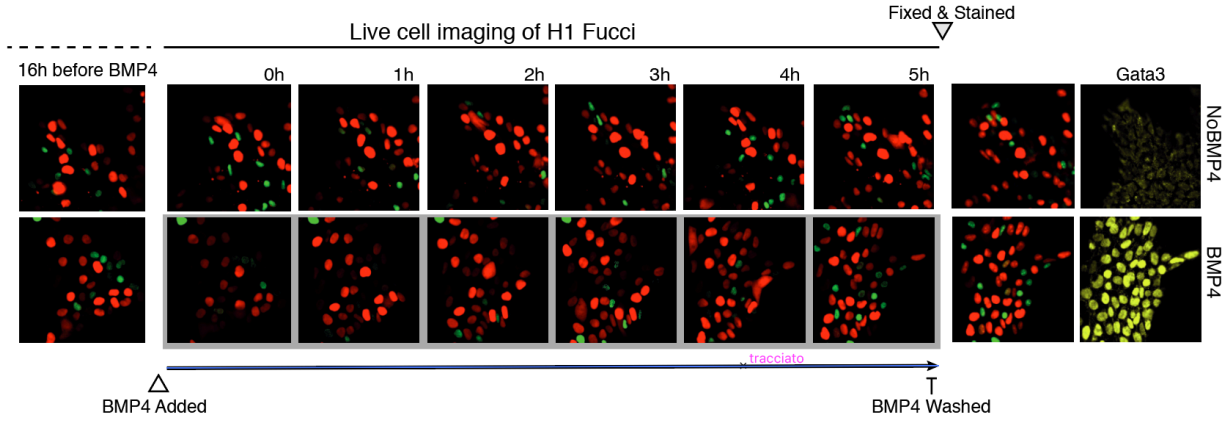


Figure 4.1 Experimental workflow used to determine the correlation between cell fate/commitment to differentiation and cell cycle in single cells. 16 hours of live cell imaging were followed by 5 hours of BMP4 stimulation and subsequent IF staining for the early commitment marker, GATA3.

Positive GATA3 cells were analysed to verify in which phase of the cell cycle were when they received the BMP4 stimulus. Approximately 30% of cells were in G1-phase while the rest was in S/G2/M phase. This distribution mirrors the normal cell cycle in hESCs (Figure 4.2A)

In order to verify if there was any correlation between expression of GATA3 and both cell cycle probes, the intensity of Cdt1 and Geminin was plotted against GATA3 intensity. The G1-phase marker, Cdt1, did not show any correlation with the early differentiation marker (Pearson correlation coefficient, $r = 0.35$). When plotting S/G2/M phase marker, Geminin, against GATA3 intensity a more significant correlation was shown (Pearson correlation coefficient, $r = 0.47$). in particular, two populations started to appear (Figure 4.2B). This result might be explained by the fact that cells could have switch phase during the 5 hours BMP4 treatment.

To take into consideration the possibility of cells switching phase during those 5 hours, a different analysis was performed considering two populations of GATA3 positive cells: cells that were in G1-phase or cells that were in S/G2/M phase at the end of the 5 hours treatment. Taken these two population of cells, we followed their cell cycle history back to determine whether cells were in G1- or S/G2/M phase when they received the BMP4 stimulus. As showed in Figure 4.2 C, 15% of cells remained in G1-phase for the full length of BMP4 treatment, while 85% of cells that were in S/G2/M phase at the beginning of BMP4 treatment switch to G1-phase during those 5 hours. On the other hand, 47% of cells progress from G1- to S/G2/M phase. Interestingly, 53% of cells remained in S/G2/M during BMP4 stimulation (Figure 4.2C) suggesting that G1-phase in hESCs might not be the only phase during where cells can decode external stimuli.

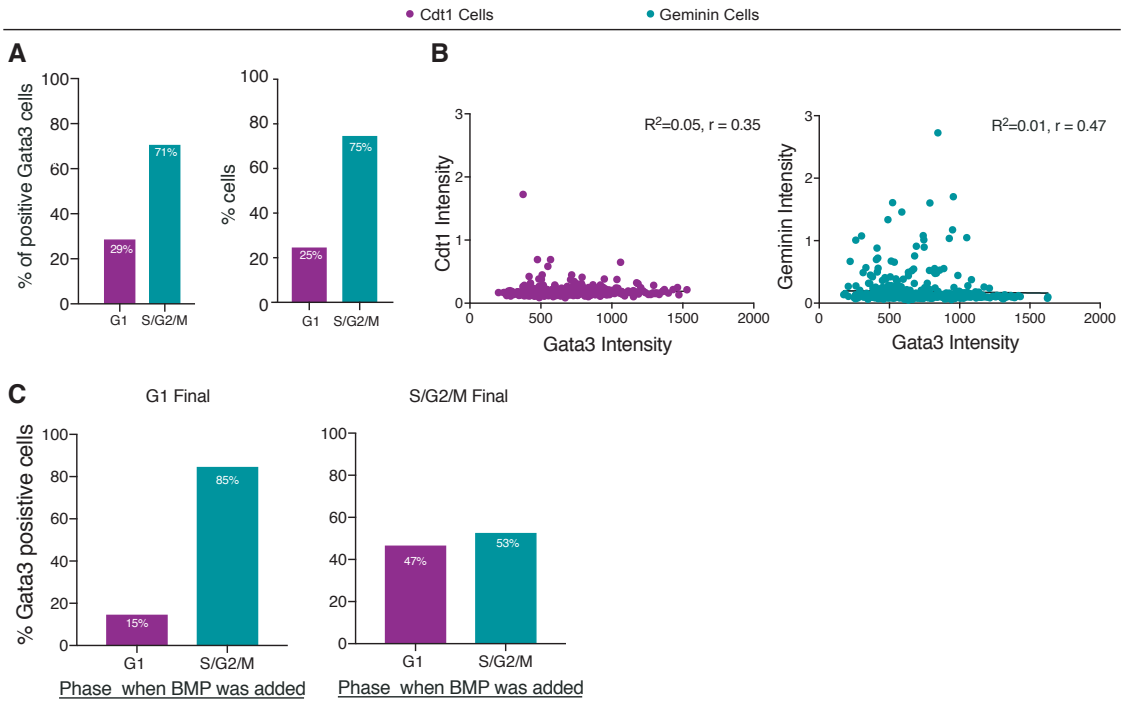


Figure 4.2 Correlation between cell cycle phases and commitment. A. Left plot: analysis of cell cycle distribution of GATA3 positive cells after 5 hours of BMP4 (50μg/ml) treatment. Right plot: analysis of the distribution of a generic population of cells in the cell cycle (n>100). **B.** Left plot: GATA3 intensity as a function of Cdt1 intensity in single cells. Right plot: GATA3 intensity as a function of Geminin intensity. Coefficient of determination (R^2) and Pearson correlation coefficient (r) are shown (n>500). **C.** GATA3 positive cells that were either in G1- or S/G2/M phase at the end of the experiment are separately plotted. In each graph is reported the percentage of cells (n>100) that were either in G1- or S/G2/M phase when BMP4 was added.

This preliminary result highlights further differences between G1-phase control in pluripotent and differentiated cells. Since G1-phase in hES cells is significantly shorter, it might be that these cells have different mechanisms that allow to integrate and respond to external signals compared to somatic cells. Further studies will be important to shed light on whether the same behaviour in hESCs is seen when differentiating towards different lineages.

4.4 The cell cycle remodels after 3 days of BMP4 treatment, but how many cell divisions is this?

Upon BMP4-driven differentiation, hES cells undergo several changes: visible morphology alteration, global variation in gene expression (Wang, Oron et al. 2012), epigenetic modifications (Gifford, Ziller et al. 2013, Xie, Schultz et al. 2013) and finally cell cycle remodelling all happening within 3 days. As shown in Chapter 3 of this thesis, G1-phase lengthening is one of the most striking cell cycle changes observed during differentiation. Employing cell cycle biosensors and live cell imaging, this study has shown at single cell level that G1-phase remodels during differentiation in a switch-like manner. During sustained stimulation with BMP4 driving hESCs towards the mesoderm lineage, cells start to remodel G1-phase length after 2 cell cycle divisions (as seen in 3.3). In order to verify if the timing of G1-phase remodelling had any correlation with the expression of differentiation markers, the following experiment was performed: H1 hES cells expressing NLS-mCherry biosensor were imaged for 36 hours in presence of BMP4 to measure subsequent cell divisions. Imaging for 36 hours, due to cell cycle length variation, allowed to capture cells that divided either 2, 3 or 4 times. After 36 hours, BMP4 was washed away and immunofluorescence assay (IF) was performed fixing and staining cells for two differentiation markers specific for mesoderm, Cdx2 and Brachyury (Bry) (Bernardo, Faial et al. 2011). Protein levels for Cdx2 and Bry were quantified using Cell Profiler software in order to identify positive cells for each marker. Finally, the number of cell divisions for positive cells was determined by analysing the live cell imaging (Figure 4.3).

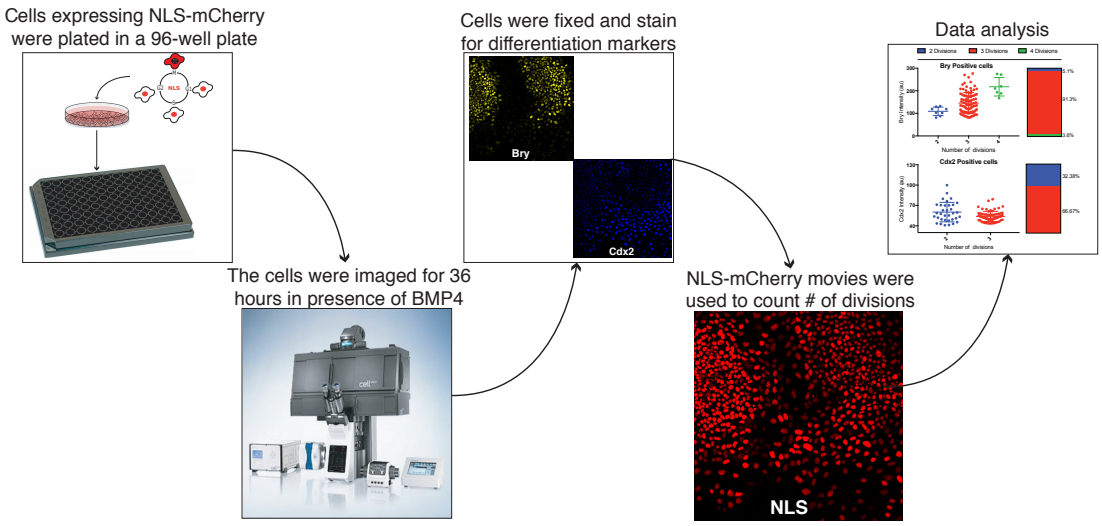


Figure 4.3 Pipeline to study the correlation between differentiation markers expression and cell division during BMP4-driven differentiation. hES cell line expressing NLS-m-Cherry biosensor were plated in a 96-well imaging plate. Cells were imaged for 36 hours every 20 minutes in presence of BMP4. After 36 hours, the BMP4 was wash away and cells were fixed and stained for mesoderm specific markers (Cdx2 and Bry). Positive cells for these markers were traced back to determine the number of cell divisions they went through during the BMP4 treatment. Data was analysed to determine correlation between number of cell division cycles and expression of differentiation markers.

This analysis showed that 91.3% of cells expressing Brachyury went through 3 divisions while 5.1% only divided twice and 3.6% of positive cells divided four times and showed higher values of Bry intensity. On the other hand, 32.38% of positive cells for Cdx2 divided twice while 66.6% divided three times (Figure 4.4).

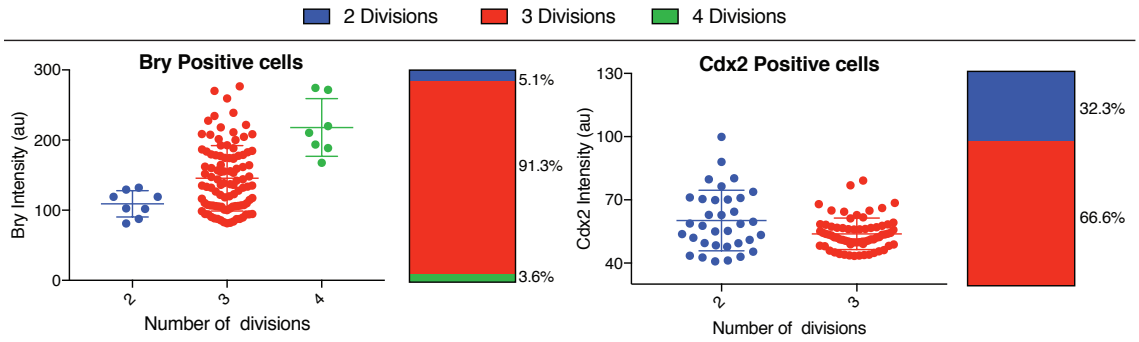


Figure 4.4 Differentiation markers are expressed after at least 2 divisions in hESC during BMP4-driven differentiation. Dot plots show positive cells for Bry and Cdx2 plotted depending on the number of cell division that the cell went through since the start of BMP4-stimulation. Bar graphs show quantify as a percentage what shown in the dot plots (n=100).

Taken together these results suggest that the expression of differentiation markers follows the same dynamics of cell cycle and G1-phase remodelling, needing at least 3 division before starting to rise.

The down regulation of pluripotency genes and the upregulation of differentiation genes happen simultaneously during hESC differentiation. Interplay between pluripotency genes and cell cycle regulators has been reported. For example, Nanog can directly bind Cdk6 and Cdc25A promoters, which encode for proteins involved in the G1/S transition (Zhang, Neganova et al. 2009). It is interesting to observe that the expression of differentiation markers shows a certain level of correlation with cell division. Further experiments will be necessary in order to confirm this correlation and understanding which are the mechanisms underlying these processes.

4.5 Cell cycle biosensors and live cell imaging: advantages and disadvantages

Research studies on cell cycle have been fundamental to understand the mechanisms controlling this life-depending process. Great knowledge has been derived from studies employing techniques that analysed static population of cells, such as DNA synthesis and levels of cell cycle regulators. However, most of these methods rely on cell-fixation, that only offers a snapshot view of the cell cycle, or on cell synchronization, that can affect the natural cell cycle dynamics.

Recent years have seen the development of new tools, known as cell cycle biosensors, that have opened a new horizon for cell cycle studies. These biosensors combined with live cell imaging have now open the doors to a new way of studying cell cycle dynamics with the advantage of having a high resolution, single cell, real time approach. Moreover, these tools can be very useful for comparative studies of cell cycle dynamics of different type of cells.

One of the aims of the work presented in this thesis was to establish stable hES cell lines expressing cell cycle biosensors that allowed to measure cell cycle dynamics during differentiation. In order to monitor all cell cycle phases and the overall changes in cell cycle dynamics, two biosensors were employed: PCNA-YFP and NLS-mCherry and Fucci (CA) (described in chapter 2 and 3). To avoid that any artefacts would be induced by the over-expression of these biosensors in the cells, few precautions were taken. Firstly, cell lines were sorted by FACS selecting for lowest levels of expression but still distinguishable from non-expressing cells. Secondly, two different biosensors were used to measure each cell cycle phase.

The results obtained with these two biosensors were comparable, when looking at cell cycle dynamics. However, slight differences could also be noted. This discrepancy can be due to quantification error in how different cell cycle phases are recognised and measured. For example, the end of G1-phase using in the PCNA-YFP and NLS-mCherry sensor is determined by the appearance of nuclear speckles that can be more challenging to detect compared to the disappearance of Cdt1-mCherry signal that is used in the Fucci (CA) biosensor to resolve G1-phase duration. Moreover, the S- to G2-phase transition can be challenging to determine with the Fucci (CA) sensor since it requires to identify the accumulation of Cdt1-mCherry in cells that are already expressing Geminin-YFP. Unlike its degradation at the end of G1-phase, Cdt1-mCherry accumulates slowly starting at the beginning of G2-phase, making the boundary between S- and G2-phase more difficult to determine. On the other hand, the PCNA-YFP and NLS-mCherry allows an easier identification of this transition that is observed by the rapid disappearance of nuclear speckles. These observations highlight the need for using multiple cell cycle biosensors when quantitatively measuring cell cycle dynamics.

4.6 hES cells as a novel model system to study cell cycle remodelling

The cell cycle has been studied through the years employing many different model organisms from yeast to human cell lines. The early processes of development have been studied as well in a wide range of organisms, both invertebrate and vertebrate. In order to study both these processes in this work, we decided to use human ES cells. These cells have been previously adopted in studies focused on understanding the principal events involved in early human development and have been proven to be a great *in vitro* system to test *in vivo* processes. Even though many important studies have been previously performed in mouse ES cells, translating the results to humans is not always easy. This is due to the fact that species-specific differences have developed during evolution and also to the difficulty in comparing different stages of development.

When studying the cell cycle remodelling during differentiation, hESCs show a series of advantages compared to previously used models:

- Easy to manipulate: cells can grow in different format vessels allowing for high-throughput analysis, allow for genetic manipulation and can proliferate in culture indefinitely.
- Can be differentiated towards the 3 primary germ layers that will give rise to all cell types in the body and differentiation protocols are usually short.
- Trackable: they grow in 2D colonies and are easy to follow in live cell experiments.
- Important role in clinical research: they share multiple characteristics with cancer cells and iPS cells and they can be used as a model to study human development.

hES and cancer cells share a similar cell cycle profile, displaying a shorter proliferation time and absence of the main cell cycle checkpoints control. However, hESCs maintain their ability to respond to external stimuli and differentiate to form a full organism while cancer cells induce pathological outcomes. Understanding the mechanisms controlling hES cell cycle and comparing them with those acting in cancer cells might be useful in order to define the important players in diseased cells.
Finally studying cell cycle remodelling in hES cells will be important to improve reprogramming techniques. It has been previously demonstrated that cell cycle regulation seen in hES cells is fundamental in self-renewal and pluripotency (Ruiz, Diep et al. 2012). Moreover, the reversion to a short cell cycle in human induced pluripotent stem cells (hIPSCs) is one of the characteristics established during the later stages of reprogramming (Singh, Chappell et al. 2014). The overexpression of cyclin D1/D2 or cyclin E2, controlling Cdks activity, together with the inhibition of the p53/p21 pathway have been shown to increase remodelling efficiency (Hanna, Saha et al. 2009, Ruiz, Diep et al. 2012)

Taken together, these discoveries suggest how studying cell cycle remodelling in hESCs could improve the efficiency of the current techniques employed in cell reprogramming and highlight the power of using hESCs as a model system to study cell cycle regulation.

Chapter 5. Future perspectives and final conclusions

5.1 Cdk activity is key for cell cycle remodelling during hES differentiation

The work presented in this thesis was aimed to establish and use methodologies to monitor and quantitatively measure changes in cell cycle dynamics during hES cells BMP4-driven differentiation. The knowledge derived from these studies highlighted the fundamental role of Cdk activity and its control during differentiation as playing a central role in cell cycle remodelling during differentiation. Further studies will be crucial to better understand the role of Cdks activity in this process. First, it would be important to understand whether specific Cdk activities are needed or whether global changes in Cdk activity are sufficient for cell cycle changes. One way to address this is to test Cdks pharmacological inhibitors, already available on the market, in order to verify whether inhibiting Cdks activity can drive differentiation. Moreover, using inhibitors specific for each Cdks, such as Palbociclib (Cdk4/6), Roscovitine (Cdk2) and RO-3306 (Cdk1), will enable us to investigate which Cdk activity has role in the remodelling process, whether is a specific one, a combination or any of them acts on cell cycle remodelling. The use of these inhibitors can be combined with live cell imaging and cell cycle biosensors to assess their effect on cell cycle dynamics. In addition, the expression of pluripotency and differentiation markers could be investigated at mRNA and protein level through IF and qPCR experiments to gain knowledge on whether Cdk activation impacts on pluripotency and/or differentiation in addition to cell cycle remodelling. The use of pharmacological inhibitors could then be combined with genetic knockdowns of individual Cdks using CRISPR technology.

5.2 Cell fate specificity in cell cycle remodelling

Finally, it would be important to investigate whether the mechanisms involved in cell cycle remodelling during BMP4-driven mesoderm differentiation are conserved during the differentiation towards other germ layers. Protocols to differentiate cells towards the endoderm and ectoderm lineage are already been developed (Xu, Chen et al. 2002, Chambers, Fasano et al. 2009, Evseenko, Zhu et al. 2010, Bernardo, Faial et al. 2011) and preliminary data from the lab (Gunne-Braden et al., unpublished) showed that the dynamics of cell cycle remodelling happens in all differentiation protocols (Figure 5.1). In the future, it could be interesting to explore how Cdks inhibitors, such as p15 and p21, and activators are expressed throughout differentiation towards different lineages and if inhibiting Cdks activity, as described previously, affects cell cycle remodelling in other lineages as well.

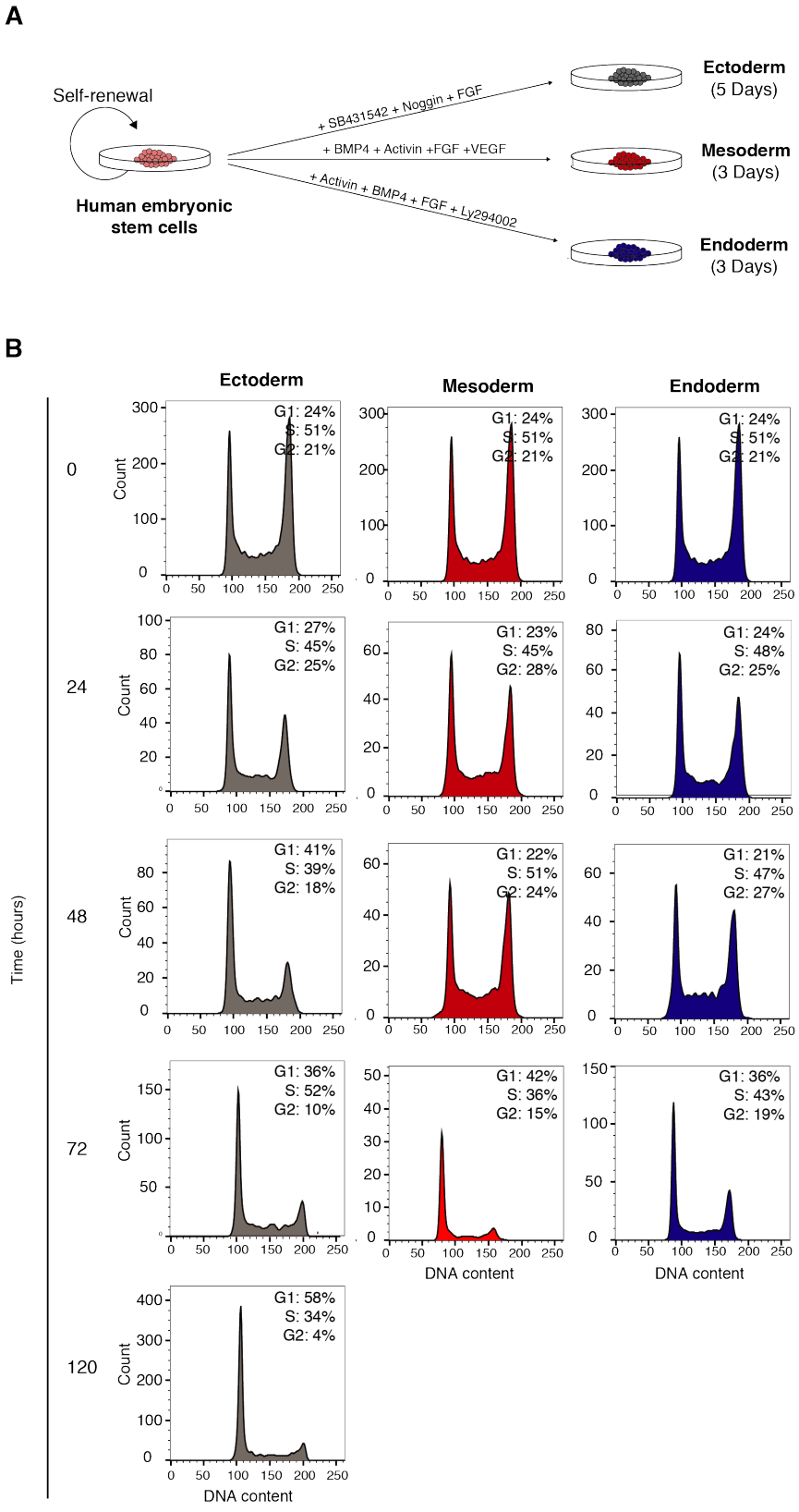


Figure 5.1 Cell cycle remodels with different speeds depending on cell fate. A. hESC can be differentiated in the 3 germ layers using protocols available from literature **B.** Plots show DNA content measured by propidium iodide during 120 hours of differentiation towards ectoderm, trophoblast, mesoderm and endoderm (Gunne-Braden et al., unpublished).

Final Conclusions

The differences between the somatic and pluripotent cell cycles have been studied in the last 20 years mainly by looking at levels of mRNA and proteins in population of fixed cells. Furthermore, most of these studies were performed in mouse ES cells, while less of them focused on human ES cells.

The work presented in this thesis aimed at gaining further knowledge on how the cell cycle changes during BMP4-driven hES cells differentiation by employing cell cycle biosensors combined with live cell imaging in order to quantitatively characterise cell cycle dynamics in single hES cells.
We show that cell cycle dynamics of hESCs, specifically Gap phases, changes during differentiation in live, single cells. The correlation between cell cycle duration and Gap phases length also changes after differentiation suggesting a potentially different regulatory mechanism for these phases in hES and differentiated cells. In addition, we provided evidence that G1-phase remodelling happens in a switch-like manner during BMP4-treatment.

Secondly, we show that the activity of cyclin-dependent kinases might be responsible for G1-phase remodelling. Previous data obtained from our lab (Gharibi et al., unpublished) highlighted 3 known regulators of Cdk activity, p15, p21 and cyclin A1, to be differentially expressed at mRNA in hES and differentiate cells. Upregulation of p15 and p21 and downregulation of cyclin A1 induced G1-phase lengthening in hESCs, confirmed the role of these proteins in cell cycle regulation in hESCs. These results emphasized the central role of Cdk activity and its control during differentiation. Further studies will be necessary to understand whether specific or global Cdk activity are sufficient for cell cycle remodelling and whether they might affect the differentiation process.

The methodologies employed in this work, combining stable hES cell lines expressing cell cycle biosensors and live cell imaging followed by single cell analysis, showed how hESCs could be used a model system to study cell cycle. Our work highlights the many advantages of studying cell cycle regulation in these cells and how they can improve our knowledge of physiological events and propose that hESCs can be used in the future to study pathological mechanisms.

References

Abe, T., A. Sakaue-Sawano, H. Kiyonari, G. Shioi, K. Inoue, T. Horiuchi, K. Nakao, A. Miyawaki, S. Aizawa and T. Fujimori (2013). "Visualization of cell cycle in mouse embryos with Fucci2 reporter directed by Rosa26 promoter." Development **140**(1): 237-246.

Araujo, A. R., L. Gelens, R. S. Sheriff and S. D. Santos (2016). "Positive Feedback Keeps Duration of Mitosis Temporally Insulated from Upstream Cell-Cycle Events." Mol Cell **64**(2): 362-375.

Artus, J., C. Babinet and M. Cohen-Tannoudji (2006). "The cell cycle of early mammalian embryos: lessons from genetic mouse models." Cell Cycle **5**(5): 499-502.

Bajar, B. T., A. J. Lam, R. K. Badiee, Y. H. Oh, J. Chu, X. X. Zhou, N. Kim, B. B. Kim, M. Chung, A. L. Yablonovitch, B. F. Cruz, K. Kulalert, J. J. Tao, T. Meyer, X. D. Su and M. Z. Lin (2016). "Fluorescent indicators for simultaneous reporting of all four cell cycle phases." Nat Methods **13**(12): 993-996.

Ballabeni, A., I. H. Park, R. Zhao, W. Wang, P. H. Lerou, G. Q. Daley and M. W. Kirschner (2011). "Cell cycle adaptations of embryonic stem cells." Proc Natl Acad Sci U S A **108**(48): 19252-19257.

Barnum, K. J. and M. J. O'Connell (2014). "Cell cycle regulation by checkpoints." Methods Mol Biol **1170**: 29-40.

Becker, K. A., P. N. Ghule, J. A. Therrien, J. B. Lian, J. L. Stein, A. J. van Wijnen and G. S. Stein (2006). "Self-renewal of human embryonic stem cells is supported by a shortened G1 cell cycle phase." J Cell Physiol **209**(3): 883-893.

Bernardo, A. S., T. Faial, L. Gardner, K. K. Niakan, D. Ortmann, C. E. Senner, E. M. Callery, M. W. Trotter, M. Hemberger, J. C. Smith, L. Bardwell, A. Moffett and R. A. Pedersen (2011). "BRACHYURY and CDX2 mediate BMP-induced differentiation of human and mouse pluripotent stem cells into embryonic and extraembryonic lineages." Cell Stem Cell **9**(2): 144-155.

Bertoli, C., J. M. Skotheim and R. A. de Bruin (2013). "Control of cell cycle transcription during G1 and S phases." Nat Rev Mol Cell Biol **14**(8): 518-528.

Besson, A., S. F. Dowdy and J. M. Roberts (2008). "CDK inhibitors: cell cycle regulators and beyond." Dev Cell **14**(2): 159-169.

Boyer, L. A., T. I. Lee, M. F. Cole, S. E. Johnstone, S. S. Levine, J. P. Zucker, M. G. Guenther, R. M. Kumar, H. L. Murray, R. G. Jenner, D. K. Gifford, D. A. Melton, R. Jaenisch and R. A. Young (2005). "Core transcriptional regulatory circuitry in human embryonic stem cells." Cell **122**(6): 947-956.

Bravo, R., R. Frank, P. A. Blundell and H. Macdonald-Bravo (1987). "Cyclin/PCNA is the auxiliary protein of DNA polymerase-delta." Nature **326**(6112): 515-517.

Cao, L., F. Chen, X. Yang, W. Xu, J. Xie and L. Yu (2014). "Phylogenetic analysis of CDK and cyclin proteins in premetazoan lineages." BMC Evol Biol **14**: 10.

Carlson, M. E., M. Hsu and I. M. Conboy (2008). "Imbalance between pSmad3 and Notch induces CDK inhibitors in old muscle stem cells." Nature **454**(7203): 528-532.

Chambers, S. M., C. A. Fasano, E. P. Papapetrou, M. Tomishima, M. Sadelain and L. Studer (2009). "Highly efficient neural conversion of human ES and iPS cells by dual inhibition of SMAD signaling." Nat Biotechnol **27**(3): 275-280.

Cheng, T., N. Rodrigues, H. Shen, Y. Yang, D. Dombkowski, M. Sykes and D. T. Scadden (2000). "Hematopoietic stem cell quiescence maintained by p21cip1/waf1." Science **287**(5459): 1804-1808.

Coudreuse, D. and P. Nurse (2010). "Driving the cell cycle with a minimal CDK control network." Nature **468**(7327): 1074-1079.

Evseenko, D., Y. Zhu, K. Schenke-Layland, J. Kuo, B. Latour, S. Ge, J. Scholes, G. Dravid, X. Li, W. R. MacLellan and G. M. Crooks (2010). "Mapping the first stages of mesoderm commitment during differentiation of human embryonic stem cells." Proc Natl Acad Sci U S A **107**(31): 13742-13747.

Fellmann, C., T. Hoffmann, V. Sridhar, B. Hopfgartner, M. Muhar, M. Roth, D. Y. Lai, I. A. Barbosa, J. S. Kwon, Y. Guan, N. Sinha and J. Zuber (2013). "An optimized microRNA backbone for effective single-copy RNAi." Cell Rep **5**(6): 1704-1713.

Fluckiger, A. C., G. Marcy, M. Marchand, D. Negre, F. L. Cosset, S. Mitalipov, D. Wolf, P. Savatier and C. Dehay (2006). "Cell cycle features of primate embryonic stem cells." Stem Cells **24**(3): 547-556.

Fujii-Yamamoto, H., J. M. Kim, K. Arai and H. Masai (2005). "Cell cycle and developmental regulations of replication factors in mouse embryonic stem cells." J Biol Chem **280**(13): 12976-12987.

Geley, S., E. Kramer, C. Gieffers, J. Gannon, J. M. Peters and T. Hunt (2001). "Anaphase-promoting complex/cyclosome-dependent proteolysis of human cyclin A starts at the beginning of mitosis and is not subject to the spindle assembly checkpoint." J Cell Biol **153**(1): 137-148.

Gerard, C. and A. Goldbeter (2009). "Temporal self-organization of the cyclin/Cdk network driving the mammalian cell cycle." Proc Natl Acad Sci U S A **106**(51): 21643-21648.

Gibson, D. G., L. Young, R. Y. Chuang, J. C. Venter, C. A. Hutchison, 3rd and H. O. Smith (2009). "Enzymatic assembly of DNA molecules up to several hundred kilobases." Nat Methods **6**(5): 343-345.

Gifford, C. A., M. J. Ziller, H. Gu, C. Trapnell, J. Donaghey, A. Tsankov, A. K. Shalek, D. R. Kelley, A. A. Shishkin, R. Issner, X. Zhang, M. Coyne, J. L. Fostel, L. Holmes, J. Meldrim, M. Guttman, C. Epstein, H. Park, O. Kohlbacher, J. Rinn, A. Gnirke, E. S. Lander, B. E. Bernstein and A. Meissner (2013). "Transcriptional and epigenetic dynamics during specification of human embryonic stem cells." Cell **153**(5): 1149-1163.

Guhr, A., A. Kurtz, K. Friedgen and P. Loser (2006). "Current state of human embryonic stem cell research: an overview of cell lines and their use in experimental work." Stem Cells **24**(10): 2187-2191.

Hanna, J., K. Saha, B. Pando, J. van Zon, C. J. Lengner, M. P. Creyghton, A. van Oudenaarden and R. Jaenisch (2009). "Direct cell reprogramming is a stochastic process amenable to acceleration." Nature **462**(7273): 595-601.

Hannon, G. J. and D. Beach (1994). "p15INK4B is a potential effector of TGF-beta-induced cell cycle arrest." Nature **371**(6494): 257-261.

Hartwell, L. H., R. K. Mortimer, J. Culotti and M. Culotti (1973). "Genetic Control of the Cell Division Cycle in Yeast: V. Genetic Analysis of cdc Mutants." Genetics **74**(2): 267-286.

Hartwell, L. H. and T. A. Weinert (1989). "Checkpoints: controls that ensure the order of cell cycle events." Science **246**(4930): 629-634.

Jeffrey, P. D., A. A. Russo, K. Polyak, E. Gibbs, J. Hurwitz, J. Massague and N. P. Pavletich (1995). "Mechanism of CDK activation revealed by the structure of a cyclinA-CDK2 complex." Nature **376**(6538): 313-320.

Julian, L. M., R. L. Carpenedo, J. L. Rothberg and W. L. Stanford (2016). "Formula G1: Cell cycle in the driver's seat of stem cell fate determination." Bioessays **38**(4): 325-332.

Kalaszczynska, I., Y. Geng, T. Iino, S. Mizuno, Y. Choi, I. Kondratiuk, D. P. Silver, D. J. Wolgemuth, K. Akashi and P. Sicinski (2009). "Cyclin A is redundant in fibroblasts but essential in hematopoietic and embryonic stem cells." Cell **138**(2): 352-365.

Kapinas, K., R. Grandy, P. Ghule, R. Medina, K. Becker, A. Pardee, S. K. Zaidi, J. Lian, J. Stein, A. van Wijnen and G. Stein (2013). "The abbreviated pluripotent cell cycle." J Cell Physiol **228**(1): 9-20.

Kippin, T. E., D. J. Martens and D. van der Kooy (2005). "p21 loss compromises the relative quiescence of forebrain stem cell proliferation leading to exhaustion of their proliferation capacity." Genes Dev **19**(6): 756-767.

Koledova, Z., A. Kramer, L. R. Kafkova and V. Divoky (2010). "Cell-cycle regulation in embryonic stem cells: centrosomal decisions on self-renewal." Stem Cells Dev **19**(11): 1663-1678.

Lake, J., J. Rathjen, J. Remiszewski and P. D. Rathjen (2000). "Reversible programming of pluripotent cell differentiation." J Cell Sci **113 (Pt 3)**: 555-566.

Leonhardt, H., H. P. Rahn, P. Weinzierl, A. Sporbert, T. Cremer, D. Zink and M. C. Cardoso (2000). "Dynamics of DNA replication factories in living cells." J Cell Biol **149**(2): 271-280.

Li, L., J. Wang, J. Hou, Z. Wu, Y. Zhuang, M. Lu, Y. Zhang, X. Zhou, Z. Li, W. Xiao and W. Zhang (2012). "Cdk1 interplays with Oct4 to repress differentiation of embryonic stem cells into trophectoderm." FEBS Lett **586**(23): 4100-4107.

Livak, K. J. and T. D. Schmittgen (2001). "Analysis of relative gene expression data using real-time quantitative PCR and the 2(-Delta Delta C(T)) Method." Methods **25**(4): 402-408.

Lois, A. F., L. T. Cooper, Y. Geng, T. Nobori and D. Carson (1995). "Expression of the p16 and p15 cyclin-dependent kinase inhibitors in lymphocyte activation and neuronal differentiation." Cancer Res **55**(18): 4010-4013.

Lukas, J., J. Bartkova and J. Bartek (1996). "Convergence of mitogenic signalling cascades from diverse classes of receptors at the cyclin D-cyclin-dependent kinase-pRb-controlled G1 checkpoint." Mol Cell Biol **16**(12): 6917-6925.

Lukas, J., T. Herzinger, K. Hansen, M. C. Moroni, D. Resnitzky, K. Helin, S. I. Reed and J. Bartek (1997). "Cyclin E-induced S phase without activation of the pRb/E2F pathway." Genes Dev **11**(11): 1479-1492.

Mailand, N., J. Falck, C. Lukas, R. G. Syljuasen, M. Welcker, J. Bartek and J. Lukas (2000). "Rapid destruction of human Cdc25A in response to DNA damage." Science **288**(5470): 1425-1429.

Malumbres, M. and M. Barbacid (2009). "Cell cycle, CDKs and cancer: a changing paradigm." Nat Rev Cancer **9**(3): 153-166.

Muller-Tidow, C., P. Ji, S. Diederichs, J. Potratz, N. Baumer, G. Kohler, T. Cauvet, C. Choudary, T. van der Meer, W. Y. Chan, C. Nieduszynski, W. H. Colledge, M. Carrington, H. P. Koeffler, A. Restle, L. Wiesmuller, J. Sobczak-Thepot, W. E. Berdel and H. Serve (2004). "The cyclin A1-CDK2 complex regulates DNA double-strand break repair." Mol Cell Biol **24**(20): 8917-8928.

Murray, A. W. and M. W. Kirschner (1989). "Cyclin synthesis drives the early embryonic cell cycle." Nature **339**(6222): 275-280.

Nakayama, K. and K. Nakayama (1998). "Cip/Kip cyclin-dependent kinase inhibitors: brakes of the cell cycle engine during development." Bioessays **20**(12): 1020-1029.

Neganova, I., K. Tilgner, A. Buskin, I. Paraskevopoulou, S. P. Atkinson, D. Peberdy, J. F. Passos and M. Lako (2014). "CDK1 plays an important role in the maintenance of pluripotency and genomic stability in human pluripotent stem cells." Cell Death Dis **5**: e1508.

Neganova, I., X. Zhang, S. Atkinson and M. Lako (2009). "Expression and functional analysis of G1 to S regulatory components reveals an important role for CDK2 in cell cycle regulation in human embryonic stem cells." Oncogene **28**(1): 20-30.

Nigg, E. A. (1995). "Cyclin-dependent protein kinases: key regulators of the eukaryotic cell cycle." Bioessays **17**(6): 471-480.

Nishitani, H., Z. Lygerou, T. Nishimoto and P. Nurse (2000). "The Cdt1 protein is required to license DNA for replication in fission yeast." Nature **404**(6778): 625-628.

Nurse, P. (1994). "Ordering S phase and M phase in the cell cycle." Cell **79**(4): 547-550.

Nurse, P., P. Thuriaux and K. Nasmyth (1976). "Genetic control of the cell division cycle in the fission yeast Schizosaccharomyces pombe." Mol Gen Genet **146**(2): 167-178.

Pedersen, R. A. (1994). "Studies of in vitro differentiation with embryonic stem cells." Reprod Fertil Dev **6**(5): 543-552.

Prelich, G., C. K. Tan, M. Kostura, M. B. Mathews, A. G. So, K. M. Downey and B. Stillman (1987). "Functional identity of proliferating cell nuclear antigen and a DNA polymerase-delta auxiliary protein." Nature **326**(6112): 517-520.

Robson, C. N., V. Gnanapragasam, R. L. Byrne, A. T. Collins and D. E. Neal (1999). "Transforming growth factor-beta1 up-regulates p15, p21 and p27 and blocks cell cycling in G1 in human prostate epithelium." J Endocrinol **160**(2): 257-266.

Ruiz, S., D. Diep, A. Gore, A. D. Panopoulos, N. Montserrat, N. Plongthongkum, S. Kumar, H. L. Fung, A. Giorgetti, J. Bilic, E. M. Batchelder, H. Zaehres, N. G. Kan, H. R. Scholer, M. Mercola, K. Zhang and J. C. Izpisua Belmonte (2012). "Identification of a specific reprogramming-associated epigenetic signature in human induced pluripotent stem cells." Proc Natl Acad Sci U S A **109**(40): 16196-16201.

Sakaue-Sawano, A., H. Kurokawa, T. Morimura, A. Hanyu, H. Hama, H. Osawa, S. Kashiwagi, K. Fukami, T. Miyata, H. Miyoshi, T. Imamura, M. Ogawa, H. Masai and A. Miyawaki (2008). "Visualizing spatiotemporal dynamics of multicellular cell-cycle progression." Cell **132**(3): 487-498.

Sakaue-Sawano, A., M. Yo, N. Komatsu, T. Hiratsuka, T. Kogure, T. Hoshida, N. Goshima, M. Matsuda, H. Miyoshi and A. Miyawaki (2017). "Genetically Encoded Tools for Optical Dissection of the Mammalian Cell Cycle." Mol Cell **68**(3): 626-640.e625.

Santamaria, D., C. Barriere, A. Cerqueira, S. Hunt, C. Tardy, K. Newton, J. F. Caceres, P. Dubus, M. Malumbres and M. Barbacid (2007). "Cdk1 is sufficient to drive the mammalian cell cycle." Nature **448**(7155): 811-815.

Satyanarayana, A. and P. Kaldis (2009). "Mammalian cell-cycle regulation: several Cdks, numerous cyclins and diverse compensatory mechanisms." Oncogene **28**(33): 2925-2939.

Savatier, P., H. Lapillonne, L. A. van Grunsven, B. B. Rudkin and J. Samarut (1996). "Withdrawal of differentiation inhibitory activity/leukemia inhibitory factor up-regulates D-type cyclins and cyclin-dependent kinase inhibitors in mouse embryonic stem cells." Oncogene **12**(2): 309-322.

Schratt, G., B. Weinhold, A. S. Lundberg, S. Schuck, J. Berger, H. Schwarz, R. A. Weinberg, U. Ruther and A. Nordheim (2001). "Serum response factor is required for immediate-early gene activation yet is dispensable for proliferation of embryonic stem cells." Mol Cell Biol **21**(8): 2933-2943.

Sherr, C. J. and F. McCormick (2002). "The RB and p53 pathways in cancer." Cancer Cell **2**(2): 103-112.

Shiomi, Y., N. Suenaga, M. Tanaka, A. Hayashi and H. Nishitani (2014). "Imaging analysis of cell cycle-dependent degradation of Cdt1 in mammalian cells." Methods Mol Biol **1170**: 357-365.

Singh, A. M., J. Chappell, R. Trost, L. Lin, T. Wang, J. Tang, B. K. Matlock, K. P. Weller, H. Wu, S. Zhao, P. Jin and S. Dalton (2014). "Cell-Cycle Control of Developmentally Regulated Transcription Factors Accounts for Heterogeneity in Human Pluripotent Cells." Stem Cell Reports **2**(3): 398.

Snow, M. H. and D. Bennett (1978). "Gastrulation in the mouse: assessment of cell populations in the epiblast of tw18/tw18 embryos." J Embryol Exp Morphol **47**: 39-52.

Solter, D., N. Skreb and I. Damjanov (1971). "Cell cycle analysis in the mouse EGG-cylinder." Exp Cell Res **64**(2): 331-334.

Spencer, S. L., S. D. Cappell, F. C. Tsai, K. W. Overton, C. L. Wang and T. Meyer (2013). "The proliferation-quiescence decision is controlled by a bifurcation in CDK2 activity at mitotic exit." Cell **155**(2): 369-383.

Sporbert, A., P. Domaing, H. Leonhardt and M. C. Cardoso (2005). "PCNA acts as a stationary loading platform for transiently interacting Okazaki fragment maturation proteins." Nucleic Acids Res **33**(11): 3521-3528.

Stead, E., J. White, R. Faast, S. Conn, S. Goldstone, J. Rathjen, U. Dhingra, P. Rathjen, D. Walker and S. Dalton (2002). "Pluripotent cell division cycles are driven by ectopic Cdk2, cyclin A/E and E2F activities." Oncogene **21**(54): 8320-8333.

Stein, G. H., L. F. Drullinger, A. Soulard and V. Dulic (1999). "Differential roles for cyclin-dependent kinase inhibitors p21 and p16 in the mechanisms of senescence and differentiation in human fibroblasts." Mol Cell Biol **19**(3): 2109-2117.

Sugiyama, M., A. Sakaue-Sawano, T. Iimura, K. Fukami, T. Kitaguchi, K. Kawakami, H. Okamoto, S. Higashijima and A. Miyawaki (2009). "Illuminating cell-cycle progression in the developing zebrafish embryo." Proc Natl Acad Sci U S A **106**(49): 20812-20817.

Swaffer, M. P., A. W. Jones, H. R. Flynn, A. P. Snijders and P. Nurse (2016). "CDK Substrate Phosphorylation and Ordering the Cell Cycle." Cell **167**(7): 1750-1761 e1716.

Sweeney, C., M. Murphy, M. Kubelka, S. E. Ravnik, C. F. Hawkins, D. J. Wolgemuth and M. Carrington (1996). "A distinct cyclin A is expressed in germ cells in the mouse." Development **122**(1): 53-64.

Teofili, L., M. Martini, A. Di Mario, S. Rutella, R. Urbano, M. Luongo, G. Leone and L. M. Larocca (2001). "Expression of p15(ink4b) gene during megakaryocytic differentiation of normal and myelodysplastic hematopoietic progenitors." Blood **98**(2): 495-497.

Thomson, J. A., J. Itskovitz-Eldor, S. S. Shapiro, M. A. Waknitz, J. J. Swiergiel, V. S. Marshall and J. M. Jones (1998). "Embryonic stem cell lines derived from human blastocysts." Science **282**(5391): 1145-1147.

Wang, Z., E. Oron, B. Nelson, S. Razis and N. Ivanova (2012). "Distinct lineage specification roles for NANOG, OCT4, and SOX2 in human embryonic stem cells." Cell Stem Cell **10**(4): 440-454.

Warrier, S., M. Van der Jeught, G. Duggal, L. Tilleman, E. Sutherland, J. Taelman, M. Popovic, S. Lierman, S. Chuva De Sousa Lopes, A. Van Soom, L. Peelman, F. Van Nieuwerburgh, D. I. M. De Coninck, B. Menten, P. Mestdagh, J. Van de Sompele, D. Deforce, P. De Sutter and B. Heindryckx (2017). "Direct comparison of distinct naive pluripotent states in human embryonic stem cells." Nat Commun **8**: 15055.

White, J. and S. Dalton (2005). "Cell cycle control of embryonic stem cells." Stem Cell Rev **1**(2): 131-138.

Xie, W., M. D. Schultz, R. Lister, Z. Hou, N. Rajagopal, P. Ray, J. W. Whitaker, S. Tian, R. D. Hawkins, D. Leung, H. Yang, T. Wang, A. Y. Lee, S. A. Swanson, J. Zhang, Y. Zhu, A. Kim, J. R. Nery, M. A. Urich, S. Kuan, C. A. Yen, S. Klugman, P. Yu, K. Suknuntha, N. E. Propson, H. Chen, L. E. Edsall, U. Wagner, Y. Li, Z. Ye, A. Kulkarni, Z. Xuan, W. Y. Chung, N. C. Chi, J. E. Antosiewicz-Bourget, I. Slukvin, R. Stewart, M. Q. Zhang, W. Wang, J. A. Thomson, J. R. Ecker and B. Ren (2013). "Epigenomic analysis of multilineage differentiation of human embryonic stem cells." Cell **153**(5): 1134-1148.

Xu, R. H., X. Chen, D. S. Li, R. Li, G. C. Addicks, C. Glennon, T. P. Zwaka and J. A. Thomson (2002). "BMP4 initiates human embryonic stem cell differentiation to trophoblast." Nat Biotechnol **20**(12): 1261-1264.

Yang, R., C. Muller, V. Huynh, Y. K. Fung, A. S. Yee and H. P. Koeffler (1999). "Functions of cyclin A1 in the cell cycle and its interactions with transcription factor E2F-1 and the Rb family of proteins." Mol Cell Biol **19**(3): 2400-2407.

Yu, P., G. Pan, J. Yu and J. A. Thomson (2011). "FGF2 sustains NANOG and switches the outcome of BMP4-induced human embryonic stem cell differentiation." Cell Stem Cell **8**(3): 326-334.

Zhang, P., C. Wong, D. Liu, M. Finegold, J. W. Harper and S. J. Elledge (1999). "p21(CIP1) and p57(KIP2) control muscle differentiation at the myogenin step." Genes Dev **13**(2): 213-224.

Zhang, X., I. Neganova, S. Przyborski, C. Yang, M. Cooke, S. P. Atkinson, G. Anyfantis, S. Fenyk, W. N. Keith, S. F. Hoare, O. Hughes, T. Strachan, M. Stojkovic, P. W. Hinds, L. Armstrong and M. Lako (2009). "A role for NANOG in G1 to S transition in human embryonic stem cells through direct binding of CDK6 and CDC25A." J Cell Biol **184**(1): 67-82.

Zielke, N., J. Korzelius, M. van Straaten, K. Bender, G. F. Schuhknecht, D. Dutta, J. Xiang and B. A. Edgar (2014). "Fly-FUCCI: A versatile tool for studying cell proliferation in complex tissues." Cell Rep **7**(2): 588-598.